universiteit hasselt
KNOWLEDGE IN ACTION

2015 | Faculty of Sciences

DOCTORAL DISSERTATION

Study of zinc oxide coatings for improvement of the gas barrier, UV-protection and photodegradation characteristics of the bioplastic poly-(3-hydroxybutyrate-co-hydroxyvalerate) (PHBV).

Doctoral dissertation submitted to obtain the degree of
Doctor of Science: Chemistry, to be defended by

Lize Jaspers

Promoter: Prof. Dr Marlies K. Van Bael
Co-promoters: Prof. Dr Roos Peeters
Prof. Dr An Hardy

D/2015/2451/71

universiteit hasselt | imec
IMO - IMOMEC
INSTITUUT VOOR MATERIAALONDERZOEK

Members of the Jury

Chairman

Prof. dr. Karin CONINX
Dean Faculty of Sciences, UHasselt

Promoter

Prof. dr. Marlies K. VAN BAEL, UHasselt

Co-promoters

Prof. dr. Roos PEETERS, UHasselt
Prof. dr. An HARDY, UHasselt

Members of the Jury

dr. Nadia LEPOT, UHasselt
Prof. dr. Ir. Mieke BUNTINX, UHasselt
Prof. dr. Jan D'HAEN, UHasselt
Prof. dr. Ir. Peter RAGAERT, Universiteit Gent
Prof. dr. Mualla ÖNER, Yildiz Technical University

Dankwoord

Dit boekje is het resultaat van een helse en lange tocht, waarop vele mensen mij direct of indirect gesteund en geholpen hebben. Ik wil dan ook even de tijd nemen om deze mensen te bedanken.

In de eerste plaats zou ik mijn promotor, Marlies Van Bael, willen bedanken voor het mogelijk maken van dit doctoraat en me bij te sturen als ik weer eens te veel als een ingenieur aan het denken was.

Ook mijn copromotoren mogen niet vergeten worden. Roos, een groot deel van dit werk is tot stand gekomen door jouw begeleiding. Ik heb enorm veel bewondering voor jou omdat je ondanks het feit dat je vice-decaan van FIIW, docent en hoofd van het VerpakkingsCentrum bent, nog altijd tijd voor me vond. Dook er een probleem op, ik kon altijd bij jou terecht. Bedankt hiervoor. Jij liet me ook vrij om alle aspecten van verpakking te ontdekken en ik kan je daar alleen maar om bedanken. De reden dat ik nu een droomjob heb is juist omdat je me zo vrijgelaten hebt en me niet beperkt hebt in mijn kennis. An, je stond altijd klaar om mijn artikels en abstracten na te lezen. Jouw input zorgde er voor dat het meer wetenschappelijk en een aaneenhangend geheel werd.

Nadia, jij maakte deel uit van mijn doctoraatscommissie en was heel nauw betrokken met het tot stand komen van dit doctoraat. Je hebt hetzelfde traject als ik doorlopen en je deelde maar al te graag jouw ervaringen en gaf me de nodige tips om het toch tot een goed einde te brengen, bedankt hiervoor.

Ik wil ook nog Heidi van den Rul bedanken, in het prille begin van mijn doctoraat maakte je nog deel uit van mijn commissie en heb jij me op weg geholpen met de depositie van ZnO, bedankt hiervoor.

Doordat mijn doctoraat een samenwerking was tussen IIW Verpakkingstechnologie en Anorganische en Fysische Chemie heb ik het geluk gehad deel uit te maken van 2 onderzoeksgroepen en veel mensen te leren kennen.

Allereerst wil ik de mensen van het VerpakkingsCentrum en de opleiding IIW Verpakkingstechnologie bedanken. In de voorbije jaren heb ik verschillende mensen zien passeren en hopelijk vergeet ik niemand. Ik ga beginnen met de mensen van ons oude bureautje. Philip, ik herinner me nog de leuke gesprekken in de auto en vooral dat je zo vriendelijk was om me af en toe in Berchem af te zetten. Ik heb ook enorm veel geleerd van jou, zoals werken met Europese en Amerikaanse standaarden en waar op te letten tijdens de verschillende metingen. Jouw technische kennis van de verschillende meettechnieken en meetapparatuur is gewoon enorm, ging er iets kapot, 9 kansen van de 10 kon je het zelf herstellen. Dat ik een cursus over papieren en kartonnen verpakkingsmaterialen heb kunnen schrijven, heb ik ook grotendeels aan jou te danken. Ik vond het dan ook heel jammer toen je naar het BVI vertrok. Wies, ik weet nog goed hoe je me hielp met maken van mijn visitekaartjes en het maken van de infomappen voor de wetenschapsweek of andere activiteiten. Voor de creatieve ideeën kon ik altijd bij jou terecht. Ook gewoon voor een leuke babbel of als ik even stoom moest aflaten, stond je altijd klaar. Stan, je kritische kijk en ondernemingszin zorgde er voor dat je altijd boordenvol nieuwe ideeën zat en je was een inspiratie om steeds naar beter en meer te verlangen en het beste na te streven. Je altijd goed humeur en geweldig gevoel voor humor zorgde ook voor vele leuke en hilarische momenten die ik niet gauw zal vergeten. Momenteel ben je met Heleen een huis aan het verbouwen en aan de foto's te zien leveren jullie prachtig werk! Ik ken Heleen dan ook niet anders dan een hardwerkende collega, die altijd iets te doen moet hebben. Heleen, je nam altijd de touwtjes in handen en als ik hulp nodig had wegens tijdgebrek, stond je ook altijd voor me klaar. Bedankt hiervoor. Gert, in de meer theoretische opleiding die ik heb gevolgd leerde je niet echt creatief te zijn of met design programma's om te gaan. Jij hebt dan ook moeite moeten doen om me de basis begrippen van CAD bij te brengen en ik ben je daar enorm dankbaar voor, zeker aangezien ik voor mijn huidige job nog regelmatig in contact kom met CAD en andere designprogramma's. Het zal me ook altijd bijblijven hoe je een bestelwagen hebt omgetoverd tot een soort van caravan, kan niet anders dat je er al vele leuke avonturen mee beleefd hebt. Mieke, als opleidingshoofd IIW Verpakkingstechnologie wil je alleen maar het beste voor de opleiding. We hebben dan ook verschillende uren samen doorgebracht om de

opleidingsonderdelen zo academisch mogelijk maken. Bij activiteiten zoals de wetenschapsweek, opendeurdagen, enz. was het ook steeds duidelijk hoe klein onze groep wel niet was en deed je altijd je best om zo veel mogelijk mensen te motiveren en enthousiasmeren om steeds weer klaar te staan voor de organisatie van de verschillende activiteiten. Ook al maakte je geen deel uit van mijn doctoraatscommissie, ik kon altijd op je rekenen om mijn artikels, presentaties, enz. na te lezen en de nodige input te geven, bedankt hiervoor. Dimitri, jij bent één van de weinigen die al in het VerpakkingsCentrum werkte toen ik een aantal jaren geleden begon en nu nog altijd een groot deel van je leven daar doorbrengt. Je hebt me met de Mocons leren werken en de nodige tips gegeven bij het uitvoeren van de permeabiliteitsmetingen. Jij hebt ook onnoemelijk veel keren jouw meetschema moeten aanpassen aan mijn schema, echt bedankt, weet dat dat niet altijd even makkelijk was. Gudrun, jij bent meer de stille werkkracht. Je staat altijd klaar voor iedereen, zonder te klagen en niets is te veel gevraagd. Ben ook stiekem jaloers op je vele bezoekjes aan Vegas, als ik er ooit nog eens geraak, kom ik zeker langs voor enkele tips. Bram en Griet, jullie kwamen toen ik in de laatste fase van mijn doctoraat zat, wij hebben dan ook niet zo veel tijd met elkaar kunnen doorbrengen. Waarschijnlijk kwam dit ook doordat we niet aan dezelfde projecten werkten. Toch moet ik jullie bedanken voor de leuke babbels die we op die enkele momenten hadden en die me steeds hielpen de stress even te vergeten.

Willem, jij was net als ik doctoraatsassistent en de enkele jaren dat je er was hebben we dan ook veel samengewerkt. Doordat je al ervaring had in de plasticindustrie, was je kennis hiervan heel uitgebreid. Ik heb dan ook veel geleerd van jou, hoe plastics verwerkt worden, waar de industrie naar kijkt, wat belangrijk is om in rekening te brengen. Bedankt hiervoor. Jens, met jou heb ik veel lief en leed gedeeld. We kwamen regelmatig voor de zelfde obstakels te staan en je stond samen met Kenny altijd voor me klaar om mijn geklaag te aanhoren. Ik wens je veel moed en sterkte deze laatste maanden. Als assistent IIW Verpakkingstechnologie heb ik ook het geluk gehad met vele andere mensen binnen de opleidingen IIW Verpakkingstechnologie en Nucleaire technologie te mogen samenwerken. Kenny, Inge, Sonja, Els, Ida en alle anderen bedankt voor de mooie tijd.

En dan nu de mensen van labo anorganische en fysische chemie. Christopher, de perfectionist, de tijd die je steekt in anderen zodat ook hun werk aan jouw normen voldoet is onvoorstelbaar. Altijd en overal sta je voor iedereen klaar, zelfs als postdoc voerde je taken uit die eigenlijk niet tot je takenpakket behoorden. Je gaat een groot gemis zijn voor de groep. Naast dat je een toffe en behulpzame collega was, hebben we ook veel leuke momenten gehad buiten de werkuren. De dinertjes met onze club van drie, trouwens de agenda's moeten dringend naast elkaar gelegd worden voor de ***, CT, lopen, enz. Samen met Linny en Hanne ben je niet enkel een collega, maar ook een echte vriend. Linny, allebei werkten we met ZnO, je hebt me dan ook vaak goede raad gegeven voor het aanpassen van de synthesemethoden. Jouw enthousiasme, energie en doorzettingsvermogen is ongezien, het geluid dat je kan produceren ook en dan zeggen ze dat ik soms luid spreek! Ik herinner me de zomers waar we vaak enkel met zijn tweetjes in het labo stonden en de radio loeihard stond, lagen afzetten was nooit plezieriger! Ook met jou heb ik vele mooie momenten beleefd na de uren, de concerten, musicals, dansen, restaurant bezoekjes, enz. Zelfde geldt voor jou als voor Christopher, haal de agenda maar boven, een weekendje in de Vlaanders komt er aan! Daan, wij gaan al heel lang terug, samen aan de UHasselt begonnen, samen naar Antwerpen, waar we een kamer hadden in hetzelfde gebouw en was dat nog niet genoeg, kwamen we elkaar weer tegen op de UHasselt. De onderwerpen van onze doctoraten lagen misschien iets te ver uit elkaar om echt te kunnen samenwerken, maar je stond altijd klaar voor een leuke babbel en een luisterend oor. Ken, stille waters hebben diepe gronden, dat heb ik wel ontdekt bij de eerste quiz die we samen speelden. De hoeveelheid vragen die jij kon beantwoorden, ongelooflijk. Het was leuk met jou samen te werken. Alexander, de onzin die jij kan verkopen, ongelooflijk. Een liedjestekst in 1, 2, 3 omtoveren tot een hilarisch stuk of ideeën spuien voor de CT of de act voor iemands doctoraatsverdediging, jij kan het als de beste. Volgens mij missen ze je op zulke momenten enorm. Kevin, lange tijd hebben we naast elkaar gezeten in het landschapsbureel, we hebben dan ook heel wat af gelachen. Ik bewonder het enorm dat je voor je eigen geluk hebt gekozen en je altijd je eigen ding bent blijven doen. Jij was een van de weinigen die effectief durfde zeggen en doen wat iedereen dacht en wilde, chapeau. Ik moet je ook enorm bedanken voor alle stalen die je voor mij hebt gemeten. Nick, kapitein

van ons CT team, je chiro skills kwamen tijdens de CT goed van pas. Net als Christopher streefde je in het labo naar perfectie en hielp je mee aan allerlei projecten om het labo en de veiligheid in het labo te verbeteren. Als postdoc stond je ook altijd klaar met raad en goede ideeën voor het batterijteam. Anke, net als mij babbel je nogal graag en ik vond het dan ook enorm leuk dat we gewoon over alles en niets konden tetteren. Bertie, ik heb je pas beter leren kennen op het einde van je doctoraat, toen we eventjes een bureau deelden. Ik kijk met veel plezier terug op die tijd. Giedrius, thank you for the Raman measurements. I enjoyed the talks about your dog and about the travels you made. Nikolina, even though we didn't have much contact, you were a good colleague. Hanne, waar moet ik beginnen, ik denk dat wij gewoon gelijktijdig door alle fases in ons doctoraat zijn gegaan. We hebben samen gelachen en gehuild, je was een grote steun. De leuke dingen die we samen hebben gedaan zijn niet meer te tellen: sh'bam, zumba, last minute concerten, shoppen, sauna, … Doordat we het allebei enorm druk hebben gehad de laatste 3 maanden, hebben we wat minder tijd gehad voor deze dingen. Ik kijk dan ook uit naar januari zodat we onze tradities in stand kunnen houden. Sven, je was een aangename collega, veel succes met je nieuwe job. Thomas, het is je vergeven dat je een android man bent. Net als Ken, ben je eerder van het stille type, al kan je af en toe zeer gevat uit de hoek komen. Veel succes met het schrijven van je doctoraat. Ellen, jij staat altijd en overal voor iedereen klaar en wil alles tot in perfectie regelen. Je hebt een slimme keuze genomen, ik wens je ongelooflijk veel succes in alles wat je doet. Giulia, it was a delight to know you, I love your optimism and work spirit. Wouter & Boaz, als ik jullie zie, word ik spontaan goed gezind. Jullie spontaniteit en enthousiasme zijn gewoon aanstekelijk, hou die eigenschappen goed vast, het wordt jullie sterkste troef. Maarten, jij stond altijd klaar met duizend-en-een vragen, zoals het een echte wetenschapper betaamt. Gilles en Jonathan, doordat ik al in de laatste fase van mijn doctoraat zat, hebben wij elkaar ook niet zo goed leren kennen, maar ik wens jullie veel succes met jullie doctoraat.

Ik wil ook iedereen van de andere onderzoeksgroepen waar ik heb mee samengewerkt bedanken, te beginnen bij de mensen van TANC. Prof. dr. Carleer omdat ik mocht gebruik maken van de meettoestellen van zijn onderzoeksgroep. Guy voor de vele metingen die ik op de DSC heb mogen uitvoeren en de hulp bij het bedienen van de Q200. Jenny voor de GPC metingen, Martine voor de ATR metingen en Elsy en Yvo voor de aangename momenten in het labo. Huguette omdat ik de UV metingen bij haar mocht uitvoeren. Van de onderzoeksgroep materiaalfysica, Jan d' Haen en Bart Ruttens voor de SEM en XRD metingen, Tim Vangerven voor de DEKTAK metingen en Stoffel voor het aanleren van de contacthoekmetingen.

I would also like to thank the members of the jury for reading and improving my thesis.

Ook wil ik mijn familie bedanken. Mama en papa, jullie staan altijd en overal voor me klaar en steunen me onvoorwaardelijk. Dankzij jullie heb ik kunnen studeren en doctoreren. Bedankt voor alles wat jullie voor me gedaan hebben en nog altijd doen, zonder jullie stond ik nergens. Tine, mijn allerliefste zus, op jou kan ik altijd rekenen voor steun en goede raad en als dat nog niet genoeg is, heb je me het mooiste geschonken wat iemand me ooit kan geven, Jente, mijn engel van een metekindje. De uitstapjes met haar deden me onmiddellijk alle stress en wrevel van mijn doctoraat vergeten en hielpen me er weer tegen aan te gaan. De geboorte van Sverre was ook een lichtpuntje in mijn laatste doctoraatsjaar. Van de eeuwige lach op zijn gezichtje kan je niet anders dan gelukkig worden. Tante Marita, jou wil ik ook speciaal bedanken omdat je meer bent dan een gewone tante, als er iets was, ik kon altijd met je praten en je hielp me de dingen relativeren. Bedankt daarvoor.

En dan als laatste wil ik nog de allerbelangrijkste persoon in mijn leven bedanken, mijn vriend Tom. Het was niet altijd even gemakkelijk, zeker de laatste twee jaar van mijn doctoraat niet, maar toch stond je altijd voor me klaar om me op te peppen, te troosten of te kalmeren. Je bent de beste vriend die iemand zich kan inbeelden. Je geeft me de vrijheid en steun om te zijn wie ik ben en ik ben je daar ongelooflijk dankbaar voor.

Publications

★ Described in this thesis

E. Debie, **L. Jaspers**, P. Bultinck, W. Herrebout, B. Van der Veken, *Induced solvent chirality: A VCD study of camphor in CDCl3*, Chem Phys Lett, 450 (2008) 426-430.

★ **L. Jaspers**, N. Lepot, K. Schellens, A. Hardy, R. Peeters, M.K. Van Bael, *Influence of Zinc Oxide (ZnO) nanolayers on the oxygen barrier of the bioplastic poly(3-hydroxybutyrate-co-3- hydroxyvalerate) (PHBV),* Proceedings of 26th IAPRI Symposium on Packaging 10-13 August 2013, Espoo, Finland.

★ **L. Jaspers**, N. Lepot, A. Hardy, R. Peeters and M.K. Van Bael, *Study on the influence of zinc oxide (ZnO) nanolayers on the permeability of the bioplastic poly(3-hydroxybutyrate-co-3-hydroxyvalerate) (PHBV),* Proceedings of the 5th International Conference on Nanotechnology: Fundamentals and Applications, Prague, Czech Republic, August 11-13, 2014.

★ ***L. Jaspers****, N. Lepot, G. Degutis, M. Buntinx, A. Hardy, R. Peeters, M.K. Van Bael,* Influence of Zinc Oxide (ZnO) nanolayers on the gas barrier and UV degradation properties of the bioplastic poly(3-hydroxybutyrate-co-3-hydroxyvalerate) (PHBV)*, submitted.*

★ **L. Jaspers**, N. Lepot, A. Hardy, R. Peeters, M.K. Van Bael, *Low Temperature Deposition of Zinc Oxide (ZnO) on bioplastic poly(3-hydroxybutyrate-co-3-hydroxyvalerate) (PHBV) and Polyethylene terephthalate (PET),* submitted.

Conference contributions

Oral Presentations

L. Jaspers, N. Lepot, A. Hardy, R. Peeters and M.K. Van Bael, *Low temperature solution deposition of ZnO thin films on the bioplastic PHBV.*
ChemCYS 2012, Blankenberge, Belgium, March 1-2 2012

L. Jaspers, N. Lepot, A. Hardy, R. Peeters and M.K. Van Bael, *Zinc oxide: a promising material for future food packaging.*
EMPACK Brussels 2012, Brussel, Belgium, September 26-27 2012

L. Jaspers, N. Lepot, A. Hardy, R. Peeters and M.K. Van Bael, *Low temperature deposition of zinc oxide (ZnO) nanoparticles on (bio)polymers.*
ECERS 2013, Limoges, France, June 23-27 2013

L. Jaspers, N. Lepot, M. Buntinx, R. Peeters, A. Hardy and M.K. Van Bael, *Study on the influence of zinc oxide (ZnO) nanolayers on the permeability of the bioplastic poly(3-hydroxybutyrate-co-3-hydroxyvalerate) (PHBV).*
5th International Conference on Nanotechnology: Fundamentals and Applications, Prague, Czech Republic, August 11-13, 2014

L. Jaspers, N. Lepot, M. Buntinx, R. Peeters, A. Hardy and M.K. Van Bael, *The effect of zinc oxide (ZnO) nanolayers on the gas barrier properties of the bioplastic poly(3-hydroxybutyrate-co-3-hydroxyvalerate) (PHBV).*
2nd International Conference on Biobased Polymers and Composites, Visegrád, Hungary, August 24-28, 2014

Poster Presentations

L. Jaspers, N. Lepot, K. Elen, R. Peeters, J. Mullens, A. Hardy and M.K. Van Bael, *Zinc oxide: a promising material for improving future food packaging.*
NanoSymposium 2010, Brussel, Belgium, November 10, 2010

L. Jaspers, N. Lepot, A. Hardy, R. Peeters and M.K. Van Bael, *Low temperature solution deposition of Zinc Oxide coatings on flexible polymer substrates.*
EMRS 2011 Fall Meeting, Warsaw, Poland, September 17-21, 2012

L. Jaspers, N. Lepot, A. Hardy, R. Peeters and M.K. Van Bael, *Improving characteristics of (bio)plastics by low temperature deposition of zinc oxide (ZnO) nanoparticles.*
2013 BCerS Annual Meeting, Hasselt, Belgium, April 19, 2013

L. Jaspers, N. Lepot, A. Hardy, R. Peeters and M.K. Van Bael, *Influence of zinc oxide (ZnO) nanolayers on the oxygen barrier of the bioplastic poly(hydroxyvaleratehydroxybutyrate) (PHBV).*
26th IAPRI Symposium on Packaging, Espoo, Finland, June 10-13, 2013

L. Jaspers, N. Lepot, A. Hardy, R. Peeters and M.K. Van Bael, *Improving the gas barrier properties of the bioplastic poly(3-hydroxybutyrate-co-3-hydroxyvalerate) (PHBV) through Zinc Oxide (ZnO) nanolayers.*
ChemCYS 2014, Blankenberge, Belgium, February 27-28, 2014

Table of contents

Nederlandstalige samenvatting

Verpakking is onmisbaar geworden in de voedingsindustrie. Verpakte producten kunnen op een efficiëntere manier getransporteerd en geïdentificeerd worden en de verpakte producten worden beter beschermd tijdens transport en opslag. Voedsel wordt niet alleen beschermd tegen schokken en stoten, maar ook tegen omgevingsfactoren. Zo kunnen temperatuur, vochtigheid, licht en zuurstof een grote invloed hebben op de houdbaarheid van voedingswaren.

Aangezien sommige producten van het ene naar het andere continent verscheept worden, is kwaliteitsbehoud van de producten meer dan ooit belangrijk. Om de houdbaarheid van voedsel te verlengen, wordt gebruik gemaakt van barrière-materialen. Barrière-materialen kunnen zowel zuurstof, koolstofdioxide, stikstof, vocht en licht buiten houden, als zuurstof, koolstofdioxide, stikstof en vocht in de verpakking houden.

Plastics zijn één van de meest gebruikte verpakkingsmaterialen. Meer dan 50% van de producten wordt in plastic verpakt. Plastics hebben onder andere het grote voordeel dat ze in verschillende vormen kunnen geproduceerd worden en ze licht in gewicht zijn. Ondanks de voordelen, zijn er ook nadelen. Voor de productie is niet alleen ruwe olie nodig, maar ook energie waardoor er broeikasgassen, zoals methaan en CO_2 vrijkomen. Daarnaast zijn plastics niet biologisch afbreekbaar en dragen ze bij tot het afvalprobleem. Bioplastics daarentegen worden geproduceerd uit biomassa en/of zijn biologisch afbreekbaar. Hierdoor worden ze gezien als interessant verpakkingsmateriaal om plastic te vervangen. Biogebaseerde polyethyleentereftalaat (Bio-PET), biogebaseerde polypropyleen (Bio-PP) en biogebaseerde polyethyleen (Bio-PE) nemen geleidelijk aan de plaats in van hun conventionele tegenhangers. Deze materialen zijn echter enkel gebaseerd op biomassa en niet biologisch afbreekbaar. Polymelkzuur (PLA) daarentegen is zowel gebaseerd op biomassa en biologisch afbreekbaar. PLA heeft het nadeel bros en thermisch instabiel te zijn. Polyhydroxyalkanoaten (PHA's) worden gezien als een beter alternatief. Polyhydoxybutyraat-co-hydroxyvaleraat (PHBV) behoort tot de groep van de

PHA's en heeft vergelijkbare mechanische eigenschappen als polypropyleen (PP). Het is een semi-kristallijn polymeer met een smeltpunt rond de 180°C, afhankelijk van de valeraat concentratie. De gasbarrière van dit materiaal voldoet echter niet aan de voorwaarden van een goede barrière, ≤ 1 cc.mm/(m^2.dag.atm), en dient dus geoptimaliseerd te worden om een ruimer toepassingsgebied te creëren.

Er zijn verschillende methoden om de gasbarrière te optimaliseren. Men kan het materiaal mengen met een materiaal met hogere barrière-eigenschappen. Er kunnen lagen hoog barrièremateriaal op het polymeer afgezet worden of er kunnen deeltjes barrièremateriaal in de polymeermatrix gemengd worden. In de verpakkingswereld blijkt het inmengen van anorganische deeltjes zoals aluminiumoxide (Al_2O_3), montmorilloniet (MMT) en siliciummonoxide (SiO) en siliciumdioxide (SiO_2) een goede techniek voor de verbetering van de gasbarrière. Het inmengen van anorganische deeltjes in een polymeermatrix heeft echter ook nadelen. Vaak zorgt de chemische incompatibiliteit tussen het anorganische deeltje en de polymeermatrix er voor dat er agglomeraten worden gevormd en dat de barrière-eigenschappen afnemen, tegengesteld aan het feitelijke doel. Een mogelijke oplossing hiervoor is het aanbrengen van barrière-lagen op het polymeeroppervlak. Voor dit onderzoek werd gekozen om zinkoxide (ZnO) nanolagen aan te brengen op het oppervlak van de bioplastic PHBV. Er werd gekozen voor ZnO omdat ZnO zuurstof adsorbeert, beschermt tegen UV licht en antibacteriële eigenschappen heeft.

Er zijn verschillende technieken ter beschikking om lagen aan te brengen op het oppervlak van polymeren. Bij de meeste van deze technieken, zoals chemische dampdepositie (CVD), wordt ZnO slechts afgezet bij temperaturen boven de 200 °C. Aangezien PHBV ontbindt bij temperaturen boven de 200 °C is het dus belangrijk dat er een techniek gebruikt wordt waarmee een afzettingstemperatuur onder de 100 °C kan gehanteerd worden. Technieken zoals atomaire laag depositie (ALD) en sputteren voldoen aan deze voorwaarden, maar zijn duur. Een goedkopere oplossing is het gebruik van de sol-gel techniek in combinatie met de chemisch bad methode. Een ander voordeel van deze techniek is dat door aanpassing van enkele parameters, zoals

zuurtegraad (pH), temperatuur en concentratie van de oplossingen, de vorm van de afgezette deeltjes kan aangepast worden. Nanodeeltjes met een hoge aspectratio vormen betere barrière-materialen dan deeltjes met een lage aspectratio. Aangezien de afzetting verschilt van substraat tot substraat is het belangrijk de pH, depositietemperatuur en duur van de depositie aan te passen. Aangezien de depositie van ZnO nanolagen op het substraat PHBV nog niet bestudeerd werd en de bestaande sol-gel methoden vaak werkingstemperaturen boven de 100°C gebruiken, werd de ZnO laag eerst geoptimaliseerd op een PET substraat.

In hoofdstuk 4 wordt de synthese van de ZnO nanolagen besproken. Het gebruik van kiemlagen bleek noodzakelijk voor de afzetting van ZnO nanolagen. Door de kiemlaag af te zetten bij 30 °C werden betere ZnO nanolagen verkregen. Na het afzetten van de kiemlagen werden de substraten ondergedompeld in een chemisch bad. Temperatuur, duur van de behandeling en de molaire ratio van de precursor werden gevarieerd om tot de vorming van ZnO nanolagen te komen. Zowel zinknitraat hexahydraat ($Zn(NO_3)_2.6H_2O$) als zinkacetaat dihydraat ($Zn(CH_3COO)_2.2H_2O$) werden gebruikt als Zn^{2+} bron. Voor de afzetting van ZnO nanolagen op PET bleek het chemisch bad van $Zn(NO_3)_2.6H_2O$ en DETA de meeste dichte afzetting te leveren. De substraten werden ondergedompeld in het mengsel en 4u in een oven op 95°C geplaatst. Door PHBV substraten 2u onder te dompelen op 95°C in een mengsel van $Zn(CH_3COO)_2.2H_2O$ en HMT, werden voor deze substraten de meest dense lagen ZnO gevormd. Verlaging van de temperatuur naar 75°C leidde tot een slechtere depositie. De ZnO nanolaag werd gekarakteriseerd door middel van SEM, XRD, Raman en FTIR-ATR. De gevormde lagen hebben een dikte tussen de 140 en 270 nm en bestaan uit wurtziet ZnO die groeien in (002) richting. De depositie van de ZnO nanolagen had geen invloed op de mechanische en thermische eigenschappen van PHBV en PET.

De depositie van ZnO nanolagen op PHBV leidde tot een verbetering van de zuurstof, CO_2 en waterdamp barrière-eigenschappen van PHBV (hoofdstuk 5). Door de temperatuur te verhogen van 10 °C naar 23 °C naar 38 °C werd aangetoond dat door de afzetting van de ZnO nanolagen, PHBV op 38°C betere

barrière-eigenschappen heeft dan PHBV zonder ZnO op 23 °C. De permeabiliteit van PHBV met ZnO op 38 °C was lager dan de permeabiliteit van puur PHBV op 23 °C. De activeringsenergie voor permeabiliteit werd bepaald voor zowel PET, PHBV, PET met ZnO en PHBV met ZnO. Hierdoor kan de permeabiliteit van deze materialen bij verschillende temperaturen bepaald worden. Door de vochtigheidsgraad te verhogen van 0% naar 40% naar 80% voor zuurstof- en CO_2 doorlaatbaarheid en de vochtigheidsgraad te verlagen van 100% naar 80% naar 40% voor waterdampdoorlaatbaarheid kan aangetoond worden dat door ZnO af te zetten op PHBV, de PHBV ook bij hogere vochtigheidsgraad kan gebruikt worden als barrière-materiaal. Doordat het PET staal al goede barrière-eigenschappen had, kon er geen verandering in permeabiliteitseigenschappen worden waargenomen na afzetting van de ZnO nanolagen.

Alhoewel de depositie van de ZnO op PHBV leidde tot een verbetering van de barrière-eigenschappen, dienen de ZnO lagen geoptimaliseerd te worden. De PHBV stalen met ZnO nanolagen vertonen geen merkbare verbetering ten opzichte van de stalen met ZnO kiemlagen. Dit komt doordat er nog te veel defecten aanwezig zijn in de nanolaag zelf. De lagen kunnen geoptimaliseerd worden door de pH en de molaire ratio van de precursor aan te passen.

In hoofdstuk 6 wordt aangetoond dat ZnO PHBV ook beschermt tegen UV licht. De UV degradatie van PHBV volgt een proces van crosslinking en ketensplitsing zoals aangetoond wordt door GPC-metingen. De ATR-metingen toonden aan dat er ook ketenafbraak plaatsvindt door β-oxidatie en in beperkte mate door de Norrish I en Norrish II reactie. Bestraling van PHBV met UV licht veroorzaakt verkleuring door een verandering in de chemische samenstelling van het polymeer. Toevoeging van ZnO aan de PHBV substraten vermindert de verkleuring en vergeling met een kleine hoeveelheid. Er kon pas een verandering in treksterkte, het aantal gemiddeld molecuulgewicht (Mn) en het gewicht gemiddeld molecuulgewicht (Mw) gedetecteerd worden na 24u bestraling, terwijl een toename van de keto- en ester-carbonyl index al zichtbaar was na 12u bestraling. De PHBV stalen met een ZnO nanolaag bleken beter beschermd te zijn dan de PHBV stalen met enkel ZnO kiemlagen. De O_2 en

CO_2 permeabiliteit van PHBV met ZnO kiemlaag bleven stabiel, zelfs na 36u bestraling, terwijl de permeabiliteit van puur PHBV daalt na 36u bestraling.

Er kan dus besloten worden dat de depositie van ZnO op PHBV de O_2, CO_2 en waterdampbarrière van PHBV verhoogt en PHBV beschermt tegen UV licht.

Abbreviations and symbols

a	Aspect ratio
A	Surface area
ALD	Atomic layer deposition
Al_2O_3	Aluminium oxide
ATR-FTIR	Attenuated Total Reflectance Fourier Transform Infra Red
BIF	Barrier improvement factor
C	Concentration
CB	Chemical bath
CBD	Chemical bath deposition
$(CH_2)_6N_4$	Hexamethylene tetramine
$(CH_2)_4N_3H_5$	Diethylenetriamine
CH_3OH	Methanol
CI	Crystallinity index
C_{md}	Dimensional constant
CNT	Carbon nanotubes
CVD	Chemical vapour deposition
CO_2	Carbon dioxide
D	Diffusion coefficient
D_0	Temperature-independent diffusion factor
DETA	Diethylenetriamine
DSC	Differential scanning calorimetry
E_d	Activation energy of diffusion,
E_p	Activation energy of permeability
EVOH	Ethylene vinyl alcohol
FDA	Food & Drug Administration
GHG	Greenhouse gases
GRAS	Generally recognized as safe
GPC	Gel permeation chromatography
HDPE	High density polyethylene
HMT	Hexamethylene tetramine
H_2O	Water

H_2O_2	Hydrogen peroxide
HB	Hydrobuterate
HV	Hydroxyvalerate
J	Diffusion flux
LDPE	Low density polyethylene
M_n	Number-average molecular weight
M_w	Weight-average molecular weight
MAF	Mobile amorphous fraction
MAP	Modified Atmosphere Packaging
MgO	Magnesium oxide
MMT	Montmorillonite
MOCVD	Metalorganic chemical vapour deposition
N_2	Nitrogen
NaOH	Sodium hydroxide
O^{2-}	Oxygen ion
O_2	Oxygen gas
OTR	Oxygen transmission rate
p	Partial Pressure
P	Permeability coefficient
P_b	Permeability polymer with oxide layer
P_c	Permeability of coating
P_{CO2}	Carbon dioxide permeability coefficient
P_{comp}	Permeability of composite
P_{la}	Permeability through lattice
P_{nd}	Permeability through nanodefects
P_{O2}	Oxygen permeability coefficient
P_p	Permeability of polymer
P_{poly}	Permeability of polymer
P_{WV}	Water Vapour permeability coefficient
PA	Polyamide
PBAT	Polybutylene adipate-co-terephthalate
PEG	Polyethylene glycol
PEN	Polyethylene naphthalate

PEO	Polyethylene oxide
PET	Polyethylene terephthalate
PHA	Polyhydroxyalkanoate
PHB	Polyhydroxybutyrate
PHBV	Poly(3-hydroxybutyrate-co-hydroxyvalerate)
PLA	Polylactic acid
PP	Polypropylene
PS	Polystyrene
PVOH	Poly(vinyl alcohol)
PVC	Polyvinyl chloride
PVDC	Poly(vinylidene chloride)
Q	Total amount of permeant
r	Intermolecular distance
R	Universal gas constant
RAF	Rigid amorphous fraction
RF	Radio-frequency
RH	Relative humidity
SiO	Silicon monoxide
SiO_2	Silicon dioxide
S	Solubility coefficient
S_0	Temperature-independent solubility factor
SEM	Scanning electron microscopy
t	Time
T	Temperature
T_d	Decomposition temperature
T_R	Room temperature
T_m	Melting temperature
TiO_2	Titanium dioxide
TGA	Thermal gravimetric analyse
TR_{O2}	Oxygen transmission rate
UV	Ultra Violet
V	Volume
VTR	Vapour transmission rate

W	Weight
w_b	Weight sample before UV exposure
w_a	Weight sample after UV exposure
WV	Water vapour
x	Thickness film
X_c	Coating thickness
X_P	Polymer thickness
XRD	X-ray diffraction
Zn^{2+}	Zinc ion
$Zn(CH_3COO)_2.2H_2O$	Zinc acetate dehydrate
$ZnCl_2$	Zinc chloride
$Zn(NO_3)_2.6H_2O$	Zinc nitrate hexahydrate
ZnO	Zinc oxide
ZrO_2	Zirconium oxide
Δb	Yellowing index
ΔH_f°	Enthalpy of formation of a 100% crystalline polymer
ΔH_f^{obs}	Observed enthalpy of the polymer
ΔH_S	Enthalpy of solution
ΔL	Lightness
Δp	Change in permeant partial pressure
δ	Function angular depence of the dipole-dipole interaction energy
ε	Maximum energy of action
σ	Collision diameter
σ_{max}	Tensile strength
φ_{np}	Volume fraction nanoparticle
ϕ_g	Thickness oxide layer
ϕ_P	Thickness polymer

Chapter 1

Introduction

1.1 Functions of packaging

Through its numerous functions, packaging has become indispensable in the food industry. The first reason for using packaging is the ease in handling. While not so long ago, fruit, vegetables, flour and other products were sold loose, they are now packed in containers, jars, boxes, etc.. This makes it easy to hold and transport the products. Products can also be packed in bulk making it easy to handle larger amounts. The colour, shape, size and text on the package enables us to identify the product. Through labelling extra information about the packaged good can be provided. The ingredient list, nutrition values, product use, possible hazards, etc. can be put on the package. Packaging also complicates tampering with the products. It shows once a package has been opened. Next to this, packaging ensures physical protection of the product. During transport and storage, products are protected against shocks, vibrations, compressions, humidity and temperature. Thanks to packaging materials, some food products are protected against contact with substances, such as air, light and moisture, protecting them against spoilage. These materials that protect against air, light, moisture and other substances are called barrier materials [1-3].

In the last years quality preservation has become one of the most important functions of packaging. Products come from all over the world. For some food products this means that several days or months pass until the product is consumed. Ingredients in food however have a low chemical stability, making them easy to digest. Numerous reactions with the environment can lead to spoilage. Air and humidity are the most important parameters for food spoilage. In air it is especially oxygen (O_2) that can lead to a decrease in food quality. Oxygen can cause damage to food in several ways. For instance a number of bacteria, all moulds and most yeast (aerobes), need O_2 to grow. There are also

bacteria that only grow in the absence of O_2 (anaerobes)[4]. Polyphenol oxidase and peroxidase are two oxidizing enzymes in vegetables and fruit that speed up the oxidative reactions of phenolic compounds causing vegetables and fruit to brown [5]. This reaction often leads to loss in flavour and odours. Another kind of spoilage through O_2 is oxidative spoilage. In fatty food lipids oxidize and short chain carbon compounds are formed. These compounds have a bad flavour and a strong odour. Next to O_2, moisture can lead to food spoilage. Moulds and yeast need water to grow. So excessive water increases mould and yeast growth. Moisture condensing on the surface of food products can lead to soggy products. While moisture loss can lead to too dry products [6].

A way to extend the shelf life of food is to use modified atmosphere packaging (MAP). The atmospheric air inside a package is substituted with a gas mixture. Mostly the oxygen content is decreased and the carbon dioxide (CO_2) is increased. CO_2 at high levels is both bacteriostatic and fungistatic, preventing moulds to grown [7]. The third gas that is used is nitrogen (N_2). N_2 is used to replace O_2 [1].

O_2, CO_2 and humidity are the most important factors in extending the shelf life of products. To keep these gases in or out the packaging, the barrier properties of the packaging materials are important. As shown in table 1.1 different products need different O_2, CO_2 and water vapour (WV) barriers. For example red meat needs a high barrier all over, while fish needs a low water vapour barrier [8]. A high barrier has a permeability of less than 1 $cc.mm/m^2.day.atm$ for the O_2 and CO_2 gasses and a permeability of less than 1 $g.mm/m^2.day.atm$ for water vapour. Low gas barriers have a permeability value higher than 10 $cc.mm/m^2.day.atm$ and low water vapour barriers have a permeability of higher than 10 $g.mm/m^2.day.atm$. The different needs of packaged food makes it necessary to know the O_2, CO_2 and WV permeability of the materials used as packaging. The concept permeability is further explained in chapter 2.

Table 1.1: Barrier requirements of packaging materials for different foods [8].

Food	Preservation time	Preservation temperature	O2	CO2	WV
Red meat	6 - 14 d	0 - 5 °C	High barrier	High barrier	(High barrier)
Other meat	1 d - 6 w	0 - 5 °C	High barrier	High barrier	(High barrier)
Fat fish	1 - 7 d	0 - 5 °C	High barrier	High barrier	Low barrier
Low fat fish	1 - 7 d	0 - 5 °C	High barrier	High barrier	Low barrier
Fermented milk	16 -18 d	2 - 5°C	High barrier	High barrier	High barrier
Fresh cheese	1 - 8 w	< 5 °C	High barrier	High barrier	High barrier
Fresh pasta	4w	2 - 5 °C	High barrier	High barrier	(High barrier)
Dried pasta	1 - 6 md	room temp.	/	/	High barrier
Most vegetables	1 w	0 - 25 °C	High barrier	High barrier	High barrier
Most fruits	1 w	0 - 18 °C	High barrier	High barrier	High barrier
Flour	3 yr	2 °C - room temp.	/	/	High barrier
Breakfast cereals	1 yr	room temp.	High barrier	Low barrier	High barrier

1.2 Plastic food packaging

Many different packaging materials are used in the food industry, such as paper, board, glass and metal. In Western Europe up to 50% of the products are packed in plastic [9], this because of among others the lightweight of plastics and their capacity to be shaped in many different forms. Yearly 45.9 Mt plastic is produced in Europe alone. 39.4% of the total plastics demand comes from packaging applications [10]. The most commonly used plastics for packaging application are polyethylene terephthalate (PET), high density polyethylene (HDPE), low density polyethylene (LDPE), polypropylene (PP), polyamide (PA) and polyvinyl chloride (PVC) [11]. Each plastic has its own properties, depending on these properties they are used for different purposes. For instance PET has excellent water barrier properties and is widely used in drink bottles. While PET is a transparent material, PE is more opaque and used for milk containers. PP on

the other hand has high strength properties and is used in bags. Polystyrene (PS) is heat-resistant and can be used for cups for warm drinks, such as coffee [12].

In spite of these great characteristics, plastics have several drawbacks. For the production of plastics, crude oil is used. The formation of crude oil takes millions of years. The remains of microscopic ocean plants and animals were buried in layers of sand and mud at the bottom of the sea. The layers turned into sedimentary rock and through high pressure and heat the remains were transformed into crude oil, a mixture of hydrocarbons, sulphur, nitrogen and oxygen compounds [13]. Crude oil has a finite supply. The limited amount of crude oil creates an unstable price market. Currently there is an ongoing inflation of the plastic prizes. In addition the energy needed for the production of plastic pellets and the breakdown of plastics release CO_2 and methane [14]. These greenhouse gases (GHG) contribute to global warming. Therefore in 1997 the Kyoto protocol was introduced. The protocol states that industrialised countries have to reduce their GHG emissions by at least 5% over the period 2008-2020 [15]. This means that also the emission of GHG through traditional plastic production needs to be reduced. Plastics are also non-biodegradable. In 2012 25.2 Mt of the 45.9 Mt produced plastic ended up as waste in Europe. Only 8% is recycled, the rest of the waste ends up in landfills and in the ocean, where it harms and kills sea life. To tackle this problem the European Parliament adopted the resolution to reach the zero plastics waste to landfills by 2020 [10]. Even though the amount of plastic waste decreased in the last five years, there is still a long way to go.

The oil shortage and the environmental problems ask for research into other possible solutions. Next to the further development of concepts for reusing and recycling plastics in a closed loop, bioplastics could be a solution.

1.3 Bioplastics

Bioplastics are biobased and/or biodegradable polymers. Biobased products are derived from biomass. The most used biomass for bioplastics are corn,

sugarcane and wood pulp [16]. The use of biomass has several advantages. Biomass can be grown in a year and can be first used for materials and afterwards for energy regeneration. GHG emission could be reduced for some materials. And most important it could be possible to abandon the crude oil route. The concern that bioplastics are obtained for edible materials that are in direct competition with food and animal feedstock, such as sugar and starch, led to research into non-edible biomass.

Biodegradability is a possible solution for the waste problems. Biodegradable polymers are converted into water, CO_2 and biomass by microorganisms available in the environment. Environmental conditions are of importance to the biodegradation process. Therefore in 2008, Belgium was the first European country to define the requirements for biodegradation. According to these requirements a material is called biodegradable if it degrades at room temperature (20 °C - 30 °C) for 90% over a period of 24 months or less [17].

As shown in figure 1.1, bioplastics can be divided into three categories. The first category are the materials that are biobased, but not biodegradable. Materials that are biodegradable but not biobased belong to the second category. The third and last category belongs to the group of materials that are both biobased and biodegradable.

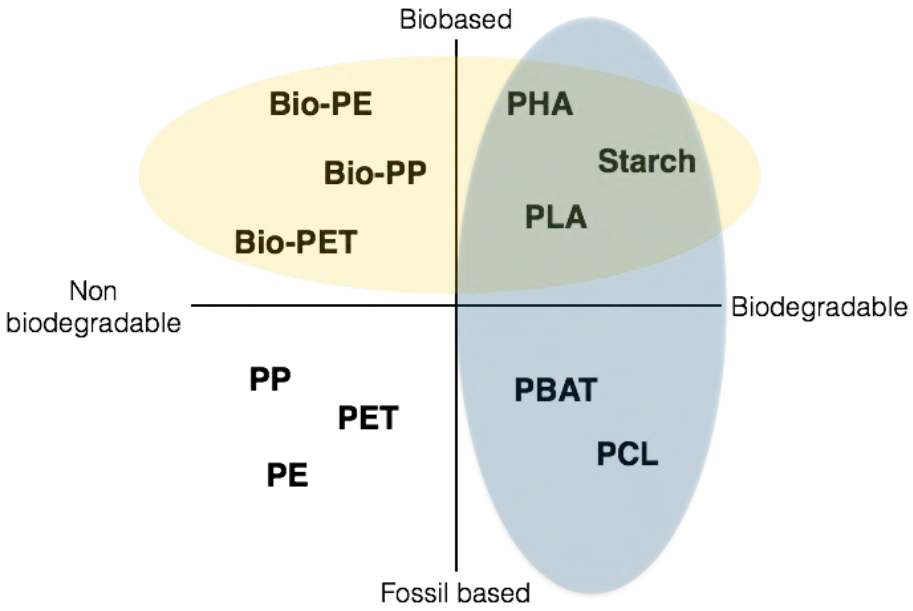

Figure 1.1: The 3 categories of bioplastics [18].

Currently, mostly biobased PE, PP and PET are used as alternative packaging materials. As indicated in table 1.2, biobased PE and PET can be used for bottles and biobased PP for closure of bottles and cups [19]. The reason why these materials are used the most is that they have almost the same properties as conventional PE and PET. However the disadvantage of these materials is that they are only biobased and not biodegradable [9].

Table 1.2: Use of biobased packaging material [19].

Type of packaging	Application	Material choice	Alternative material choice
Bottles	Carbonated Soft Drinks	PET	Bio-PET
Bottles, bricks	Still beverages	PET	Bio-PET, PLA
Bottles	Liquid dairy, personal care (shampoo, shower gel)	HDPE, PET	Bio-HDPE, Bio-PET
Cups	Semi-liquid dairy products (e.g. yoghurt)	PP, PS	PLA, BIO-PP
Closures	Beverages	PP	Bio-PP

From the materials that are both biodegradable and biobased, polylactic acid (PLA) has the highest production capacity. Of the 1.4 Mt bioplastics that were produced in 2012, 13.4 % consisted of PLA [20]. However, PLA has some drawbacks. The thermal instability limits the processability of PLA and the brittleness of PLA causes food packaging to break at very little deformation and limits the use as flexible packaging material [2]. Therefore Polyhydroxyalkanoate (PHA) can be considered as a possible alternative for PLA.

In 2012 2.4 % of the produced bioplastics were PHA's [20]. PHA 's are biopolyesters and are obtained by microbial production. Various types of PHA's can be formed depending on the type carbon sources. Both homopolymers and copolymers can be synthesized [21]. Polyhydroxybutyrate (PHB) was one of the first PHA's researched. PHB is a semi-crystalline polymer and has a melting point

of approximately 180 °C [22]. PHB has several interesting properties, such as water resistant, insoluble in water and has similar tensile strength and elasticity properties as PP [22]. However, PHB is brittle and difficult to process. To solve this problem PHB can be blended with other polymers, such as polybutylene adipate-co-terephthalate (PBAT) and polyethylene oxide (PEO). Another possibility is the use of the copolymer poly(3-hydroxybutyrate-co-hydroxyvalerate) (PHBV) [22-25].

PHBV is more flexible than PHB, has a higher impact resistance and an improved processability. As can be seen in table 1.3, the melting temperature decreases with increasing hydroxyvalerate (HV) concentration [26].

Table 1.3: Physical properties of different composition of PHBV [26].

%HV	Melting point (°C)	Glass transition temperature (°C)	Young's Modulus (GPa)	Tensile Strength (MPa)
0	179	10	3.5	40
3	170	8	2.9	38
9	162	6	1.9	37
14	150	4	1.5	35
20	145	-1	1.2	32
25	137	-6	0.7	30

The brittleness of the polymers decreases with increasing amount of HV, as is shown in table 1.3, through the decreasing glass transition temperatures. This allows use at lower temperatures. The decrease in elastic modulus indicates the improving flexibility of PHBV with a higher HV concentration. The melting point of PHBV decreases with increasing %HV, while the processing window is widened [26]. The crystallinity increases slightly with increasing %HV. The

chemical and mechanical properties of PHBV are comparable with the properties of PP. PHBV and PP have similar melting temperature, crystallinity and tensile strength properties. Therefore PHBV is a possible substitute for PP [27].

As will be discussed in chapter 2, PHBV has P_{O2} of 5 cc.mm/m^2.day.atm and higher. As can be seen in table 1.1, most food products require packaging material with a P_{O2} lower than 1 cc.mm/m^2.day.atm. Therefore, it is necessary to improve the O_2 barrier properties of PHBV. Moreover, literature reports on the CO_2 permeability of PHBV are limited. Consequently, more research into the CO_2 barrier of PHBV is necessary.

1.4 Methods to improve the gas barrier properties of plastics

There are different ways to improve the barrier properties of plastics. Thicker plastic films can be used. However, this limits the range of applications and increases the costs [28]. Therefore, one of the most used methods to improve the barrier properties is the addition of barrier material to the polymer. One can add barrier layers to the polymer or one can mix barrier material into the polymer matrix [3].

One of the most used barrier layer in the packaging industry is aluminium. Aluminium is impermeable to light, gasses and moisture. Sheets of a few micrometers thick can be laminated to a plastic film or a layer of a few nanometers thick can be vacuum-deposited on the plastic, metallized film. A standard aluminium sheets of 25 µm provides almost a total oxygen barrier of 0.2 cc.mm/m^2.day.atm or less [29]. However, the main disadvantage of laminating aluminium is the high cost [30]. Metallizing plastic can lower the cost [29], but also reduces the effectiveness of aluminium as barrier material [31]. Other disadvantages of aluminium are that aluminium reacts with acidic food and that it takes a lot of energy to produce aluminium [29]. Although transparency is a quality that is required for several food applications, sheets of aluminium are non-transparent and metallized plastics have a reduced transparency [32].

Another way to create a barrier layer is through lamination or co-extrusion of plastics with high barrier polymers. Examples of these high barrier polymers are poly(vinylidene chloride) (PVDC), ethylene vinyl alcohol (EVOH), poly(vinyl alcohol) (PVOH) and PA. These polymers display good oxygen barrier characteristics in dry conditions. This means that they have to be sandwiched between good water vapour barrier layers, increasing the cost of the package. Co-extrusion of these polymers shows the same limitation. Packaging manufactures are limiting the amount of PVDC used in packaging since burning waste with PVDC can lead to formation of dioxins [29, 33, 34].

Mixing a high barrier material into the polymer matrix can also increase the barrier properties. This method is called blending. Mostly a small amount of a barrier polymer is mixed into the polymer matrix of a more common polymer [35, 36]. However more recently inorganic nanoparticles are mixed into the polymer matrix. Polymers with nanoparticles in the matrix are a kind of nanocomposites. Adding inorganic nanoparticles to a polymer can improve the barrier properties of a polymer because of two reasons. The first reason is that inorganic particles are impermeable and replace permeable polymer. The second reason is the increase in tortuous path. The permeant has to travel around the impermeable inorganic nanoparticles [37, 38]. Nielsen was the first to develop a model to calculate the tortuous path [39]:

$$\frac{P_{comp}}{P_{poly}} = \frac{1-\varphi_{np}}{1+a\varphi_{np}} \quad (1.1)$$

Where P_{comp} is the permeability of the composite, P_{poly} the permeability of the polymer without nanoparticles, a the aspect ratio and φ_{np} the volume fraction of the nanoparticle.

Nielsen's model shows that the tortuous path is determined by the aspect ratio of the nanoparticles [29]. Two-dimensional (2D) nanoplates, such as clays, have a higher aspect ratio than zero-dimensional (0) nanoparticles and one-dimensional (1D) nanorods or nanotubes. Through the use of nanoplates an improvement of the barrier properties of the order of 50 or higher can be obtained [29]. However, the Nielsen model is only applicable for loading

percentages lower than 10 %. Higher loading percentages will cause particle agglomeration [40].

Besides the aspect ratio, the extent of dispersion of the nanoparticles in the polymer matrix determines the decrease in permeability. When there is a maximum degree of dispersion, an exfoliated morphology, the permeability is solely dependent on the aspect ratio and will decrease significantly [41]. The extent of dispersion depends on the compatibility between the polymer and the nanoparticles. Weak interaction between polymer and nanoparticles will lead to agglomeration and thus a low degree of dispersion [42]. The agglomeration of the nanoparticles is the result of a combination of van der Waals attraction force and Brownian motion between the nanoparticles. This problem has occurred when combining non-polar polymers, such as PE, with polar nanostructures, such as montmorillonite (MMT) [43].

MMT is one of the most commonly used organophilic-layered silicates for improving the gas barrier of polymers. PE, PA, PVC and PLA are only a few of the polymers used in combination with MMT [43-46]. The use of nanoclays can reduce the gas permeability up to 75% [47, 48]. Sanchez-Garcia reported that PHBV/mica (5%wt) nanocomposites reduce the oxygen and water vapour permeability with 32% and 75%, respectively. For PHBV/mica (10%) the oxygen permeability increased and the water vapour permeability decreased with only 47% [49]. More recently Corêa reported a 12% reduction in oxygen permeability for PHBV/Cloisite 30B nanocomposites [50]. Other inorganic materials that are used to decrease permeability in polymers are carbon nanotubes (CNT) and magnesium oxide (MgO), zirconium oxide (ZrO_2), titanium dioxide (TiO_2), silicon dioxide (SiO_2) and Zinc oxide (ZnO) nanoparticles [37, 40, 51, 52]. SiO_2, TiO_2, MgO and ZnO are also studied for their UV blocking abilities and more recently antimicrobial properties of ZnO, TiO_2 and MgO are studied [53]. Because of the additional antimicrobial properties of ZnO, ZnO can be considered interesting for food packaging applications. The literature found on the influence of ZnO on the permeability of PHBV is even more limited than the literature on nanoclays and PHBV. Diez-Pascual reported that PHBV/ZnO nanocomposites reduce the oxygen and water vapour permeability with 35%

and 69%, respectively [54]. Although the information on PHBV/ZnO nanocomposites is limited, ZnO nanocomposites have been proven to increase the oxygen barrier of polymers such as PE, PP and PET and prolong shelf life of products such as fresh orange juice [37, 55-57].

Given inorganic material is almost impermeable to gasses, a more effective way to reduce the permeability of a plastic is to deposit a coating of inorganic nanoparticles. As will be further discussed in chapter 2, a layer of only a few ten to hundred nanometers can provide high barrier properties [58]. The most frequently used coatings for reducing the gas permeability in packaging material are silicon oxide (SiO_2) and aluminium oxide (Al_2O_3). The coatings are mostly between 10 and 100 nm thick and can be deposited using different techniques. The influence of inorganic coatings on bioplastics has only been investigated recently. However, a combination of PLA and SiO_2 has been proven successful in extending the shelf life of packed goods [59]. A SiO_2 coating can reduce the oxygen permeability with one magnitude [60]. Deposition of an Al_2O_3 coating on top of the PLA surface can reduce the permeability with a magnitude of 2 [61].

As discussed, ZnO can be considered as a worthy substitute for SiO_2 and Al_2O_3. Currently ZnO nanolayers are mainly used in the steel industry for protection against corrosion [62]. However, a ZnO of 50 nm deposited on the surface of Polyethylene naphthalate (PEN) decreases the oxygen permeability with one magnitude [63]. ZnO coatings are also used for the protection of PEN against ultra violet (UV) light [63, 64]. In addition to the use of ZnO as photo-protector, ZnO is also used for its photo-catalytic effect [65-67]. Literature does not give a clear indication when using a ZnO coating leads to photo-protection and when ZnO causes degradation.

The effect of ZnO nanolayers on the permeability of PHBV hasn't been reported before. Therefore, it is interesting to study this effect. As discussed, ZnO also has UV protection properties. Even though the reports on the influence of UV light on PHBV are limited, it can be assumed that exposure of PHBV to UV light can lead to changes in the chemical composition of PHBV. Therefore, next to the

permeability properties, it is interesting to study the influence of UV light on PHBV and PHBV with ZnO nanolayer.

1.5 Zinc Oxide (ZnO)

ZnO crystallizes preferably in the hexagonal (c = 0.512 nm and a = 0.325 nm) wurtzite structure (Fig. 1.2). The wurtzite structure consists of alternating planes composed of tetrahedral coordinated Zn^{2+} (yellow) and O^{2-} (grey) ions, stacked along the c-axis [68]. ZnO oxide can also crystallize as zinc blend or cubic rocksalt. However ZnO only exists in the rocksalt structure at pressures around 9 GPa and zinc blende structures are only formed when they are grown on cubic substrates [69].

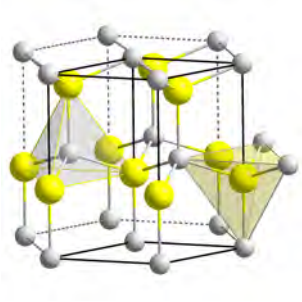

Figure 1.2: The wurtzite structure [70].

ZnO is an n-type semiconductor with an excess of Zn^{2+} and O^{2-} vacancies. This non-stoichiometric form of ZnO makes it possible to adsorb O_2. This process is called chemisorption [71]. The wide band gap of ZnO (3.37 eV) makes ZnO transparent and colorless to visible light, but not for Ultra Violet (UV) light. ZnO thin films are capable of absorbing UV radiation up to 380 nm [72]. The low transmission in the UV range makes ZnO an ideal photo-protector.

ZnO also has photo-catalytic properties. Irradiation of ZnO with UV light causes ZnO to excite an electron from the valence band to the conduction band forming a hole in the valence band. The formed electron / hole pair can directly react with other molecules to form radicals. These radicals may promote the oxidation

of organic components and thus cause degradation of these components [65-67].

ZnO exhibits also antibacterial activity. The underlying process of the antibacterial activity is not clear yet. However, it is suggested that the induction of intercellular reactive oxygen species, including hydrogen peroxide (H_2O_2), a strong oxidizing agent is harmful to bacterial cells. ZnO can be activated by UV and visible light and generate H_2O_2 [73, 74]. Smaller particles, such as nanoparticles, have high surface-to-volume ratio and allow better interaction with the bacteria. Therefore ZnO nanoparticles have a more pronounced antibacterial effect [75].

Other interesting properties of ZnO are the thermal properties such as high heat capacity and good thermal conductivity [76]. The wurtzite structure of ZnO exhibits piezoelectric properties [77].

Another advantage is that ZnO is listed by the Food & Drug Administration (FDA) as "a generally recognized as safe" (GRAS) material [78] and is found in many daily life applications such as in drug delivery, cosmetics and medical devices [57].

Though most importantly, ZnO can be synthesized into many shapes, such as nanorods, nanowires, etc. [72, 76, 79-87], and has a low cost.

1.6 ZnO thin layer deposition

There are many different ways to deposit ZnO nanolayers. One can use a chemical deposition technique, such as chemical vapour deposition (CVD), atomic layer deposition (ALD), sol gel deposition and chemical bath deposition (CBD) or a physical deposition technique, such as sputtering.

1.6.1 Chemical vapour deposition (CVD)

CVD is one of the most used techniques to deposit thin layers. It is a process in which one or more chemical precursors are vaporised and react and/or decompose on the heated substrate surface. The advantages of this technique

are high growth rates and good reproducibility. A disadvantage for ZnO deposition with this technique is the high substrate temperature, mostly above 500 °C [88, 89]. As can be seen in table 1.3, PHBV has a melting temperature between 130 °C and 180 °C and can not handle such high substrate temperature. Although there are chemical vapour deposition techniques that have lower substrate temperatures, such as metal organic CVD (MOCVD), the minimum substrate temperature found for ZnO deposition is between 100°C and 150°C [90, 91] and temperatures below 100 °C are necessary to deposit ZnO films on the surface of PHBV substrates.

1.6.2 Atomic layer deposition (ALD)

The principal of ALD is similar to CVD. First the surface is exposed to a first precursor. Chemisorption of the first precursor on the substrate surface occurs. The excess precursor is purged away. Then adsorption of the second precursor occurs. The two precursors react at the substrate surface and excess of the second precursor and the reaction by-products are purged of. By repeating these steps a film is formed [92]. For the formation of ZnO layers different precursors can be used. Zinc acetate and water were the first precursors ever used for ALD. For the reaction between zinc acetate and water to occur, deposition temperatures of 280°C or higher are required [92, 93]. However, the most common used Zn precursor is diethyl zinc. Typical reactions between these precursors occur in a temperature range of 100-200°C, but there are also reports of deposition at 60°C [94, 95]. The disadvantage of this technique is that it is very expensive and has a slower deposition rate [96].

1.6.3 Solution-based deposition

Solution-based deposition techniques, such as chemical bath deposition (CBD) and sol gel deposition, have an easy setup and are less expensive alternatives for the previous techniques. Simple metal salts, solvents and deposition techniques are used. During chemical bath deposition, substrates are placed in a precursor solution for a certain period in time. Through heterogeneous nucleation, a dense layer of a metal oxide can be deposited on a substrate surface. ZnO layers can be grown at temperatures between 60°C and 95°C [97,

98]. The deposition of ZnO through chemical bath deposition on conventional plastics, such as PET and PEN, occurs at temperatures between 90-200°C [99]. To promote the formation of ZnO a combination of sol-gel and chemical bath deposition is often used [100]. The sol-gel method consists of a sol phase followed by a gel phase. The sol phase consist of solid nanoparticles dispersed in a liquid. These nanoparticles agglomerate to form a network in the liquid, called the gel. To remove the liquid the gels are heated. The sol can be deposited on the substrate by means of spraying, spinning or dipping. The advantage of these techniques is that one can control the morphology of the ZnO. This can be interesting since for nanocomposites, nanoparticles with a higher aspect ratio, such as platelets, provide better barrier properties [40]. The formation of the nanolayer is dependent on several parameters. Duration of the process, pH, temperature, concentration of the solution, the reagents used and the surface roughness of the substrate will influence the layer. The influence of these parameters differs for different substrate materials. This will be discussed further in chapter 3.

Since there are no reports on the deposition of ZnO on PHBV or other bioplastics substrates, the deposition of ZnO on PHBV substrates will provide an important contribution. However, different parameters are used for different substrates and the parameters of known combination methods of sol-gel and chemical bath deposition will have to be adjusted. Therefore, it will be a challenge to deposit fully-grown ZnO nanolayers on top of PHBV substrates.

1.6.4 Sputtering

Sputtering is a process in which material particles are emitted from a solid target material by bombarding with energetic ions. The particles are then deposited on the material. Important for this technique is that there is the possibility to keep the substrate temperature below 60 °C, so that PHBV will undergo no thermal change. For the deposition of ZnO, the substrate temperatures are in the range of 50°C - 150°C [101, 102]. Other advantages are good adhesion of the coated layer on the substrate, broader coverage and increased film density [63]. The quality of the film is strongly dependent on the

sputter conditions, such as radio frequency (RF) power, the sputtering pressure and the distance between target and substrate. The required values of these parameters vary from substrate to substrate. When using this technique the most efficient value for each parameter should be found. The disadvantages for this process are the expensive sputtering targets, between 200 and 300 € for a ZnO sputtering target with a thickness of 3 mm and a diameter of 25 mm, formation of heat that needs to be removed and in reactive sputtering the gas composition needs to be controlled to prevent poisoning the sputter target [103].

1.7 Outline of the thesis

This thesis is divided into 7 chapters.

As shown in previous paragraphs a general introduction is given in chapter 1. The necessity of substituting plastics by a more environmental friendly solution is shown. Bioplastics are being suggested to be a suitable alternative. For this research the biobased and biodegradable bioplastic PHBV was used. As mentioned before, the gas permeability properties of this biopolymer are not suitable for high barrier packaging applications. Therefore, a ZnO nanolayer was added to PHBV to improve the barrier properties of this material. The theory of permeability is discussed in chapter 2 and the theory of sol gel and chemical bath deposition is discussed in chapter 3.

My first aim was to deposit a uniform ZnO nanolayer on top of PHBV. A combination of the sol gel and chemical bath method was used. To form a uniform layer, different parameters were investigated. Different reagents and different molar fractions were used. The necessity of a seed layer was researched. Also the influence of temperature of the deposition process was investigated. The influence of these parameters on the deposition of ZnO on PHBV was compared to the influence of these parameters on the deposition of ZnO on PET. The difference between a sputtered layer and a layer formed through the combination of the sol gel and chemical bath method was studied. The outcome of this research will be reported in chapter 4.

The second goal was to improve the O_2, CO_2 and WV barrier properties through the application of a ZnO nanolayer. In chapter 5 the research into the barrier properties of PHBV and PET is reported. The influence of ZnO on these properties is discussed.

The last goal was to research the influence of UV radiation on PHBV and PHBV with ZnO. The outcome of this research is discussed in chapter 6.

The conclusions of the research are given in chapter 7, together with an outlook towards further research.

1.8 References

1. Han, J.H., *Innovations in Food Packaging*. 2005, Academic Press.
2. Robertson, G.L., *Food Packaging Principles and Practice*. 3rd ed. 2013, Florida: CRC Press.
3. Ebnesajjad, S., *Plastic Films in Food Packaging: Materials, Technology and Applications*. 2012: William Andrew.
4. Richard Coles, M.J.K., *Food and Beverage Packaging Technology*. 2011: John Wiley & Sons.
5. Vitti, M.C.D., et al., *Activity of Enzymes Associated with the Enzymatic Browning of Minimally Processed Potatoes.* Brazilian Archives of Biology and Technology, 2011. **54**(5): p. 983-990.
6. Déak, T., *Handbook of Food Spoilage Yeasts*. 2nd ed. 2008, Florida: CRC.
7. Knechtges, P.L., *Food Safety: Theory and Practice*. 2012, London: Jones & Bartlett Learning.
8. Petersen, K., et al., *Potential of biobased materials for food packaging.* Trends in Food Science & Technology, 1999. **10**(2): p. 52-68.
9. *Bioplastics packaging - Combining performance with sustainability*. 2014 January 2014 [cited 2014 22 July]; Available from: http://en.european-bioplastics.org/wp-content/uploads/2011/04/fs/Packaging_eng.pdf.
10. PlasticsEurope, *Plastics - the Facts 2013*, 2013.
11. Makers, A.P. http://www.plasticpackagingfacts.org/Plastic-Packaging. 2011-2014 [cited 2014 20 August].
12. Otto G. Piringer, A.L.B., *Plastic Packaging Materials for Food: Barrier Function, Mass Transport, Quality Assurance, and Legislation*. 2008: John Wiley & Sons.
13. Spilsbury, R., L. Spilsbury, *The oil industry*. Development or destruction? 2012, New York: The Rosen Publishing Group.

14. Tucker, N.M.j., *Low Environmental Impact Polymers*. 2004, Shawbury: rapra technology.

15. *Tackling climate change*. 04.04.2011 [cited 2014 23 July]; Available from: http://europa.eu/legislation_summaries/environment/tackling_climate_change/l28060_en.htm.

16. Bioplastics, E. *What are bioplastics?* 2014 [cited 2014 23 July]; Available from: http://en.european-bioplastics.org/wp-content/uploads/2011/04/fs/Bioplastics_eng.pdf.

17. *Koninklijk besluit houdende vaststelling van productnormen voor composteerbare en biologisch afbreekbare materialen.* 2008 [cited 2014 23 July]; Available from: http://www.ejustice.just.fgov.be/cgi_loi/change_lg.pl?language=nl&la=N&table_name=wet&cn=2008090947.

18. Bioplastics, E. *Faq bioplastics*. 2014 [cited 2014 14 September]; Available from: http://en.european-bioplastics.org/technologymaterials/materials/.

19. Bioplastics, E. *Benefits of Biobased Rigid Packaging*. Fact Sheets 2013 [cited 2014 23 July]; Available from: http://en.european-bioplastics.org/wp-content/uploads/2013/publications/EuBP_FS_Rigid Packaing_March2013.pdf.

20. bioplastics, E. *Materials*. 2014 [cited 2014 23 July]; Available from: http://en.european-bioplastics.org/technologymaterials/materials/.

21. Bastioli, C., *Handbook of Biodegradable Polymers*. 2005, Shawbury: Rapra Technology Limited.

22. Bucci, D.Z., L.B.B. Tavares, and I. Sell, *PHB packaging for the storage of food products.* Polymer Testing, 2005. **24**(5): p. 564-571.

23. Reis, K.C., et al., *Characterization of polyhydroxybutyrate-hydroxyvalerate (PHB-HV)/maize starch blend films.* Journal of Food Engineering, 2008. **89**(4): p. 361-369.

24. Luzier, W.D., *Materials Derived from Biomass Biodegradable Materials.* Proceedings of the National Academy of Sciences of the United States of America, 1992. **89**(3): p. 839-842.

25. Miao, L.Q., et al., *Fully biodegradable poly(3-hydroxybutyrate-co-hydroxyvalerate)/poly(ethylene succinate) blends: Phase behavior, crystallization and mechanical properties.* Reactive & Functional Polymers, 2008. **68**(2): p. 446-457.

26. Kaplan, D., *Biopolymers from Renewable Resources*. 1998, Berlin: Springer.

27. Pilla, S., *Handbook of Bioplastics and Biocomposites Engineering Applications*. 2011, Hoboken: John Wiley & Sons.

28. Massey, L.K., *Permeability Properties of Plastics and Elastomers*. Vol. William Andrew Publishing. 2003, USA.

29. Lange, J. and Y. Wyser, *Recent innovations in barrier technologies for plastic packaging - a review.* Packaging Technology and Science, 2003. **16**(4): p. 149-158.

30. Marsh, K. and B. Bugusu, *Food packaging - Roles, materials, and environmental issues.* Journal of Food Science, 2007. **72**(3): p. R39-R55.

31. Garnier, G., et al., *Influence of Structural Feature of Aluminum Coatings on Mechanical and Water Barrier Properties of Metallized PET Films.* Journal of Applied Polymer Science, 2010. **115**(5): p. 3110-3119.

32. Niaounakis, M., *Biopolymers: Processing and Products*. 2015, Oxford, UK: William Andrew Publications.

33. Siracusa, V., *Food Packaging Permeability Behaviour: A Report.* International Journal of Polymer Science, 2012.

34. Mueller K. , C.S., H.-C. Langowski, *Thin Laminate Films for Barrier Packaging Application – Influence of Down Gauging and Substrate Surface Properties on the Permeation Properties.* Packaging Technology and Science, 2011. **25**(3): p. 137-148.

35. De Petris, S.P.L.M.M.M.P.M.Z., *Study of blends of nylon 6 with EVOH and carboxyl-modified EVOH and a preliminary approach to films for packaging applications.* Journal of Applied Polymer Science, 1998. **68**: p. 637-648.

36. Nir Y, N.M., Siegmann A., *Permeation through strongly interacting polymer blends: EVOH/ Copolyamide-6/6.9. .* Polymer Networks Blends 1997. **7**.

37. Lepot, N., et al., *Influence of Incorporation of ZnO Nanoparticles and Biaxial Orientation on Mechanical and Oxygen Barrier Properties of Polypropylene Films for Food Packaging Applications.* Journal of Applied Polymer Science, 2011. **120**(3): p. 1616-1623.

38. Suprakas, S.R., *Clay-Containing Polymer Nanocomposites: From Fundamentals to Real Applications*. 2013, Amsterdam: Elsevier.

39. Nielsen, L.E., *Models for the Permeability of Filled Polymer Systems.* Journal of Macromolecular Science: Part A - Chemistry, 1967. **1**(5): p. 929-949.

40. Duncan, T.V., *Applications of nanotechnology in food packaging and food safety: Barrier materials, antimicrobials and sensors.* Journal of Colloid and Interface Science, 2011. **363**(1): p. 1-24.

41. Maiti, P., et al., *New polylactide/layered silicate nanocomposites: Role of organoclays.* Chemistry of Materials, 2002. **14**(11): p. 4654-4661.

42. Alateyah, A.I., H.N. Dhakal, and Z.Y. Zhang, *Processing, Properties, and Applications of Polymer Nanocomposites Based on Layer Silicates: A Review.* Advances in Polymer Technology, 2013. **32**(4).

43. Dadbin, S., M. Noferesti, and M. Frounchi, *Oxygen Barrier LDPE/LLDPE/Organoclay Nano-Composite Films for Food Packaging.* Macromolecular Symposia, 2008. **274**: p. 22-27.

44. Russo, G.M., G.P. Simon, and L. Incarnato, *Correlation between rheological, mechanical, and barrier properties in new copolyamide-*

based nanocomposite films. Macromolecules, 2006. **39**(11): p. 3855-3864.

45. Kalendova, A., et al., *Polymer/clay nanocomposites and their gas barrier properties.* Polymer Composites, 2013. **34**(9): p. 1418-1424.

46. Picard, E., E. Espuche, and R. Fulchiron, *Effect of an organo-modified montmorillonite on PLA crystallization and gas barrier properties.* Applied Clay Science, 2011. **53**(1): p. 58-65.

47. Cava, D., et al., *Comparative performance and barrier properties of biodegradable thermoplastics and nanobiocomposites versus PET for food packaging applications.* Journal Of Plastic Film & Sheeting, 2006. **22**(4): p. 265-274.

48. Sanchez-Garcia, M.D., E. Gimenez, and J.M. Lagaron, *Novel pet nanocomposites of interest in food packaging applications and comparative barrier performance with biopolyester nanocomposites.* Journal of Plastic Film & Sheeting, 2007. **23**(2): p. 133-148.

49. Sanchez-Garcia, M.D. and J.M. Lagaron, *Novel Clay-Based Nanobiocomposites of Biopolyesters with Synergistic Barrier to UV Light, Gas, and Vapour.* Journal of Applied Polymer Science, 2010. **118**(1): p. 188-199.

50. Correa, M.C.S., et al., *Elaboration and Characterization of Nano-Biocomposites Based on Plasticized Poly(Hydroxybutyrate-Co-Hydroxyvalerate) with Organo-Modified Montmorillonite.* Journal of Polymers and the Environment, 2012. **20**(2): p. 283-290.

51. Sanuja, S., A. Agalya, and M.J. Umapathy, *Studies on Magnesium Oxide Reinforced Chitosan Bionanocomposite Incorporated with Clove Oil for Active Food Packaging Application.* International Journal of Polymeric Materials and Polymeric Biomaterials, 2014. **63**(14): p. 733-740.

52. Pradhan, G.C., S. Dash, and S.K. Swain, *Effect of zirconium oxide nanopowder on the thermal, chemical and gas barrier properties of starch.* Materials Science in Semiconductor Processing, 2014. **23**: p. 115-121.

53. Rhim, J.W., H.M. Park, and C.S. Ha, *Bio-nanocomposites for food packaging applications.* Progress in Polymer Science, 2013. **38**(10-11): p. 1629-1652.

54. Diez-Pascual, A.M. and A.L. Diez-Vicente, *ZnO-Reinforced Poly(3-hydroxybutyrate-co-3-hydroxyvalerate) Bionanocomposites with Antimicrobial Function for Food Packaging*. Acs Applied Materials & Interfaces, 2014. **6**(12): p. 9822-9834.

55. Llorens, A., et al., *Metallic-based micro and nanocomposites in food contact materials and active food packaging.* Trends in Food Science & Technology, 2012. **24**(1): p. 19-29.

56. Elen, K., et al., *Towards high-performance biopackaging: barrier and mechanical properties of dual-action polycaprolactone/zinc oxide nanocomposites.* Polymers for Advanced Technologies, 2012. **23**(10): p. 1422-1428.

57. Emamifar, A., et al., *Evaluation of nanocomposite packaging containing Ag and ZnO on shelf life of fresh orange juice.* Innovative Food Science & Emerging Technologies, 2010. **11**(4): p. 742-748.

58. Hanika, M., et al., *Inorganic layers on polymeric films - Influence of defects and morphology on barrier properties.* Chemical Engineering & Technology, 2003. **26**(5): p. 605-614.

59. Lija Dukalska, S.M.-B., Irisa Murniece, Ilona Dabina-Bicka, Emils Kozlinskis, and S. Sarvi, *Influence of PLA Film Packaging on the Shelf*

Life of Soft Cheese Kleo. World Academy of Science, Engineering and Technology, 2011. **5**(8).

60. Zhang, X.L., et al., *Plasma Enhanced Chemical Vapor Deposition of SiO(x) Layer on the Surface of the Poly lactic Acid(PLA) Film and Its Barrier Performance.* Thirteenth National Conference on Packaging Engineering, Tncpe 13, 2010: p. 158-162.

61. Hirvikorpi, T., et al., *Thin Al2O3 barrier coatings onto temperature-sensitive packaging materials by atomic layer deposition.* Surface & Coatings Technology, 2011. **205**(21-22): p. 5088-5092.

62. Hosseini, M.G., R. Bagheri, and R. Najjar, *Electropolymerization of Polypyrrole and Polypyrrole-ZnO Nanocomposites on Mild Steel and Its Corrosion Protection Performance.* Journal of Applied Polymer Science, 2011. **121**(6): p. 3159-3166.

63. Guedri, B., et al., *Lifetime improvement of poly(ethylene naphthalate) by ZnO adhesive coatings.* Polymer Degradation and Stability, 2005. **88**(2): p. 199-205.

64. Guedri-Knani, L., et al., *Photoprotection of poly(ethylene-naphthalate) by zinc oxide coating.* Surface & Coatings Technology, 2004. **180**: p. 71-75.

65. Peternel, I.T., et al., *Comparative study of UV/TiO2, UV/ZnO and photo-Fenton processes for the organic reactive dye degradation in aqueous solution.* Journal of Hazardous Materials, 2007. **148**(1-2): p. 477-484.

66. Chakrabarti, S., et al., *Degradation mechanism and kinetic model for photocatalytic oxidation of PVC-ZnO composite film in presence of a sensitizing dye and UV radiation.* Journal of Hazardous Materials, 2008. **154**(1-3): p. 230-236.

67. Parida, K.M. and S. Parija, *Photocatalytic degradation of phenol under solar radiation using microwave irradiated zinc oxide.* Solar Energy, 2006. **80**(8): p. 1048-1054.

68. Özgür, H.M.a.U.m., *Zinc Oxide: Fundamentals, Materials and Device Technology*. 2009, Weinheim: WILEY-VCH Verlag GmbH & Co.

69. B.S. Murty, P.S., Baldev Raj, B B Rath, James Murday, *Textbook of Nanoscience and Nanotechnology*. 2013: Springer.

70. State, S., http://commons.wikimedia.org/wiki/File%3AWurtzite_polyhedra.png.

71. Mitra, P. and A.K. Mukhopadhyay, *ZnO thin film as methane sensor.* Bulletin of the Polish Academy of Sciences-Technical Sciences, 2007. **55**(3): p. 281-285.

72. Xu, J.Q., et al., *Hydrothermal synthesis and gas sensing characters of ZnO nanorods.* Sensors and Actuators B-Chemical, 2006. **113**(1): p. 526-531.

73. Jones, N., et al., *Antibacterial activity of ZnO nanoparticle suspensions on a broad spectrum of microorganisms.* Fems Microbiology Letters, 2008. **279**(1): p. 71-76.

74. Sawai, J., *Quantitative evaluation of antibacterial activities of metallic oxide powders (ZnO, MgO and CaO) by conductimetric assay.* Journal of Microbiological Methods, 2003. **54**(2): p. 177-182.

75. Xie, Y.P., et al., *Antibacterial Activity and Mechanism of Action of Zinc Oxide Nanoparticles against Campylobacter jejuni.* Applied and Environmental Microbiology, 2011. **77**(7): p. 2325-2331.

76. Wang, J.M. and L. Gao, *Hydrothermal synthesis and photoluminescence properties of ZnO nanowires.* Solid State Communications, 2004. **132**(3-4): p. 269-271.

77. Yassitepe, E., et al., *Photocatalytic efficiency of ZnO plates in degradation of azo dye solutions.* Journal of Photochemistry and Photobiology a-Chemistry, 2008. **198**(1): p. 1-6.

78. FDA. *e-CFR PART 182—SUBSTANCES GENERALLY RECOGNIZED AS SAFE*. 2014 [cited 2014 January 9]; Available from: http://www.ecfr.gov/cgi-bin/text-idx?c=ecfr&sid=786bafc6f6343634fbf79fcdca7061e1&rgn=div5&view=text&node=21:3.0.1.1.13&idno=21 - 21:3.0.1.1.13.9.1.12.

79. Elen, K., et al., *Additive-free hydrothermal synthesis of high aspect ratio ZnO particles from aqueous solution.* Chemistry Letters, 2006. **35**(12): p. 1420-1421.

80. Lepot, N., et al., *Synthesis of ZnO nanorods from aqueous solution.* Materials Letters, 2007. **61**(13): p. 2624-2627.

81. Klaitabtim, D., S. Pratontep, and J. Nukeaw, *Effect of gas-timing technique on structure and optical properties of sputtered zinc oxide films.* Ceramics International, 2008. **34**(4): p. 1103-1107.

82. Klingshirn, C., *ZnO: Material, physics and applications.* Chemphyschem, 2007. **8**(6): p. 782-803.

83. Wang, C.L., et al., *Controllable synthesis of ZnO nanocrystals via a surfactant-assisted alcohol thermal process at a low temperature.* Materials Letters, 2005. **59**(23): p. 2867-2871.

84. Du, J.M., et al., *Control of ZnO morphologies via surfactants assisted route in the subcritical water.* Journal of Crystal Growth, 2005. **280**(1-2): p. 126-134.

85. Tao, D.L., et al., *A novel low-temperature method to grow single-crystal ZnO nanorods.* Journal of Crystal Growth, 2004. **271**(3-4): p. 353-357.

86. Bai, F.F., et al., *Size-controlled preparation of monodispersed ZnO nanorods.* Materials Letters, 2005. **59**(13): p. 1687-1690.

87. Wu, G.S., et al., *Controlled synthesis of ZnO nanowires or nanotubes via sol-gel template process.* Solid State Communications, 2005. **134**(7): p. 485-489.

88. Protasova, L.N., et al., *ZnO based nanowires grown by chemical vapour deposition for selective hydrogenation of acetylene alcohols.* Catalysis Science & Technology, 2011. **1**(5): p. 768-777.

89. Podrezova, L.V., et al., *Comparison between ZnO nanowires grown by chemical vapor deposition and hydrothermal synthesis.* Applied Physics a-Materials Science & Processing, 2013. **113**(3): p. 623-632.

90. Wenas, W.W., et al., *Textured Zno Thin-Films for Solar-Cells Grown by Metalorganic Chemical Vapor-Deposition.* Japanese Journal of Applied Physics Part 2-Letters, 1991. **30**(3B): p. L441-L443.

91. Kim, K.S., H.W. Kim, and C.M. Lee, *Effect of growth temperature on ZnO thin film deposited on SiO2 substrate.* Materials Science and Engineering B-Solid State Materials for Advanced Technology, 2003. **98**(2): p. 135-139.

92. Knisley, T.J., L.C. Kalutarage, and C.H. Winter, *Precursors and chemistry for the atomic layer deposition of metallic first row transition metal films.* Coordination Chemistry Reviews, 2013. **257**(23-24): p. 3222-3231.

93. Wojcik, A., et al., *Controlling of preferential growth mode of ZnO thin films grown by atomic layer deposition.* Journal of Crystal Growth, 2008. **310**(2): p. 284-289.

94. Szczepanik, A., et al., *ZnO nanostructures by Atomic Layer Deposition method.* Nano 2008: 2nd National Conference on Nanotechnology, 2009. **146**.

95. Ott, A.W. and R.P.H. Chang, *Atomic layer-controlled growth of transparent conducting ZnO on plastic substrates.* Materials Chemistry and Physics, 1999. **58**(2): p. 132-138.

96. Guziewicz, E., et al., *Extremely low temperature growth of ZnO by atomic layer deposition.* Journal of Applied Physics, 2008. **103**(3).

97. Li, Q.W., et al., *Controllable growth of well-aligned ZnO nanorod arrays by low-temperature wet chemical bath deposition method.* Applied Surface Science, 2010. **256**(6): p. 1698-1702.

98. Lockett, A.M., P.J. Thomas, and P. O'Brien, *Influence of Seeding Layers on the Morphology, Density, and Critical Dimensions of ZnO Nanostructures Grown by Chemical Bath Deposition.* Journal of Physical Chemistry C, 2012. **116**(14): p. 8089-8094.

99. Yi, S.H., et al., *Low-temperature growth of ZnO nanorods by chemical bath deposition.* Journal of Colloid and Interface Science, 2007. **313**(2): p. 705-710.

100. Jia, G.Z., Y.F. Wang, and J.H. Yao, *Fabrication and strain investigation of ZnO nanorods on Si composing sol-gel and chemical bath deposition method.* Journal of Physics and Chemistry of Solids, 2012. **73**(3): p. 495-498.

101. Rosa, A.M., et al., *Structural transition of ZnO thin films produced by RF magnetron sputtering at low temperatures.* Journal of Materials Science-Materials in Electronics, 2013. **24**(9): p. 3143-3148.

102. Peiris, T.A.N., et al., *Effect of ZnO seed layer thickness on hierarchical ZnO nanorod growth on flexible substrates for application in dye-sensitised solar cells.* Journal of Nanoparticle Research, 2013. **15**(12).

103. finishing, P. *Vacuum Deposition Processes*. 2014; Available from: http://www.pfonline.com/articles/vacuum-deposition-processes.

Chapter 2

Permeability theory

2.1 Diffusion-Solution model

As mentioned in previous chapter the barrier properties of packaging materials are important to maintain food quality. Because of their superior properties and low cost, polymers are commonly used as packaging material [1-3].

The permeation of gases and vapours through polymers consist of three processes (Fig. 2.1). First there is sorption, the permeating gas or vapour can be adsorbed or absorbed by the polymer. Then there is the diffusion through the polymer and finally there is desorption of the permeating gas or vapour from the polymer surface. Therefore the permeability of the polymer can be expressed as the permeability coefficient (*P*) [4]:

$$P = \frac{Qx}{At\Delta p} \tag{2.1}$$

Q is the total amount of permeant passing through a material with a thickness *x* and surface area *A* in time *t* and *Δp* is the change in permeant partial pressure across the film.

As will be proven in the following paragraphs, P can be defined as a product of the solubility coefficient (*S*) of a gas or vapour and the diffusion coefficient (*D)* through the polymer [6].

$$P = D.S \tag{2.2}$$

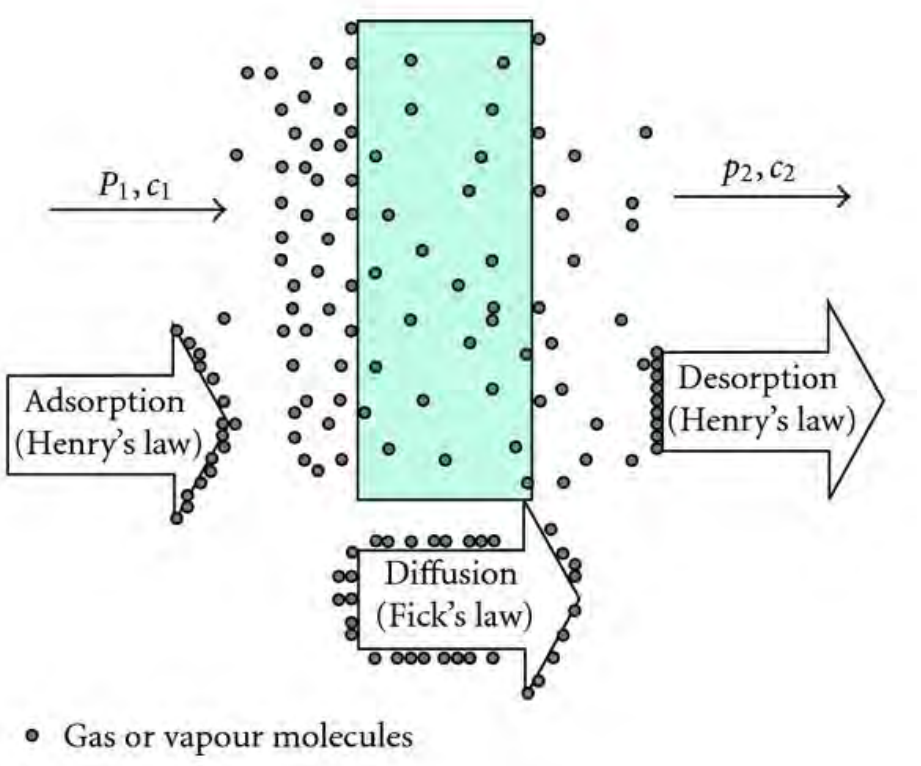

Figure 2.1: Permeation through a polymer [5].

2.1.1 Diffusion

Diffusion is the rate-limiting factor in permeability and can be described as the flow of molecules from a high concentration region to a low concentration region. One-dimensional penetrant diffusion through a polymer in steady-state can be expressed according to Fick's first law [6]:

$$J = \frac{Q}{At} = -D\frac{\delta C}{\delta x} \tag{2.3}$$

Where J is de diffusion flux. This is the amount of substance diffusing across (Q) per unit area (A) per unit time (t). D is the diffusion coefficient. C is the amount of substance per unit volume and x is the position (length) [7].

When the equilibrium of diffusion is reached, it is assumed that *J* is a constant. The integration of equation 2.3, where the diffusion coefficient is a constant, gives following equation:

$$J = \frac{Q}{At} = D\frac{(C_1 - C_2)}{x} \tag{2.4}$$

In non-steady state the diffusion can be described through Fick's second law of diffusion [6]:

$$\frac{\delta C}{\delta t} = D\left(\frac{\delta^2 C}{\delta x^2} + \frac{\delta^2 C}{\delta y^2} + \frac{\delta^2 C}{\delta z^2}\right) \tag{2.5}$$

If the diffusion occurs only in the x-direction, the equation can be simplified as follows [6]:

$$\frac{\delta C}{\delta t} = D\left(\frac{\delta^2 C}{\delta x^2}\right) \tag{2.6}$$

The diffusion coefficient in polymers is above all dependent on the concentration of the penetrant. Therefore, Fick's first law states that the volume (*V*) of the penetrant is directly proportional to the partial pressure differential (*p*). This is only the case for permanent gases that obey Henry's law, such as oxygen and carbon dioxide. Since readily soluble vapours, such as water vapour, do not obey Henry's law, Fick's first law is adjusted as follows [1]:

$$W = VTR.(A.t)/x \tag{2.7}$$

Where *VTR* is the vapour transmission rate and *W* is the weight of the penetrant.

2.1.2 Solubility

The sorption capacity of a polymer with respect to a particular permeant is indicated by solubility. At low concentrations the solubility (S) can be expressed as the volume of vapour per unit volume of polymer per unit of partial pressure by Henry's law [8, 9]:

$$C = S.p \tag{2.8}$$

Substitution of equation 2.8 in equation 2.4 gives:

$$\frac{Q}{At} = DS\frac{(p_1 - p_2)}{x} \tag{2.9}$$

Now equation 2.1 can be derived from equation 2.9 as follows:

$$P = DS = \frac{Qx}{At(p_1 - p_2)} \tag{2.10}$$

Therefore the permeability coefficient is equal to the product of the diffusion and the solubility coefficient.

2.2 Variables affecting permeability

The major factors influencing permeability can be divided into three categories: nature of the polymer, nature of the permeant and ambient conditions.

2.2.1 Nature of the polymer

The molecular structure of the polymer plays an important role in the permeability. Good O_2 and CO_2 barriers often are poor water vapour barriers. The polarity of the polymer is a good indication for the permeability of the polymer. For example, there are polymers containing hydroxyl groups. These polymers are highly polar and are excellent barriers to nonpolar permeants, such as O_2 and CO_2, and the worst barriers against polar permeant molecules, such as water vapour. In contrast, there are the hydrocarbon polymers. These polymers are nonpolar and are poor O_2 and CO_2 barriers and good water vapour barriers [6]. This is because the solubility coefficient of molecules with similar polarity is higher [10]. The effect of functional groups on the oxygen permeability (P_{O2}) is given in table 2.1. In some cases polymers containing polar groups can absorb moisture from the atmosphere. This causes the polymer to swell or plasticize, increasing diffusion rate of the permeant and thus increasing the permeability [6].

As shown in figure 2.2 PHBV is a copolymer formed by ester bounds. Esters are less polar than alcohols, but still more polar than ethers. As shown in table 2.1 ester groups lower the permeability, but they don't improve the barrier properties drastically.

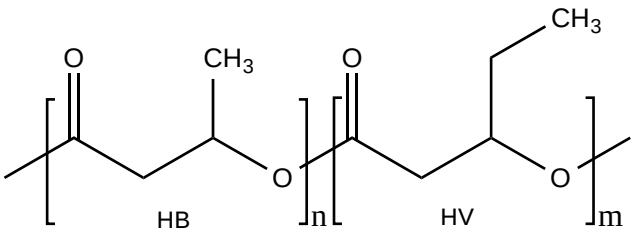

Figure 2.2: Chemical structure of PHBV.

As shown in table 2.2, linear polymers with a simple molecular structure have a lower permeability than polymers with bulky side groups. This is due to the close chain-to-chain packing in the polymer [6]. Bulky side groups can increase the free volume, increasing the diffusion of the permeant. The polarity of the side chains influences the solubility only slightly [11].

PHBV contains methyl and ethyl side groups, causing steric hindrance and decrease the packing ability. This causes the gas permeability to increase. A higher concentration of HV means a higher level of steric hindrances. The increase in permeability through increase of the percentage of HV is confirmed by literature [12-21]. PHB has a lower permeability than PHBV because PHB only consists out of methyl side groups. This is shown by Sanchez-Garcia, the P_{O2} of PHB at 24°C and 0% RH is 2.01 e^3 cc.mm/(m^2.day.atm) and the P_{O2} of PHBV is 1.41 e^4 cc.mm/(m^2.day.atm) [22].

Table 2.1: Effect of functional groups on oxygen permeability [23].

Nature of X in $-(-CH_2-CHX-)-_n$	P_{O2} (cc.mm/(m^2.day.atm))
-OH	0.004
-CN	0.016
-Cl	3.15
-F	5.90
$-COOCH_3$	6.69
$-CH_3$	59.1
$-C_6H_5$	165
-H	188

Table 2.2: Effect of side groups [6].

Polymer	Structure	Packing ability	P_{O2} (cc.mm/(m^2.day.atm)
HDPE	$-(-CH_2-CH_2-)-$	Good	43
PP	$-(-CH_2-CH(CH_3)-)-$	Fair, Hindrance of CH3 group	59
Poly-3-methyl butene-1	$-(-CH_2-CH(CH(CH_3)_2)-)-$	Poor, bulky side groups	1575

Polymers with close chain-to-chain packing are also most likely to have a higher degree of crystallinity. Generally, gas molecules are insoluble in crystallites and decrease the diffusion rate [24]. Therefore, high crystallinity leads to lower permeability [9].

PHBV is a semi-crystalline polymer, consisting of an impermeable crystalline phase and a permeable amorphous phase [25]. The amorphous phase can be divided in a mobile amorphous fraction (MAF) and a rigid amorphous fraction (RAF). The different solubility of MAF and RAF to gases and vapours helps determine the permeability [26]. Thus, the way PHBV is produced increases or decreases the permeability. A higher concentration of HV lowers the crystallinity of the polymer [27]. Thus, the permeability of PHBV is increased.

Another factor influencing the permeability is the molecular orientation. Increasing molecular orientation decreases the diffusion coefficient and thus the polymer's permeability. This effect is more pronounced for crystalline polymers than for amorphous polymers. In amorphous polymers the molecular orientation decreases the permeability with 10 to 15 %, while in crystalline polymers the permeability decreases with over 50 % [6].

Polymers with a high free volume are in general more permeable. This can be explained by the free volume theory that suggests that the permeant molecule can only diffuse through the free volume of the polymer matrix [28]. The free volume can also be related to density. The higher the density is, the lower the free volume [6]. The free volume of a polymer is dependant on the manufacturing method and processing parameters of the polymer [29]. Therefore, it is important to take in consideration how the polymer was processed when comparing permeability results.

The diffusion coefficient of a polymer usually decreases through crosslinking polymer chains. The mobility of the chains decreases, thus the permeability of the polymer will be decreased. However, when high-energy radiation is used to crosslink semi-crystalline polymers, the radiation can oxidize the polymer in the presence of O_2. The crystallinity can decrease and unsaturation and chain scission can increase, increasing the permeability [10, 30].

Addition of additives and plasticizers in the polymer matrix usually increases the permeability [9]. The additives and plasticizers are dispersed among and between polymer chains, disrupting hydrogen bonding and spreading the chains apart causing the free volume to increase [31]. However fillers can either increase or decrease the permeability depending on the degree of compatibility and adhesion between the polymer matrix and the filler [6]. Inert fillers that are compatible with the polymer matrix will take in free volume and create a tortuous path as discussed in paragraph 1.4. Therefore, the permeability decreases. When the fillers are incompatible with the polymer, voids will occur, increasing the free volume of the polymer and thus increasing the permeability [11].

Plasticizers are incorporated in the PHBV polymer matrix to improve processability, mechanical properties and thermal behaviour. Polyethylene glycol (PEG) is a commonly used plasticizer [32]. The PHBV substrates used in this work contain PEG to improve the processability. The influence of PEG on the permeability of PHBV hasn't been studied yet. However, Yuniarto showed that the addition of PEG decreased the oxygen transmission rate (OTR) of PLA up to a concentration of 5% PEG, after which the OTR increased [33] and Srinivasa showed that the P_{WV} of chitosan films increased after the addition of PEG and the P_{O2} decreased [34]. Therefore, it is important to keep in mind that PEG has been added to the PHBV substrates when comparing the results with other results found in literature.

As indicated in equation 2.10 the permeability coefficient is independent of thickness. However there are exceptions to this rule. Coated films sometimes show an increase in permeability with thickness, while the permeability decreases with thickness for films with irregular surface due to pinholes [6]. This will be discussed in paragraph 2.3.

2.2.2 Nature of the permeant

Permeability properties are affected by molecular size, shape and chemical nature of the permeant.

Molecules with a large molecular size generally reduce the diffusion and solubility of the permeant [18]. For transport phenomena the kinetic diameter is most used for the description of molecule size. The smallest effective dimension of a molecule is given by the kinetic diameter [35]. For spherical, non-polar molecules, the kinetic diameter can be obtained from the Lennard-Jones potential. This potential describes the potential energy of interaction between two molecules in dependence of their distance to each other [36]:

$$\Phi(r) = 4\varepsilon[(\sigma/r)^{12} - (\sigma/r)^{6}] \quad (2.11)$$

Where σ is the collision diameter, ε the characteristic or maximum energy of action and r the intermolecular distance. The collision diameter is the distance between two molecules of the same gas when the potential energy of action is equal to zero, thus the distance at their closest point of approach [37]. Figure 2.3 shows that both O_2 and CO_2 are linear nonpolar molecules. O_2 has a molecular diameter of 2.98 Å and CO_2 has a molecular diameter of 3.34 Å. When comparing O_2 with CO_2, CO_2 will diffuse faster than O_2. This because the kinetic diameter of O_2 (3.46 Å) is higher than the kinetic diameter of CO_2 (3.30 Å) [5]. Therefore, the diffusion coefficient of O_2 is lower than the diffusion coefficient of CO_2. Breck used the Stockmayer potential for polar substances to calculate the kinetic diameter for polar molecules, such as H_2O (Fig. 2.3) [38]:

$$\Phi(r) = 4\varepsilon[(\sigma/r)^{12} - (\sigma/r)^{6} - \delta(\sigma/r)^{3}] \quad (2.12)$$

Where δ is a function to describe the angular dependence of the dipole-dipole interaction energy. H_2O has a bent shape, a molecular diameter of 2.75 Å and a kinetic diameter of 2.65 Å [5].

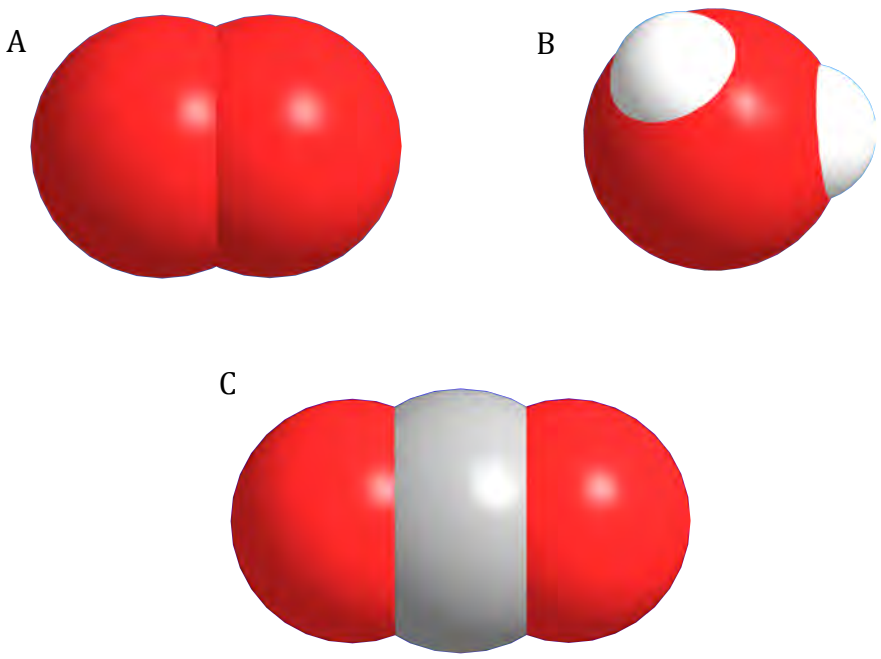

Figure 2.3: The molecular structure of O_2 (A), H_2O (B) and CO_2 (C).

As discussed in paragraph 2.2.1, the chemical similarity between the polymer and the permeant also plays an important role in the permeation properties. Because of the polar ester groups in PHBV, the P_{O2} of PHBV will be higher than the P_{H2O} of PHBV. The difference between the P_{O2} and P_{H2O} of PHBV is shown in table 2.3. Table 2.3 shows a large variance in the permeability results. This is due to the way in which PHBV is produced and the different techniques in which the permeability is determined.

Table 2.3: Literature values of P_{O2} and P_{WV} of PHBV.

% HV	T (°C)	RH (%)	P_{O2} (cc.mm/(m².day.atm))	T (°C)	RH (%)	P_{WV} (g.mm/(m².day.atm))	Ref.
3	25	80	2.23	25	100	0.0006	[17]
5	25	80	5.93	25	100	0.0007	[12]
5	23	0	4.9	37.8	90	2.9	[19]
8	21	40	8.75	21	40	0.0003	[14]
8	23	0	4.9	37.8	90	3.1	[19]
12	24	80	12.61	24	100	0.001	[16]
12	24	80	15.58	24	40	0.001	[13]
12	23	0	3.9	37.8	90	2.9	[19]

2.2.3 Ambient environment

The permeability of a polymer can be strongly affected by temperature, humidity and pressure.

2.2.3.1 Temperature

The permeability is influenced by temperature. The mobility of the gas, the partial pressure difference and the polymer configuration are directly influenced by temperature [1].

The diffusion rate increases exponentially with increasing temperature in accordance to Arrhenius law [35]:

$$D = D_0 e^{-E_D/RT} \tag{2.13}$$

E_D is the activation energy of diffusion (J. mol^{-1}), R is the universal gas constant (8,314 J. K^{-1}.mol^{-1}), T the temperature in Kelvin and D_0 a temperature-independent factor (length^2/time).

The increase in diffusion rate can be explained by the greater mobility of polymer chains at higher temperature and with an increased free volume of the polymer [18]. The energy of the permeant molecules also increases, causing the increase of diffusion rate of the permeant. It can be concluded that *D* increases with increasing temperature for both permanent gases, such as O_2 and CO_2, and vapours, such as water vapour.

The solubility is also exponentially dependant on the temperature and can be described by following equation [6]:

$$S = S_0 e^{-\Delta H_S / RT} \tag{2.14}$$

The enthalpy of solution (ΔH_S) is determined by the energy necessary for a gas molecule to condensate ($\Delta H_{condensation}$) and the pores created for the gas molecule to enter the polymer (ΔH_{mixing}). $\Delta H_{condensation}$ is generally negative and dominant for gases and vapors [6]. For low molecular weight gases, the low condensability causes the ΔH_S to be solely dependent on ΔH_{mixing}. In the case of gas adsorption, ΔH_{mixing} increases with increasing temperature, causing the solubility to decrease with increasing temperature. However, for weak interactions between the polymer and the penetrant, ΔH_{mixing} is practically stable, causing the solubility to increase with increasing temperature. Generally the solubility coefficient increases for permanent gases, such as O_2 and CO_2, and decreases for vapours, such as water vapour, with increasing temperature.

The temperature dependence of permeability can be given by combining equations 2.2, 2.13 and 2.14:

$$P = D_0 S_0 e^{(-E_D - \Delta H_S)/RT} = D_0 S_0 e^{-E_p / RT} \tag{2.15}$$

E_p is the activation energy of permeability and is determined by E_D and ΔH_S.

It is possible to determine E_p experimentally. By plotting ln *P* versus 1/*T*, with *T*

in Kelvin, E_p can be determined by following equation:

$$E_P = -\text{slope} \times R \tag{2.16}$$

For packaging materials it is interesting to know the influence of the temperature on the material. During transport temperature changes can occur when traveling through different climate zones. Currently no literature reports on the E_P of PHBV can be found. Therefore, it is important to determine the E_P of PHBV.

2.2.3.2 Humidity

Water interacts differently with polar and non-polar polymers. Non-polar polymers show only weak interaction with polar water molecules. Therefore, the solubility is low and P_{O2} and P_{CO2} are only weakly affected by humidity. Hydrophilic polar polymers do absorb moisture. The absorption of water causes the polymer to plasticize. The diffusion coefficient increases and will increase the permeability. Therefore, it is important to know the humidity of the environment to be able to interpret the measurements [1].

Martinez-Sanz reported that the P_{O2} of PHBV increases or decreases with increasing humidity depending on the percentage HV in the polymer [39]. The decrease in P_{O2} with increasing humidity is also reported for hydrophobic polymers such as PET and PLA. The decrease in the oxygen solubility is caused by the occupancy of the free volume by water molecules at higher water activity [40, 41]. However, this is the only study found on the effect of humidity on the permeability of PHBV and more research is necessary to develop a general point of view on the influence of humidity on PHBV.

2.2.3.2 Pressure

Permanent gases that obey Henry's law, such as oxygen and carbon dioxide, are in most cases independent of the pressure of the diffusing gas. This is also true for gases and vapours that show no interaction with the polymer. However, gases and vapours that show strong interaction with a polymer are dependent

on the pressure of the diffusing gas. In general, permeability increases with increasing pressure. The diffusion coefficient increases, due to the plasticizing effect [23].

2.3 Inorganic nanolayers and polymer permeability

The transport of the permeant through polymers with a barrier layer coated on its surface can be given by following equation:

$$\frac{x}{P} = \frac{x_c}{P_c} + \frac{x_p}{P_p} \tag{2.17}$$

Where x, x_c and x_p respectively are the thicknesses of the polymer with coating, the coating and the polymer, respectively. P, P_c and P_p are the permeability of the polymer with coating, the coating and the polymer.

Equation 2.17 shows that the permeability decreases with increasing coating thickness. However, this only applies for coating thickness lower than the critical coating thickness, above the critical coating thickness cracks are formed [42].

Furthermore, dense and defect-free metal oxide nanolayers should be impermeable. Nonetheless literature shows that these layers only improve the barrier two to three orders in magnitude [43]. An explanation for the fact that the nanolayer is not completely impermeable can be found in the pinhole model. This model states that the permeation is determined by the permeation through defects or pores. Many small pores give a much higher permeation than a few large holes of the same total area [44]. Thin oxide layers can contain two kinds of defects, microdefects and nanodefects. Pinholes and microcracks with sizes of the order of 1 µm are called microdefects. Microdefects, such as uncoated substrate, can be caused by a too rough surface or low surface energy of the polymer or the deposition technique [45]. Nanodefects have a size order between 0.3 nm and 1 nm and cause hindered transport, given the size of a typical permeant is between the 0.2 nm and 0.4 nm. The amorphous lattice of the oxide (interstice < 0.3 nm) can also cause hindered transport [46]. Roberts proposed following equation for the permeability in barrier films [46]:

$$P_b = C_{md} P_p + \left(\frac{\phi_p}{P_p} + \frac{\phi_g}{P_{la} + P_{nd}} \right)^{-1} \quad (2.18)$$

Where P_b is the permeability of the polymer with oxide layer and C_{md} is a dimensional constant that depends on the size and number of microdefects in the layer. P_p and ϕ_p are respectively the permeability and the thickness of the polymer. ϕ_g is the thickness of the oxide layer. P_{la} is the permeability through the lattice and P_{nd} is the permeability through the nanodefects.

It can be concluded that the barrier of polymers coated with metal oxides depends on coating defects, coating thickness, polymer roughness, polymers surface energy, deposition technique and coating density. Therefore, it is important to take in consideration these parameters when depositing a coating.

2.4 References

1. Massey, L.K., *Permeability Properties of Plastics and Elastomers*. Vol. William Andrew Publishing. 2003, USA.
2. Reddy, M.M., et al., *Biobased plastics and bionanocomposites: Current status and future opportunities.* Progress in Polymer Science, 2013. **38**(10-11): p. 1653-1689.
3. Duncan, T.V., *Applications of nanotechnology in food packaging and food safety: Barrier materials, antimicrobials and sensors.* Journal of Colloid and Interface Science, 2011. **363**(1): p. 1-24.
4. Abdel-Bary, E.M., *Handbook of Plastic Films*. 2003, UK: Rapra Technology Limited.
5. Siracusa, V., *Food Packaging Permeability Behaviour: A Report.* International Journal of Polymer Science, 2012.
6. Comyn, J., *Polymer Permeability*. 1985, London: Chapman & Hall. 383.
7. Mark, H.F., *Encyclopedia of Polymer Science and Technology, Concise*. third ed. 2013, Hoboken, New Jersey: John Wiley & Sons.
8. Van Krevelen, D.W., Te Nijenhuis, K., *Properties of Polymers*. 2009, Amsterdam: Elsevier.
9. Yam, K.L., *The Wiley Encyclopedia of Packaging Technology*. 3rd ed. 2009, USA: John Wiley & Sons.
10. Chapman, S., *Characterization and Failure Analysis of Plastics*. 2003, USA: ASM International.
11. George, S.C. and S. Thomas, *Transport phenomena through polymeric systems.* Progress in Polymer Science, 2001. **26**(6): p. 985-1017.
12. Fabra, M.J., A. Lopez-Rubio, and J.M. Lagaron, *Nanostructured interlayers of zein to improve the barrier properties of high barrier polyhydroxyalkanoates and other polyesters.* Journal of Food Engineering, 2014. **127**: p. 1-9.

13. Sanchez-Garcia, M.D. and J.M. Lagaron, *Novel Clay-Based Nanobiocomposites of Biopolyesters with Synergistic Barrier to UV Light, Gas, and Vapour.* Journal of Applied Polymer Science, 2010. **118**(1): p. 188-199.

14. Cava, D., et al., *Comparative performance and barrier properties of biodegradable thermoplastics and nanobiocomposites versus PET for food packaging applications.* Journal Of Plastic Film & Sheeting, 2006. **22**(4): p. 265-274.

15. Sanchez-Garcia, M.D., E. Gimenez, and J.M. Lagaron, *Morphology and barrier properties of nanobiocomposites of poly(3-hydroxybutyrate) and layered silicates.* Journal of Applied Polymer Science, 2008. **108**(5): p. 2787-2801.

16. Sanchez-Garcia, M.D., J.M. Lagaron, and S.V. Hoa, *Effect of addition of carbon nanofibers and carbon nanotubes on properties of thermoplastic biopolymers.* Composites Science and Technology, 2010. **70**(7): p. 1095-1105.

17. Fabra, M.J., A. Lopez-Rubio, and J.M. Lagaron, *On the use of different hydrocolloids as electrospun adhesive interlayers to enhance the barrier properties of polyhydroxyalkanoates of interest in fully renewable food packaging concepts.* Food Hydrocolloids, 2014. **39**: p. 77-84.

18. Lagaron, J.M., *Multifunctional and nanoreinforced polymers for food packaging*. 2011, Cambridge: Woodhead Publishing Limited.

19. Thellen, C., et al., *A Processing, Characterization and Marine Biodegradation Study of Melt-Extruded Polyhydroxyalkanoate (PHA) Films.* Journal of Polymers and the Environment, 2008. **16**(1): p. 1-11.

20. Sanchez-Garcia, M.D., E. Gimenez, and J.M. Lagaron, *Morphology and barrier properties of solvent cast composites of thermoplastic biopolymers and purified cellulose fibers.* Carbohydrate Polymers, 2008. **71**(2): p. 235-244.

21. Avérous, L., Pollet, E., *Environmental Silicate Nano-Biocomposites*. 2012, London: Springer-Verlag.

22. Sanchez-Garcia, M.D., E. Gimenez, and J.M. Lagaron, *Novel pet nanocomposites of interest in food packaging applications and comparative barrier performance with biopolyester nanocomposites.* Journal of Plastic Film & Sheeting, 2007. **23**(2): p. 133-148.

23. Baldwin, E.A., R. Hagenmaier, J. Bai, J.M. Krochta, *Edible Coatings and Films to Improve Food Quality*. 1994, USA: CRC Press.

24. Kofinas, P., R.E. Cohen, and A.F. Halasa, *Gas-Permeability of Polyethylene Poly(Ethylene Propylene) Semicrystalline Diblock Copolymers.* Polymer, 1994. **35**(6): p. 1229-1235.

25. Michaels, A.S. and H.J. Bixler, *Solubility of Gases in Polyethylene.* Journal of Polymer Science, 1961. **50**(154): p. 393.

26. Di Lorenzo, M.L. and M.C. Righetti, *Effect of thermal history on the evolution of crystal and amorphous fractions of poly[(R)-3-hydroxybutyrate] upon storage at ambient temperature.* European Polymer Journal, 2013. **49**(2): p. 510-517.

27. Boufarguine, M., et al., *PLA/PHBV Films with Improved Mechanical and Gas Barrier Properties.* Macromolecular Materials and Engineering, 2013. **298**(10): p. 1065-1073.

28. Mafi, A., et al., *A Comparative Study on the Free Volume Theories for Diffusivity Through Polymeric Membrane in Pervaporation Process.* Journal of Applied Polymer Science, 2014. **131**(15).

29. Cheng, M.L. and Y.M. Sun, *Relationship between free volume properties and structure of poly(3-hydroxybutyrate-co-3-hydroxyvalerate) membranes via various crystallization conditions.* Polymer, 2009. **50**(22): p. 5298-5307.

30. Lin, H.Q., et al., *The effect of cross-linking on gas permeability in cross-linked poly(ethylene glycol diacrylate).* Macromolecules, 2005. **38**(20): p. 8381-8393.

31. Mills, A., A. Lepre, and L. Wild, *Effect of plasticizer-polymer compatibility on the response characteristics of optical thin CO2 and O-2 sensing films.* Analytica Chimica Acta, 1998. **362**(2-3): p. 193-202.

32. Bugnicourt, E., et al., *Polyhydroxyalkanoate (PHA): Review of synthesis, characteristics, processing and potential applications in packaging.* Express Polymer Letters, 2014. **8**(11): p. 791-808.

33. Yuniarto, K.B.A.W.A.P.H.K.P.A.A., *Effect of Plasticizer on Oxygen Permeability of Cast Polylactic acid (PLA) Films Determined using Dynamic Accumulation Method.* Journal of Applied Packaging Research, 2014. **6**(2): p. 51-56.

34. Srinivasa, P.C., M.N. Ramesh, and R.N. Tharanathan, *Effect of plasticizers and fatty acids on mechanical and permeability characteristics of chitosan films.* Food Hydrocolloids, 2007. **21**(7): p. 1113-1122.

35. McKeen, L.W., *PERMEABILITY PROPERTIES OF PLASTICS AND ELASTOMERS*. 3rd ed. 2012, Oxford: Elsevier.

36. Weitkamp, J.P., L., *Catalysis and Zeolites: Fundamentals and Applications*. 1999, Berlin Heidelberg © Springer-Verlag Berlin Heidelberg

37. Yampolskii, Y.P., I., Freeman B.D., *Materials Science of Membranes for Gas and Vapor Separation*, ed. Y.P. Yampolskii, I., Freeman B.D. 2006, Hoboken, USA: John Wiley & Sons

38. Mourits, F.M.R., F.H. A. , *A critical evaluation of Lennard–Jones and Stockmayer potential parameters and of some correlation methods.* Canadian Journal of Chemistry, 1977. **55**(16): p. 3007-3020.

39. Martinez-Sanz, M., et al., *Characterization of polyhydroxyalkanoates synthesized from microbial mixed cultures and of their nanobiocomposites with bacterial.* New Biotechnology, 2014. **31**(4): p. 364-376.

40. M. Martínez-Sanz, A.L.-R., J.M. Lagaron, *On the optimization of the dispersion of unmodified bacterial cellulose nanowhiskers into polylactide via melt compounding to significantly enhance barrier and mechanical properties.* Biomacromolecules, 2012. **13**(11): p. 3887-3899.

41. Auras, R., B. Harte, and S. Selke, *An overview of polylactides as packaging materials.* Macromolecular Bioscience, 2004. **4**(9): p. 835-864.

42. Leterrier, Y., *Durability of nanosized oxygen-barrier coatings on polymers - Internal stresses.* Progress in Materials Science, 2003. **48**(1): p. 1-55.

43. Lewis, J.S. and M.S. Weaver, *Thin-film permeation-barrier technology for flexible organic light-emitting devices.* Ieee Journal of Selected Topics in Quantum Electronics, 2004. **10**(1): p. 45-57.

44. Rossi, G. and M. Nulman, *Effect of Local Flaws in Polymeric Permeation Reducing Barriers.* Journal of Applied Physics, 1993. **74**(9): p. 5471-5475.

45. Wagner, J., *Multilayer Flexible Packaging: Technology and Applications for the Food, Personal Care, and Over-the-Counter Pharmaceutical Industries*. 2010, London, UK: Elsevier.

46. Roberts, A.P., et al., *Gas permeation in silicon-oxide/polymer (SiOx/PET) barrier films: role of the oxide lattice, nano-defects and macro-defects.* Journal of Membrane Science, 2002. **208**(1-2): p. 75-88.

Chapter 3

Deposition techniques

3.1 Chemical bath deposition (CBD)

As mentioned in chapter 1, a chemical bath solution was used to deposit ZnO nanolayers on top of a PHBV substrate. To promote the deposition of ZnO nanolayers, ZnO seed layers were deposited using sol gel deposition before immersing the PHBV substrate in a chemical bath.

CBD is a method that allows the formation of different sorts of nanostructures through the reaction of metal ions with the necessary anions. For the deposition of ZnO through chemical bath deposition, zinc acetate dihydrate ($Zn(CH_3COO)_2.2H_2O$), zinc nitrate hexahydrate ($Zn(NO_3)_2.6H_2O$), zinc sulfate or zinc chloride can be used to provide the Zn^{2+} metal ion [1, 2]. Water (H_2O) will provide the oxygen in the form of OH^- anions [3].

There are a lot of reports on deposition of ZnO on Si and glass using chemical bath deposition. However, the literature of ZnO chemical bath deposition on plastics is limited and the deposition of ZnO nanolayers on PHBV substrates hasn't been discussed in literature. Yi et al. reported on the deposition of ZnO on PET using a chemical bath of zinc nitrate hexahydrate ($Zn(NO_3)_2.6H_2O$) and diethylene triamine (DETA) and Shabannia et al. reported on the deposition of ZnO on PET using a chemical bath of $Zn(NO_3)_2.6H_2O$ and hexamethylene tetramine (HMT) [4, 5]. The deposition methods used in the following study will be based on these methods. The different parameters that control the deposition, such as pH, temperature and composition of the solution, will be discussed [2, 6, 7].

3.1.1 ZnO seed layer

Figure 3.2: Schematic drawing of a seed layer (yellow).

The ZnO crystals are formed through heterogeneous and homogeneous nucleation. Heterogeneous nucleation will take place at the substrate surface and homogeneous nucleation in the solution [8]. To enhance heterogeneous growth, nucleation sites can be provided on the substrate surface [9]. The nucleation sites can be added by depositing a seed layer. The ZnO seed layers will increase the affinity between the active components of the nanolayers and the substrate. Since the deposition solutions are aqueous, the bonding with hydrophobic plastics is less strong than with hydrophilic surfaces [10]. The seed layer improves the wettability. The contact angle, between substrate and solution, decreases and the surface energy of the substrate, increases. The seed layer size improves control and orientation of the ZnO nanoparticles in the ZnO nanolayer [11].

The seed layers mostly consist out of ZnO nanoparticles with a diameter of less than 20 nm [12]. The ZnO seeds can be grown using the sol gel procedure. Dip coating or spin coating can be used to deposit the seeds [4, 13]. For the sol gel synthesis, metal salts, such as zinc acetate, are used to deposit ZnO. Additionally a catalyst, such as NaOH, is used to ensure hydrolysis and condensation. The following hydrothermal reaction occurs [4, 14]:

$$\mathrm{Zn(CH3COO)_2.2H_2O + 2NaOH \rightarrow ZnO + 2Na(CH_3COOH) + H_2O} \qquad (3.1)$$

Temperature, pH and time of reaction determine the rate of hydrolysis and condensation reaction. Wahid reported that the size of the particles increases

with duration of the reaction and annealing temperature [15]. Hosono reported that a pH ≥ 8 is necessary, because a sufficient amount of OH^- is needed to convert $Zn(OH)_4^{2-}$ into ZnO. However a pH ≥ 11 causes ZnO to react with OH^- and converses the reaction [16]:

$$Zn(CH_3COO)_2.2H_2O + 2NaOH \rightarrow Zn(OH)_2 + 2CH_3COONa + 2H_2O \quad (3.2)$$

$$Zn(OH)_2 + H_2O \rightarrow Zn(OH)_4^{2-} + 2H^+ \quad (3.3)$$

$$Zn(OH)_4^{2-} \Leftrightarrow ZnO + H_2O + 2OH^- \quad (3.4)$$

An increasing annealing temperature of the seed layer up till 350 °C increases the crystallinity of the seed layer. This causes the average length of the nanoparticles in the nanolayer to increase [17]. Low surface roughness of the seed layers leads to a dense ZnO layer, while high surface roughness leads to a poor orientation of the ZnO nanoparticles [17].

3.1.2 Growth of ZnO nanolayers

Figure 3.2: Schematic drawing of a ZnO nanolayer (yellow).

After the deposition of the ZnO seed layer, the ZnO nanolayer can be formed. As mentioned, ZnO nanolayers will be formed through heterogeneous and homogeneous nucleation [8]. The homogeneous nucleation can cause a preliminary stop of heterogeneous growth. To prevent this DETA or HMT is added to the solution. As shown by the following equations, DETA and HMT are ammonia (NH_3) precursors. They are added to increase the pH and hydrolysis of Zn^{2+} [3, 4, 18] and are highly soluble in water. In equation 3.5 DETA is used as NH_3 precursor and in equation 3.6 HMT is used.

$$(CH_2)_4N_3H_5 + 4H_2O \rightarrow 4HCHO + 3NH_3 + 2H_2 \quad (3.5)$$

$$(CH_2)_6N_4 + 6H_2O \rightarrow 6HCHO + 4NH_3 \quad (3.6)$$

$$NH_3 + H_2O \rightarrow NH_4^+ + OH^- \quad (3.7)$$

For the decomposition of the precursor into NH_3 heat is necessary [19]. Tak et al. showed that increasing the amount of NH_3 added to the zinc ion solution causes the solution to change from turbid to clean. Addition of only a small amount of NH_3 causes the formation of white $Zn(OH)_2$ precipitation. By increasing the amount of NH_3, more NH_4 ions are formed. This leads to the formation of the complex $Zn(NH_3)_4^{2+}$ [20]. An increase in temperature causes the complex to react with OH^- and produce ZnO crystals [21]:

$$Zn(NH_3)_4^{2+} + 2OH^- \rightarrow ZnO + 4NH_3 + H_2O \quad (3.8)$$

Although an excess of NH_3 inhibits homogeneous growth, literature shows that there is an upper limit of 10.8 pH for ZnO growth on Si substrates [20]. This can be explained by the degree of saturation, the ratio of ion product to solubility product. When the supersaturation degree is lower than 1, no precipitation will occur. When the degree of supersaturation is 1 or higher precipitation occurs. The degree of saturation has a critical value. Below this value heterogeneous nucleation occurs and above this value homogeneous nucleation occurs [9]. Increasing the NH_3 concentration increases the pH of the solution and the formation of the complex $Zn(NH_3)_4^{2+}$. This causes the crystal quality to decrease [18]. Flowerlike ZnO nanostructures are obtained at a pH ≥ 8 and rodlike nanostructures are obtained at a slightly acidic or neutral pH [22].

Crystallinity and size of the ZnO crystal can be increased through increasing the reaction time [23]. Treatments of one hour up to several days have been reported for the deposition of ZnO layers.

The growth rate of the ZnO is dependent on the concentration Zn^{2+} in the solution. The concentration of the solution controls the nucleation density.

Increasing solution concentration causes the diameter of the particles to increase and the length to decrease [24]. The higher the Zn^{2+} concentration, the higher the growth rate of the ZnO crystals [23]. For CBD with a Zn^{2+} salt and HMT, a dense and uniform layer is obtained for Zn^{2+}:NH_3 molar ratio of 1:1 to 1:3. Increasing the NH_3 concentration decreases the density and uniformity of the layers [18]. As indicated in equation 3.8, increasing the NH_3 concentration causes forced hydrolysis of Zn^{2+}.

As mentioned, the formation of ZnO is temperature dependent. Temperature controls the aspect ratio and morphology. The length, diameter and aspect ratio increase with increasing temperature [24]. Lower temperature improves uniformity of the nanoparticles. However, a minimum temperature is necessary to grow ZnO. For Si substrates this minimum temperature is 60°C [9]. For PET the lowest deposition temperature found in literature is 95°C [9].

3.2 Sputter deposition

Another technique that is used to deposit ZnO nanolayers is reactive sputtering. Reactive sputtering is a process where a metal target (e.g. elemental Zn) is eroded by a particle bombardment and subsequently deposited onto a substrate. The target material is placed in a chamber filled with a gas or a mixture of gasses (e.g. Ar + O_2) at reduced pressure and a negative potential is set. Due to the negative potential electrons will be accelerated and collide with the gas molecules. Electron-ion pairs are formed and the ions create on impact with the target surface an atomic collision cascade. Target material will be ejected and will condense onto surrounding surfaces to form a coating (e.g. ZnO coating). This means that the coating is not only formed onto the substrates, but also onto the target. This will decrease the deposition rate significantly and is called target poisoning. The thickness of the coating and the coverage of the substrate are dependent on the distance between the substrate and the target, the pressure, the ratio Ar-O_2, the power, the pulse frequency and the deposition time. The values of these parameters were set by SIRRIS. To deposit ZnO on PHBV, they used the same values as used to deposit ZnO on other plastic substrates, such as PP and PET.

3.3 References

1. Baviskar, P.K., et al., *Controlled synthesis of ZnO nanostructures with assorted morphologies via simple solution chemistry.* Journal of Alloys and Compounds, 2013. **551**: p. 233-242.
2. Parikh, H. and M.R. De Guire, *Recent progress in the synthesis of oxide films from liquid solutions.* Journal of the Ceramic Society of Japan, 2009. **117**(1363): p. 228-235.
3. Jeong, Y.I., et al., *Effect of Reactant Concentration on the Structural Properties of Hydrothermally-grown ZnO Rods on Seed-layer ZnO/Polyethylene Terephthalate Substrates.* Journal of the Korean Physical Society, 2011. **59**(3): p. 2338-2342.
4. Yi, S.H., et al., *Low-temperature growth of ZnO nanorods by chemical bath deposition.* Journal of Colloid and Interface Science, 2007. **313**(2): p. 705-710.
5. Shabannia, R. and H. Abu-Hassan, *Vertically aligned ZnO nanorods synthesized using chemical bath deposition method on seed-layer ZnO/polyethylene naphthalate (PEN) substrates.* Materials Letters, 2013. **90**: p. 156-158.
6. Schneller, T.R.W.M.K.D.P., *Chemical Solution Deposition of Functional Oxide Thin Films*. 2013, Wien: Springer-Verlag.
7. Mitzi, D.B., *Solution processing of inorganic materials*. 2009, Hoboken, New Jersey: John Wiley & Sons.
8. Kathalingam, A., et al., *Chemical bath deposition and characterization of nanocrystalline ZnO thin films.* Materials Science-Poland, 2010. **28**(2): p. 513-522.
9. Sugunan, A., et al., *Zinc oxide nanowires in chemical bath on seeded substrates: Role of hexamine.* Journal of Sol-Gel Science and Technology, 2006. **39**(1): p. 49-56.

10. Kokotov, M. and G. Hodes, *Reliable chemical bath deposition of ZnO films with controllable morphology from ethanolamine-based solutions using KMnO4 substrate activation.* Journal of Materials Chemistry, 2009. **19**(23): p. 3847-3854.

11. Zhou, Z.Y., Y.P. Zhao, and Z.S. Cai, *Low-temperature growth of ZnO nanorods on PET fabrics with two-step hydrothermal method.* Applied Surface Science, 2010. **256**(14): p. 4724-4728.

12. Guillemin, S., et al., *Critical Nucleation Effects on the Structural Relationship Between ZnO Seed Layer and Nanowires.* Journal of Physical Chemistry C, 2012. **116**(47): p. 25106-25111.

13. Chang, G.J., S.Y. Lin, and J.J. Wu, *Room-temperature chemical integration of ZnO nanoarchitectures on plastic substrates for flexible dye-sensitized solar cells.* Nanoscale, 2014. **6**(3): p. 1329-1334.

14. Sakka, S., *Sol-gel science and technology*. sol-gel processing, ed. H. Kozuko. Vol. 1. 2005, London: Kluwer.

15. Wahid, K.A., et al., *Effect of seed annealing temperature and growth duration on hydrothermal ZnO nanorod structures and their electrical characteristics.* Applied Surface Science, 2013. **283**: p. 629-635.

16. Hosono, E., et al., *Non-basic solution routes to prepare ZnO nanoparticles.* Journal of Sol-Gel Science and Technology, 2004. **29**(2): p. 71-79.

17. Kim, K.H., et al., *Growth of Zinc Oxide Nanorods Using Various Seed Layer Annealing Temperatures and Substrate Materials.* International Journal of Electrochemical Science, 2014. **9**(4): p. 2080-2089.

18. Mridha, S. and D. Basak, *Effect of concentration of hexamethylene tetramine on the structural morphology and optical properties of ZnO microrods grown by low-temperature solution approach.* Physica Status Solidi a-Applications and Materials Science, 2009. **206**(7): p. 1515-1519.

19. Govender, K., et al., *Understanding the factors that govern the deposition and morphology of thin films of ZnO from aqueous solution.* Journal of Materials Chemistry, 2004. **14**(16): p. 2575-2591.

20. Tak, Y. and K.J. Yong, *Controlled growth of well-aligned ZnO nanorod array using a novel solution method.* Journal of Physical Chemistry B, 2005. **109**(41): p. 19263-19269.

21. Wang, Z., et al., *Large-scale fabrication of tower-like, flower-like, and tube-like ZnO arrays by a simple chemical solution route.* Langmuir, 2004. **20**(8): p. 3441-3448.

22. Baruah, S. and J. Dutta, *pH-dependent growth of zinc oxide nanorods.* Journal of Crystal Growth, 2009. **311**(8): p. 2549-2554.

23. Wang, H., et al., *Growth Mechanism of Different Morphologies of ZnO Crystals Prepared by Hydrothermal Method.* Journal of Materials Science & Technology, 2011. **27**(2): p. 153-158.

24. Li, Q.W., et al., *Controllable growth of well-aligned ZnO nanorod arrays by low-temperature wet chemical bath deposition method.* Applied Surface Science, 2010. **256**(6): p. 1698-1702.

Chapter 4

Synthesis of ZnO nanoparticle layers on PET and PHBV

4.1 Introduction

The first aim of my thesis was to deposit ZnO nanoparticle layers on the surface of PHBV substrates using a chemical bath deposition.

As mentioned in chapter 3, the literature of ZnO chemical bath deposition on plastics is limited and the deposition of ZnO nanoparticle layers on PHBV substrates hasn't been discussed in literature. Therefore, known methods to deposit ZnO on PEN and PET substrates had to be used and altered were necessary. The two methods used are published by Yi et al. [1] and Shabannia et al. [2].

Before ZnO nanoparticle layers can be deposited, it is important that there is enough affinity between the substrate and the precursor. The affinity between the substrate and the precursor can be determined by measuring the contact angle. If the contact angle is 0°, the liquid has a strong affinity for the substrate. This is called total wetting. When the contact angle is more than 90° (non-wetting), there is no affinity between the substrate and liquid. To optimize the affinity between the substrate and precursor, ZnO seed layers need to be deposited on top of the PET and PHBV substrates, before depositing the ZnO nanoparticle layers. The necessity of the seed layer was studied. In this study, the seed layer was formed using sol gel deposition as mentioned by Yi et al. [1].

After the formation of the seed layer, the ZnO nanoparticle layers were deposited using to chemical bath method. To deposit ZnO nanoparticle layers Yi et al. describes a deposition temperature of 130 °C to deposit ZnO [1]. This temperature is too high for PHBV substrates. Therefore, PET substrates were used to optimize the method so that deposition at lower temperature will be possible.

To be able to evaluate and compare the methods of Yi et al. and Shabannia et al., the Shabannia method was also used to deposit ZnO on PET substrates. As is known, the deposition of ZnO nanoparticles differs from substrate to substrate. Therefore, the optimal parameters found for the deposition on PET substrates were not the same as for PHBV. The deposition method had to be examined thoroughly and altered were necessary.

4.2 Materials

The PET substrates were offered by Agfa-Gevaert NV, Mortsel, Belgium and have a thickness of 0.25 mm and a low surface roughness of 48 nm. The surface roughness of the substrate was measured by profilometry using a DEKTAK XT Standard. This was done in cooperation with the Materials Physics research group of the UHasselt. A diamond-tipped stylus was used to scan the surface and detect minute surface variations in surface topography.

Two different kinds of PHBV substrates were used.

First self-made samples from PHBV (3% HV) granulates, provided by FKUR, Willich, Germany, were studied. In this thesis these substrates will be called PHBV1. Compression moulding was used to make the PHBV1 samples. This was done at the University of Mons. Eight to nine grams of granulate was put on a compression plate with a volume of 5.5 cm^3. Both aluminium and Teflon plates were used. As was confirmed by the DEKTAK measurements (table 4.1), aluminium plates provide a smoother surface and Teflon plates a rougher surface. The temperature was set at 170 °C. The plates were closed by hydraulic pressure. Afterwards a constant pressure of 160 Bar was applied. Sheets with

thicknesses between 0.5 and 0.6 mm were obtained. The surface roughness (R_a) (table 4.1) of these PHBV1 substrates was too high for chemical bath deposition. Therefore, it was necessary to change to less rough PHBV substrates. However, we were able to deposit ZnO nanolayers on these substrates using the sputtering technique.

Table 4.1: The surface roughness of the PHBV1 samples.

Sample (side)	Thickness (mm)	Ra*(nm) direction 1	Ra*(nm) direction 2
1 (Teflon)	0.4629	612	1490
3 (aluminium)	0.6511	201	292
4 (Teflon)	0.601	835	1500
4 (aluminium)	0.601	71	223

Since we were unable to deposit ZnO nanoparticle layers onto the surface of PHBV1 substrates using the CBD method, PHBV substrates with 8% valerate were obtained from Goodfellow, Huntingdon, England. These substrates will be called PHBV2 throughout the thesis and have a thickness of approximately 0.05 mm. The PHBV2 substrates have a surface roughness of about 125 nm. This is still rougher than the 48 nm surface roughness of the PET substrate, but not as rough as the PHBV1 substrates. These substrates are much thinner than the PET substrates, but sheets of PHBV with the same thickness as PET were not available.

4.3 Deposition of ZnO seed layers

As mentioned in chapter 4.1, seed layers are used to enhance the affinity between the substrate and the precursor. The necessity of seed layers was shown through the deposition of ZnO nanolayers on PET substrates with and without ZnO seed layer.

To be able to deposit seed layers the affinity between the substrate and the seed layer solution also has to be high enough. Therefore, first the affinity between the substrate and the solvent used for depositing seed layers was determined through contact angle measurements with an OCA 15 plus apparatus via the sessile drop method. Since the seed layers are formed using the method of Yi et al., CH_3OH was used as solvent. The contact angle of PET and CH_3OH was 32±5°. As stated in chapter 3, this means that the surface energy is high enough for heterogeneous nucleation to take place.

The seed layer was deposited by adding a 65 ml solution of NaOH (> 98 %, Sigma Aldrich, Diegem, Belgium) in CH_3OH (99.8 %, Acros, Geel, Belgium) slowly to a 125 ml solution of $Zn(CH_3COO)_2.2H_2O$ (> 98 %, Sigma Aldrich, Diegem, Belgium) in CH_3OH at 60 °C and stirring the mixture over a period of 2h. Afterwards the mixture was cooled down to room temperature (T_r). The substrates were dip coated, 5 times at a speed of 35 mm/min and kept in the solution for 120 s. The solvent was removed by drying the substrates in an oven at 130°C for 5 min. The drying temperature was reduced to avoid deterioration when using the PHBV instead of PET samples. Eventually, The drying temperature could be decreased to 95°C, but this prolonged the drying time to 20 min. For optimal formation of the ZnO seed layers the ratio of Zn^{2+} and OH^- is important. Changing the ratio of the solution by using 0.03M NaOH and 0.02 M $Zn(CH_3COO)_2.2H_2O$ didn't improve the formation of ZnO nanoparticle layers, it only gave larger particles of ZnO in the solution itself. To decrease the size of the particles in the solution, the molar concentration of Zn^{2+} in the solution was decreased to 0.01M $Zn(CH_3COO)_2.2H_2O$. After decreasing the molar concentration of $Zn(CH_3COO)_2.2H_2O$, the solution turned transparent, as reported in the article. However, the seed layers didn't really improve the deposition of ZnO nanoparticle layers (see figure 4.1.B). As shown in figure 4.1.C, cooling down the mixture to 30°C instead of room temperature and dip coating at 30°C did increase the deposition of ZnO nanoparticle layers. The Scanning Electron Microscopy (SEM) images were provided by the Materials Physics research group of the UHasselt. The measurements were performed on a FEI Quanta 2000 FEG SEM.

Smaller and more ZnO particles were deposited when the PET substrate was first covered with a seed layer. The length of the ZnO particles decreased from up to 10 µm to 1 µm or less. As mentioned in chapter 3, the formation of ZnO is a hydrothermal process and probably 30°C is necessary for the ZnO particles to grow onto the PET substrates. Contact angle measurements showed that the surface energy of PET was increased through the addition of a seed layer. The contact angle between PET and H_2O, the solvent used for the two CBD methods, decreased from 89±4° to 80°±3. The high contact angle between PET and H_2O corresponds with what has been stated in literature. The affinity between plastics and aqueous precursors is low. Thus, the seed layer is necessary to enhance the growth of ZnO nanoparticle layers.

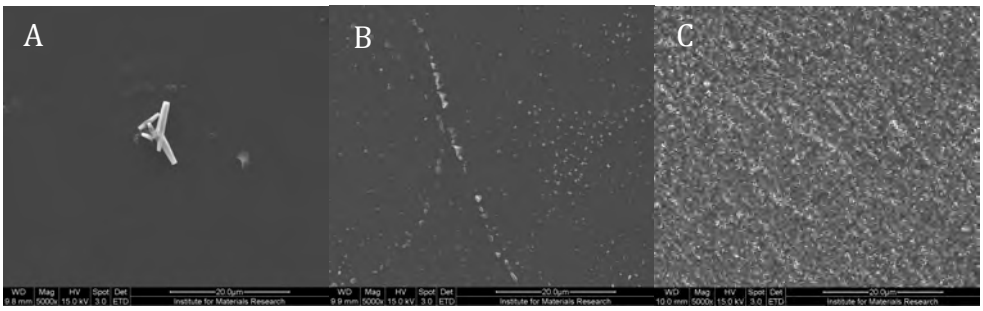

Figure 4.1: SEM images of ZnO deposition with the DETA method on PET without a seed layer (A), with a seed layer at T_k (B) and with a seed layer at 30°C (C).

Conclusion 1:

1. ***A seed layer is necessary to enhance the growth of the ZnO nanoparticle layer.***
2. ***The maximum temperature used during the deposition of seed layers is 95°C, a temperature low enough to avoid deterioration of the PHBV substrate***
3. ***Dip coating solution:***

	V	C
NaOH	65 mL	0.03 M
$Zn(CH_3COO)_2.2H_2O$	125 mL	0.01 M

4. ***Dip coating process:***

Reaction temperature	30°C
Drying temperature	95°C
Drying time	20 min

4.4 Deposition of ZnO nanoparticle layers

As mentioned before, ZnO nanoparticle layers will be deposited using the methods described by Yi et al. and Shabannia et al. A layer of ZnO nanoparticles (nanolayer) was deposited using the $Zn(NO_3)_2.6H_2O$ and DETA or HMT method. ZnO nanolayers were deposited at 90-95°C [1, 2]. Both methods describe the formation of nanorods. In the method of Yi, PET substrates were immersed in an aqueous solution of 0.025 M $Zn(NO_3)_2.6H_2O$ and 0.025 M DETA at 95°C for 1h.

In the method of shabannia, PEN substrates were immersed in an aqueous solution of 0.05M $Zn(NO_3)_2.6H_2O$ and 0.05M HMT at 95°C for 5h.

PET substrates were used to optimize the methods at lower deposition temperatures. The lowest possible deposition time for these methods was determined and the Zn^{2+}:NH_3 molar ratio was adjusted. Given that ZnO can be formed using the HMT at temperatures between 60°C and 95°C [3], the temperature of this method was decreased to determine the lowest possible temperature at which ZnO can be deposited on the substrate.

As stated, the optimal parameters found for the deposition on PET substrates are not the same as for PHBV. Therefore, the optimized deposition method for PET had to be examined thoroughly and altered were necessary when used on PHBV substrates. First the method of Yi et al. is described and afterwards the method of Shabannia.

Scanning electron microscopy (SEM) was used to determine the surface morphology of the deposited ZnO nanolayer. The measurements were performed on an FEI Quanta 2000 FEG SEM. The thickness of the layers was determined using cross-sectional SEM. The SEM images were provided by the materials physics group of the UHasselt.

4.4.1 Chemical bath deposition with DETA

4.4.1.1 Deposition of ZnO on PET substrates

PET substrates with ZnO seed layer were immersed in a chemical bath of 0.025 M $Zn(NO_3)_2.6H_2O$ (> 98 %, Sigma Aldrich, Diegem, Belgium) and 0.025 M DETA (99 %, Alfa Aesar, Belgium) aqueous solution at 95 °C for 1h. Yi et al. reported formation of ZnO nanorods after a treatment of 1h. However, even after 3h, there was no ZnO formation (see fig. 4.2). Therefore, the reaction time was prolonged to 4h, 6h and 24h. Figure 4.3 indicates that a dense layer is formed after 4h of treatment. The particles contained after 4h treatment have an average length of 2.5 µm and a diameter of up to 600 nm. Since a shorter

treatment time is economically more interesting for the packaging industry, the reaction time was held at 4h.

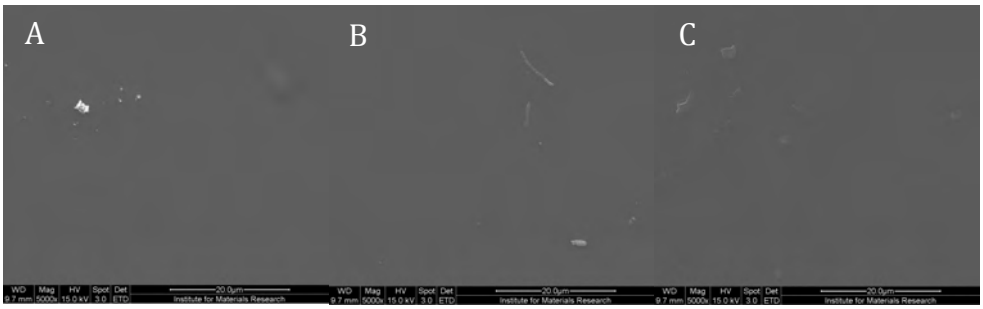

Figure 4.2: SEM images of ZnO deposition on PET with ZnO seed layer at 30 °C: 1h CBD (A), 2h CBD and 3h CBD (C).

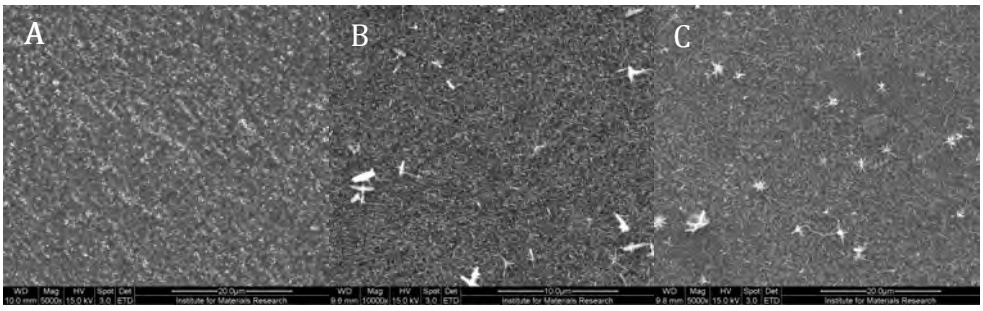

Figure 4.3: SEM images of ZnO deposition on PET with ZnO seed layer at 30 °C: 4h CBD (A), 6h CBD and 24h CBD (C).

Yogamalar reported that by using a different Zn^{2+} precursor, the morphology of the ZnO could be changed. $Zn(CH_3COO)_2.2H_2O$ would give regular shaped rodlike structures, while $Zn(NO_3)_2.6H_2O$ would give grouped ZnO nanorods. A $Zn(NO_3)_2.6H_2O$ solution has a lower basicity. This increases the reaction speed and makes a part of the crystal dissolve in the solution. Another explanation is that the growth rate dominates the nucleation rate and the crystal size decreases [4, 5]. Therefore $Zn(NO_3)_2.6H_2O$ was replaced by $Zn(CH_3COO)_2.2H_2O$. The PET substrates with ZnO seed layer were immersed in an aqueous chemical bath of 0.025 M $Zn(CH_3COO)_2.2H_2O$ and 0.025 M DETA for 4h at 95 °C. The SEM

image in figure 4.4 shows that in this case the use of $Zn(CH_3COO)_2.2H_2O$ decreased the deposition of ZnO nanoparticles. This would indicate that the reaction speed is too low to form a layer of ZnO nanoparticles.

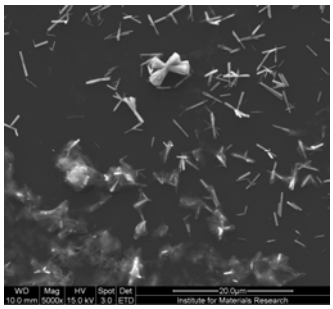

Figure 4.4: SEM image of ZnO deposition on PET with ZnO seed layer, deposited at 30°C using $Zn(CH_3COO)_2.2H_2O$ as Zn^{2+} source.

4.4.1.2 Deposition of ZnO on PHBV substrates

The affinity between PHBV2 and CH_3OH and H_2O was measured using contact angle measurements. The contact angle of PHBV2 and CH_3OH was 0°. Due to the low contact angle and thus high surface energy the formation of a seed layer was possible. The seed layer was deposited as mentioned in paragraph 4.2, by adding a 65 ml solution of NaOH in CH_3OH to a 125 ml solution of $Zn(CH_3COO)_2.2H_2O$ in CH_3OH at 60 °C and stirring it over a period of 2h. The substrates were dip coated in this solution at 30 °C and dried for 20 min at 95°C. The contact angle between PHBV2 and H_2O was 80±3°. This indicates that PHBV is slightly less hydrophobic than PET. After the deposition of a seed layer through dip coating at 30 °C the affinity of PHBV2 to H_2O increased. This is determined by a decrease in the contact angle to 74±3°.

Since PET was used to optimize the deposition procedure, PHBV2 substrates with ZnO seed layer were immersed in a solution of 0.025M $Zn(NO_3)_2.6H_2O$ and 0.025M DETA at 95 °C for 4h. As shown in figure 4.5A, for PHBV2 this led to almost no deposition of ZnO. This problem was solved by substituting $Zn(NO_3)_2.6H_2O$, the Zn^{2+} source, with $Zn(CH_3COO)_2.2H_2O$ (see fig. 4.5B). Rods with a length of up to 1 µm and a diameter of 25-55 nm were formed. This could indicate that the speed of the reaction is too high for the $Zn(NO_3)_2.6H_2O$ solution

and the crystal dissolves completely. This indicates that reaction time should be decreased. Another explanation could be that only homogeneous nucleation takes place and the amount NH_3 should be decreased.

As my goal was to deposit a ZnO nanolayer on top of PHBV substrates and this was accomplished using $Zn(CH_3COO)_2.2H_2O$, the $Zn(CH_3COO)_2.2H_2O$ and DETA method was used to study the effect of ZnO on the permeability of PHBV.

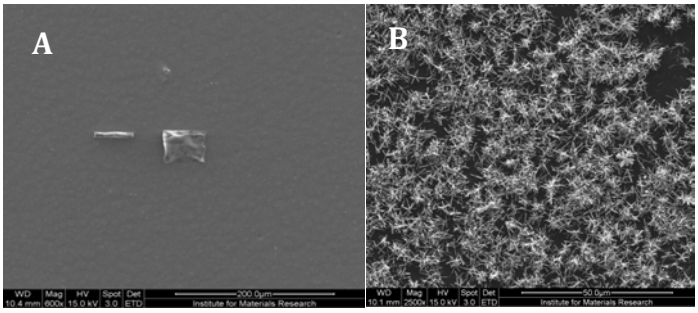

Figure 4.5: SEM image of ZnO deposition on PHBV2 with ZnO seed layer through the use of $Zn(NO_3)_2.6H_2O$ (A) and $Zn(CH_3COO)_2.2H_2O$ (B).

Conclusion 2:

1. ZnO nanoparticle layers can be deposited on PET and PHBV substrates with ZnO seed layer through CBD with DETA.

2. A minimum reaction time of 4h is necessary.

3. A minimum reaction temperature of 95°C is necessary.

4. $Zn(NO_3)_2.6H_2O$ is a better Zn-source for depositing ZnO nanoparticle layers on PET substrates.

5. $Zn(CH_3COO)_2.2H_2O$ is a better Zn-source for depositing ZnO nanoparticle layers on PHBV substrates.

4.4.2 Chemical bath deposition with HMT

4.4.2.1 Deposition of ZnO on PET substrates

PET substrates with ZnO seed layers were immersed in a solution of 0.1M $Zn(CH_3COO)_2.2H_2O$ and 0.1M HMT (99 %, Sigma Aldrich, Diegem, Belgium) in milliQ water at 95°C for 2h. The reaction time was set at 2h instead of 4h because of several reports in literature that state that ZnO layer are formed after only 1 or 2h [6, 7]. $Zn(CH_3COO)_2.2H_2O$ was used instead of $Zn(NO_3)_2.6H_2O$ because $Zn(CH_3COO)_2.2H_2O$ gave better results for PHBV2 during the DETA method. As shown in figure 4.6, ZnO nanoparticles were formed with a diameter of up to 500 nm.

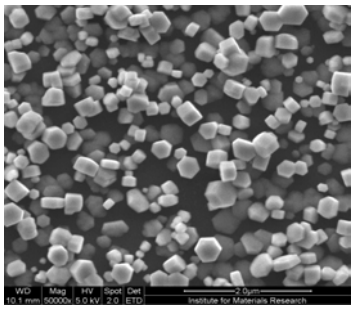

Figure 4.6: SEM image of ZnO deposition on PET with ZnO seed layer.

As mentioned in chapter 3, decreasing the Zn^{2+}:NH_3 molar ratio can decrease the diameter of the particles. Therefore, PET substrates with ZnO seed layer were immersed in solutions of 0.1M $Zn(CH_3COO)_2.2H_2O$ and 0.2M or 0.3M HMT for 2h at 95 °C. The growth of ZnO particles seemed to decrease after the increase of NH_3. This is probably due to the fact that the critical value of degree of saturation is reached, see chapter 3.

The duration of the reaction was shortened to 1 h and to 30 min, to decrease the size of the ZnO crystal. However, as shown in figure 4.7, a reaction time of 2h is necessary to fully deposit ZnO particles on the PET substrate.

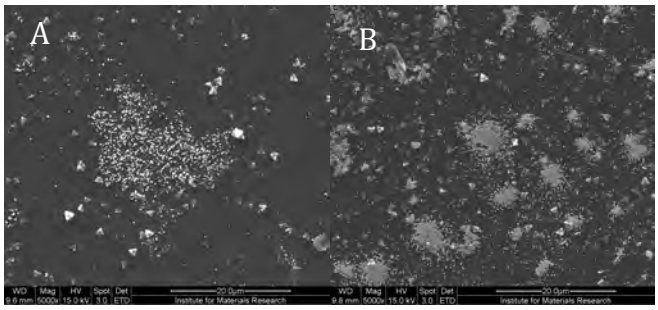

Figure 4.7: SEM images of ZnO deposition on PET with ZnO seed layer after 30 min (A) and 1h (B).

Lowering the temperature to 75°C has a negative effect on the deposition of ZnO (see fig. 4.8). Further research on the deposition at 75°C can be done by increasing the Zn^{2+} concentration or increasing the NH_3 concentration. This can determine if for the deposition of ZnO on PET a temperature of 95°C is necessary or if deposition of layers at lower temperatures is possible.

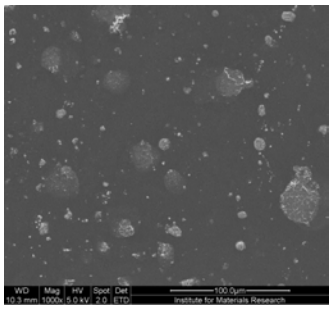

Figure 4.8: SEM images of ZnO deposition on PET with ZnO seed layer at 75°C.

Since for the DETA method deposition on the surface of PET substrates was increased using $Zn(NO_3)_2.6H_2O$ as Zn-source, the difference between using $Zn(CH_3COO)_2.2H_2O$ and $Zn(NO_3)_2.6H_2O$ as Zn-source was studied. PET substrates with ZnO seed layer were immersed in solutions of 0.1M $Zn(NO_3)_2.6H_2O$ and 0.1M HMT for 2h at 95 °C. Comparing the particles formed by using $Zn(CH_3COO)_2.2H_2O$ (fig. 4.6) and $Zn(NO_3)_2.6H_2O$ (fig. 4.9) shows that

with $Zn(NO_3)_2.6H_2O$ smaller particles are formed. The particles have a diameter of 300 nm or lower.

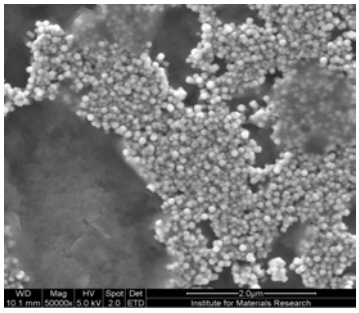

Figure 4.9: SEM image of ZnO deposition on PET with ZnO seed layer through the use of $Zn(NO_3)_2.6H_2O$.

4.4.2.2 Deposition of ZnO on PHBV2 substrates

When using $Zn(CH_3COO)_2.2H_2O$ as Zn-source, a solution of 0.1 M $Zn(CH_3COO)_2.2H_2O$ and 0.1 M HMT at 95 °C for 2h gave the best results for depositing ZnO on PET. As shown in figure 4.10A, for PHBV2, this led to the deposition of hexagonal flakes with a diameter of 100-200 nm. Since the treatment at 95 °C led to a closely packed layer, the temperature was lowered to 75 °C to see if an equally good result could be obtained. Figure 4.10 shows that a minimum of 95 °C is necessary for the deposition of a closely packed layer. The effect of using $Zn(NO_3)_2.6H_2O$ instead of $Zn(CH_3COO)_2.2H_2O$ as Zn^{2+} source was tested at 95 °C and 75 °C. Figure 4.11 shows that replacing $Zn(CH_3COO)_2.2H_2O$ with $Zn(NO_3)_2.6H_2O$ decreases the amount of ZnO that is deposited. At 95 °C a few hexagonal flakes with a diameter up to 250 nm were formed, while at 75 °C only a few spherical shaped cluster of ZnO were formed.

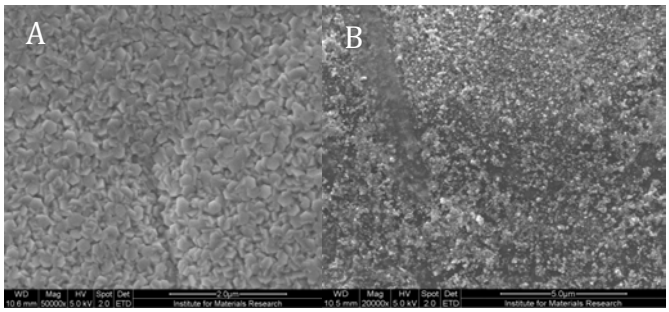

Figure 4.10: SEM images of ZnO deposition on PHBV2 with ZnO seed layer at 95°C (A) and at 75°C (B).

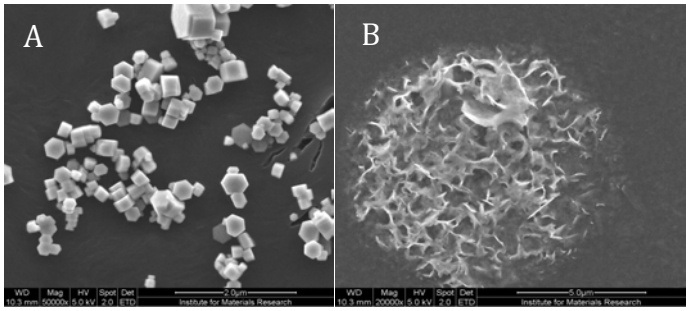

Figure 4.11: SEM images of ZnO deposition on PHBV2 with ZnO seed layer through the use of $Zn(NO_3)_2.6H_2O$ at 95°C (A) and 75°C (B).

Also for the HMT method, $Zn(CH_3COO)_2.2H_2O$ was used for the formation of the most uniform layers on PHBV. Therefore, this method was further used for the determining the influence of ZnO on the permeability of PHBV2. Since defects play a large role in the efficiency of barrier layers, the procedure of HMT 75°C was also taken into account to determine the effect of the defects in the layers.

Conclusion 3:

1. ZnO nanoparticle layers can be deposited on PET and PHBV substrates with ZnO seed layer through CBD with HMT.

2. A minimum reaction time of 2h is necessary.

3. A minimum reaction temperature of 95°C is necessary.

4. $Zn(NO_3)_2.6H_2O$ is a better Zn-source for depositing ZnO nanoparticle layers on PET substrates.

5. $Zn(CH_3COO)_2.2H_2O$ is a better Zn-source for depositing ZnO nanolayers on PHBV substrates.

General conclusion CBD:

Substrate	$Zn(CH_3COO)_2.2H_2O$ /DETA	$Zn(CH_3COO)_2.2H_2O$ /HMT	$Zn(NO_3)_2.6H_2O$ /DETA	$Zn(NO_3)_2.6H_2O$ /HMT
PHBV	+	++	--	-
PET	--	-	++	+

4.4.3 Sputtering of PHBV1 substrates

To see if the PHBV1 substrates can also be provided with a ZnO nanolayer, the sputter technique was used. As mentioned in chapter 1, sputtering provides broader coverage of the substrate and denser layers, but is more expensive than the chemical bath method. The sputtering of the ZnO nanolayers was done at SIRRIS.

For sputtering, only the samples made with Teflon plates were used. The samples were made dust-free by blowing of dust with pure dry air. The samples were taped to the machine. ZnO nanolayers were sputtered using a zinc target with a purity of 99.999 %. The substrate-target distance was kept at 8.5 cm. An Argon (Ar) -Oxygen (O_2) mixture was used as sputtering gas. Ar was introduced at a rate of 20 $ml.min^{-1}$ and O_2 at a rate of 13.8 $ml.min^{-1}$. The average supplied power was 500 W and the pulse frequency was 150 kHz. The average deposition time was 25 min. This duration is necessary to get layers of 110±10 nm thick. The maximum temperature reached during deposition was 40 °C.

The SEM images shown in figure 4.12 show uniform coverage of the PHBV1 samples. The cracks in the samples are due to the expansion coefficient of both ZnO and PHBV. The visible exfoliation is perhaps due to the scotch tape test. The adhesion of the ZnO nanolayer to the PHBV was tested using the scotch tape test.

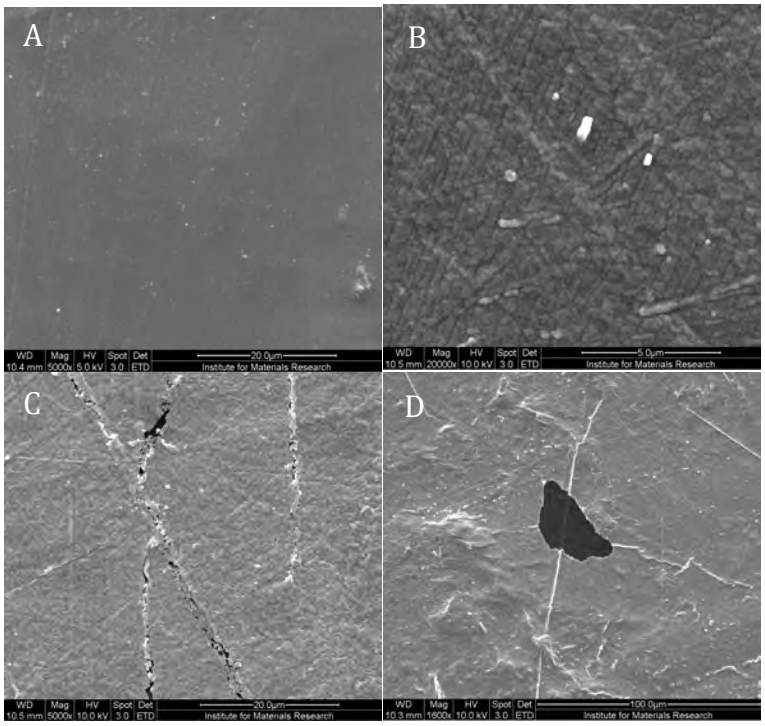

Figure 4.12: SEM images of PHBV1 (A) and PHBV1 with ZnO (B-D).

Conclusion 4:

1. For substrates with rougher surfaces, the more expensive sputter technique can be used as an alternative to deposit ZnO nanolayers.

4.5 Characterization of the ZnO nanolayer

In this paragraph, the characteristics of the ZnO nanolayers deposited on PHBV2 and PET substrates with ZnO seed layer deposited at 30 °C were studied. The ZnO nanolayers were formed using $Zn(CH_3COO)_2.2H_2O$ and 0.025M DETA at 95 °C for 4h or 0.1 M $Zn(CH_3COO)_2.2H_2O$ and 0.1 M HMT at 95 °C for 2h. The characteristics of the sputtered ZnO layer on PHBV1 substrates were also studied.

As stated in chapter 2, the thickness of the ZnO layer can play an important role in the permeability process. Thus, it is important to determine the thickness of the ZnO nanolayer.

The thickness of the ZnO layers was determined using cross-sectional SEM. The measurements were performed on an FEI Quanta 2000 FEG SEM and provided to us by the materials physics group of the UHasselt.

As shown in figure 4.13, the ZnO layers, deposited using the chemical bath methods, have a thickness between 140 and 270 nm. The thickness of the ZnO layers on PET through the use of $Zn(CH_3COO)_2.2H_2O$ and HMT couldn't be determined. The ZnO layer seemed to be too thin and increasing the magnification without deteriorating the PET substrate wasn't possible. The layers deposited on PHBV1 using the sputtering technique have a thickness of 100±10 nm.

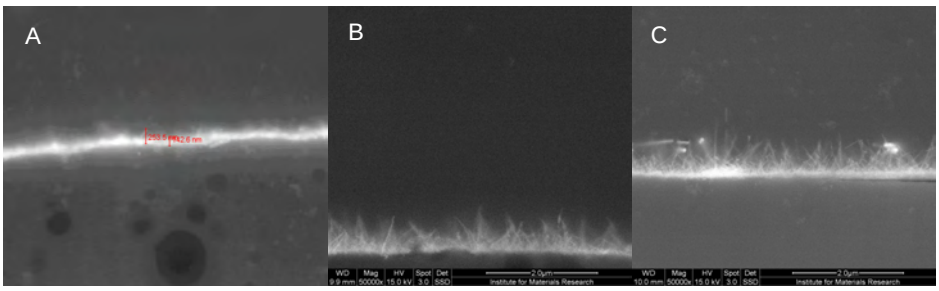

Figure 4.13: Cross-sectional SEM images of PHBV2 with ZnO nanolayers deposited through the use of $Zn(CH_3COO)_2.2H_2O$ and HMT (A) and DETA (B) and PET with ZnO nanolayers deposited through the use of $Zn(CH_3COO)_2.2H_2O$ and DETA (C).

The area of UV-transmittance can be used to characterize ZnO and give an indication whether or not the substrates are protected against UV-light.

The optical transmission measurements were carried out on a UV–VIS–NIR Varian Cary 500 spectrophotometer in the wavelength ranging from 200 nm to 800 nm.

As can be seen in figure 4.14 the chromophore groups in PHBV2 cause the polymers to strongly absorb the light up to 250 nm. PET on the other hand has more chromophore groups and strongly absorbs the light up to 310 nm (see fig. 4.15). For both PHBV2 (fig. 4.14) and PET (fig. 4.15) the area of 0% transmittance is extended to 368 nm after the deposition of the ZnO nanolayer. The absorption at 368 nm can be interpreted as an indication that ZnO is formed since this is near the absorption of bulk ZnO at 373 nm [8-10]. The extended 0% transmittance can also indicate that the addition of a ZnO layer improves the UV protection properties of the plastic. Figures 4.14 and 4.15 also show that the transmission in the region of 380 nm to 800 nm is more reduced by the HMT method for PHBV2 and by the DETA method for PET. This confirms that more dense layers are formed on PHBV2 using the HMT method and on PET using the DETA method.

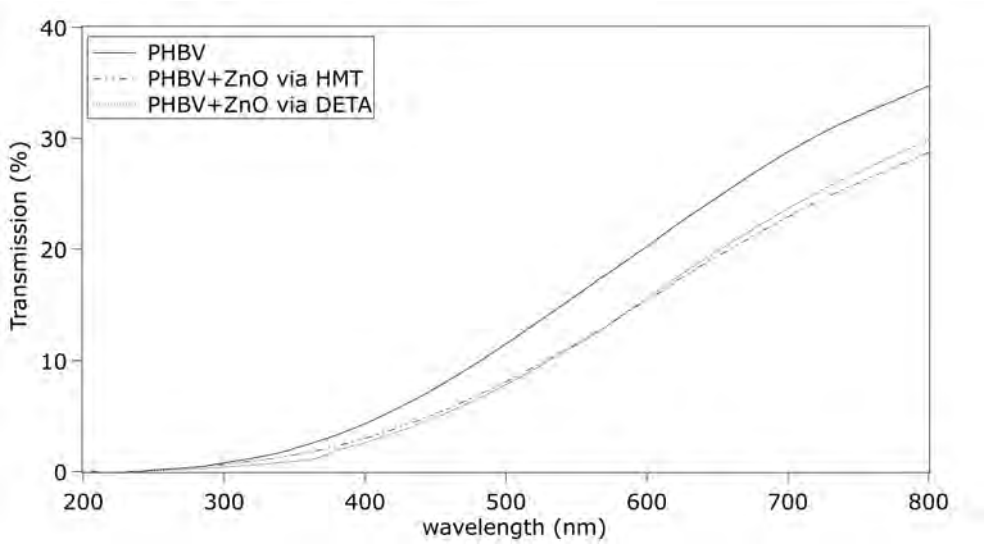

Figure 4.14: Optical transmission spectrum of PHBV2 and PHBV2 with ZnO seed layer and ZnO nanolayer.

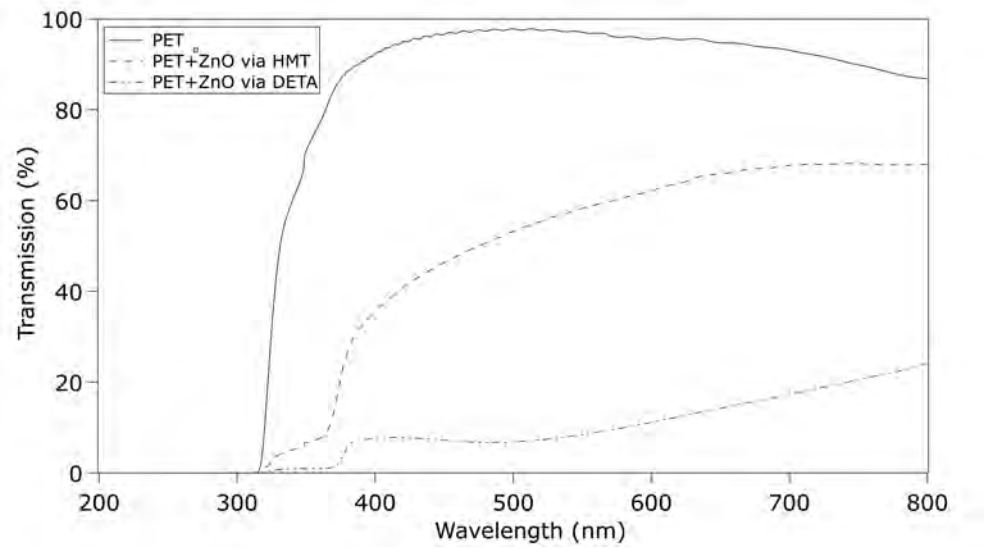

Figure 4.15: Optical transmission spectrum of PET and PET with ZnO seed layer and ZnO nanolayer.

XRD measurements were performed to characterize ZnO and to determine the crystal structure of ZnO. The crystal structure of the ZnO nanolayers was determined by X-ray diffraction (XRD) on a Siemens D-5000 diffractometer (radiation: Cu K_{a1}). The XRD diagrams were provided to us by the Materials Physics group of the UHasselt.

XRD measurements on the chemical bath substrates, showed that mostly only the diffraction peak at 34.4°, indicative for the (002) diffraction of wurtzite ZnO with a preferential orientation along the c-axis [2], appears (fig 4.16 en 4.17). Although, as shown in figure 4.18, prolonging the counting time and decreasing the step size of the measurements shows the presence of extra peaks at 31.7° and 36.3°, indicative for the (100) and (101) diffraction of the wurtzite ZnO.

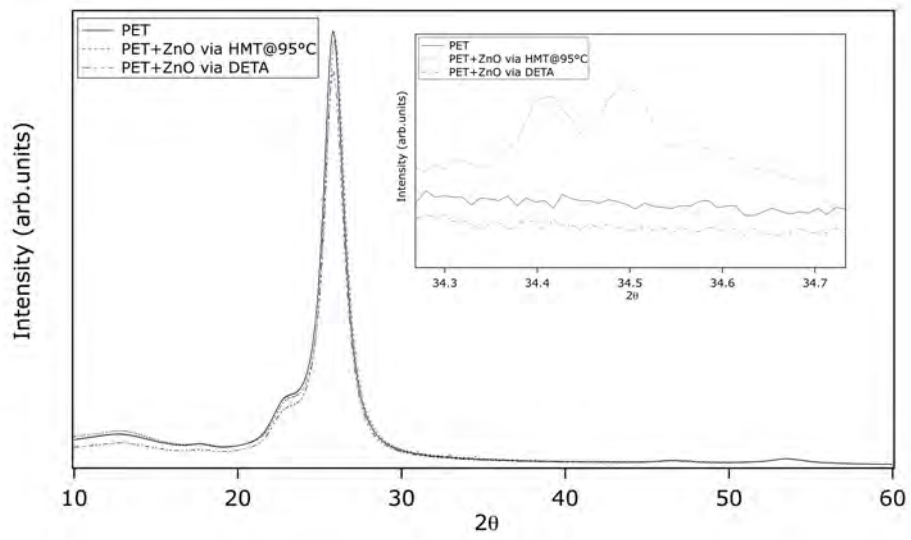

Figure 4.16: XRD pattern of PET and PET with ZnO seed layer and ZnO nanolayer.

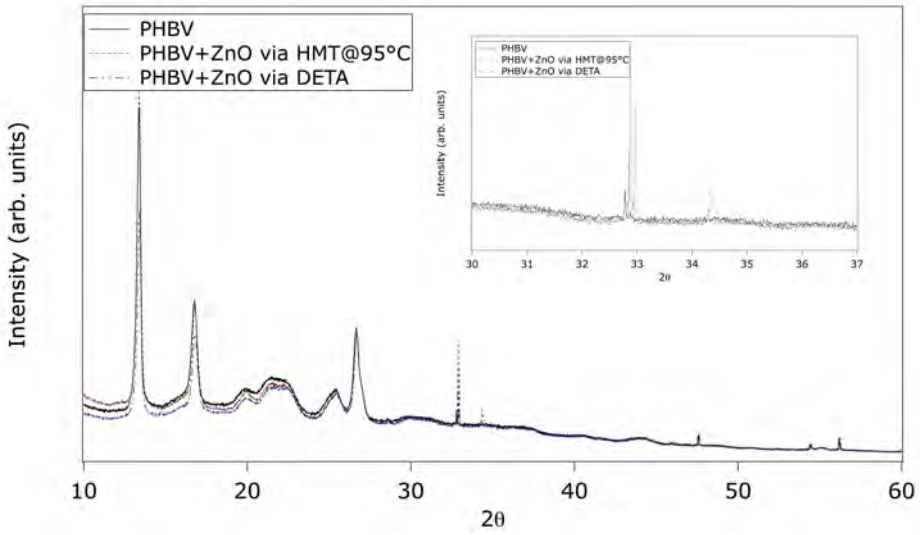

Figure 4.17: XRD pattern of PHBV2 and PHBV2 with ZnO seed layer and nanolayer.

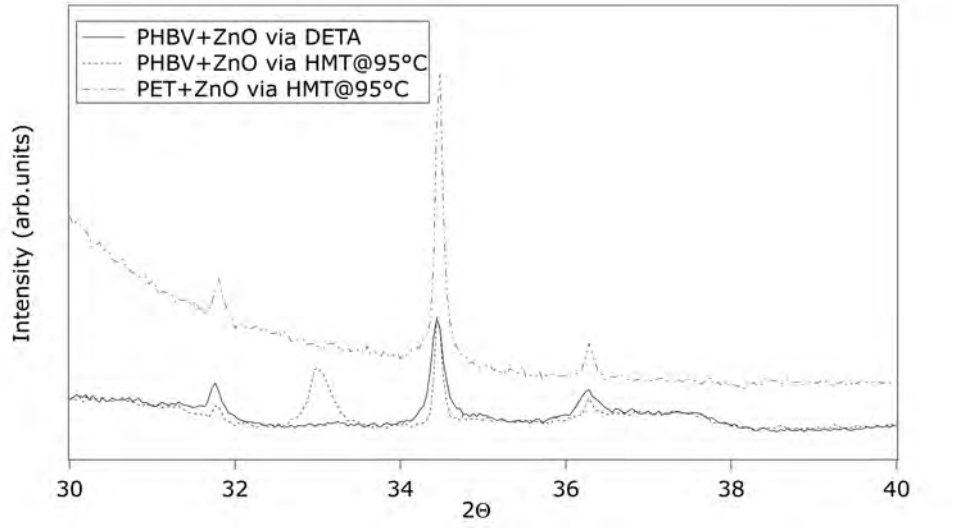

Figure 4.18: XRD pattern of PET and PHBV2 with ZnO seed layer and nanolayer using a decreased stepsize.

As shown in figure 4.19, XRD measurements of sputtered ZnO showed the formation of (002) oriented ZnO. The presence of a diffraction peak in the XRD pattern at 2θ of 34,4° is indicative for the (002) diffraction of wurtzite ZnO with a preferential orientation along the c-axis [2].

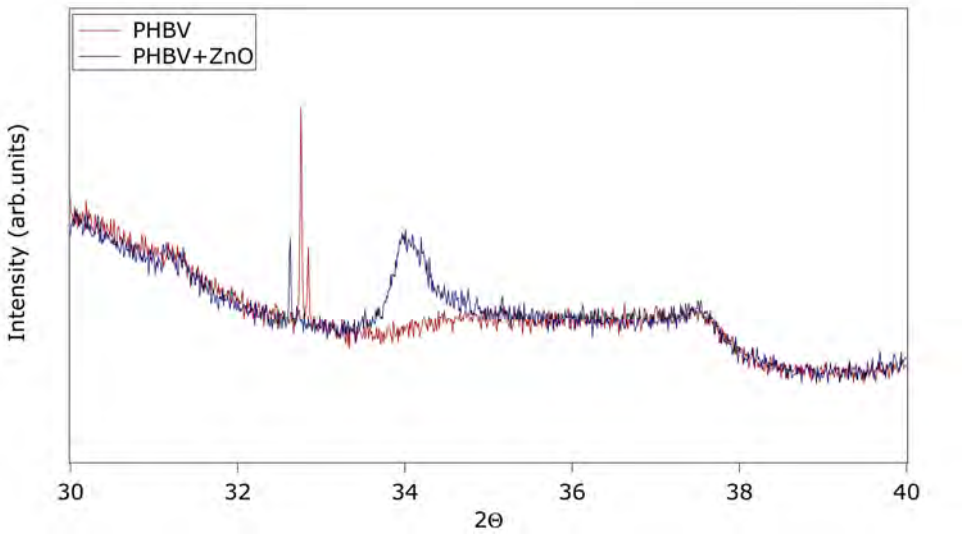

Figure 4.19: XRD of PHBV1 and PHBV1 with sputtered ZnO nanolayer.

Raman measurements were performed to identify the ZnO nanolayers. The Raman spectra of PET and PHBV2 were acquired with a Horiba Jobin Yvon T64000 confocal Raman Microscope with 244 nm excitation wavelength. According to literature, there are six Raman active modes: two E2 vibrations at 101 and 437 cm^{-1}; one transverse A1 at 381 cm^{-1} and one transverse E1 at 407 cm^{-1}; one longitudinal A1 at 574 cm^{-1} and one longitudinal E1 at 583 cm^{-1} [11, 12].

In the Raman spectra of PET (Fig. 4.20), the E_2 mode of wurtzite ZnO is shown at 438 cm^{-1} for PET with ZnO seed layer and ZnO nanolayer via the DETA and the A_1 mode at 388 cm^{-1} for PET with ZnO seed layer and ZnO nanolayer via the HMT method. Figure 4.23 shows that for PHBV2 with ZnO seed layer and ZnO via HMT both the A_1 and E_2 mode are visible, while for PHBV2 with ZnO seed layer and ZnO via DETA only the A_1 is visible.

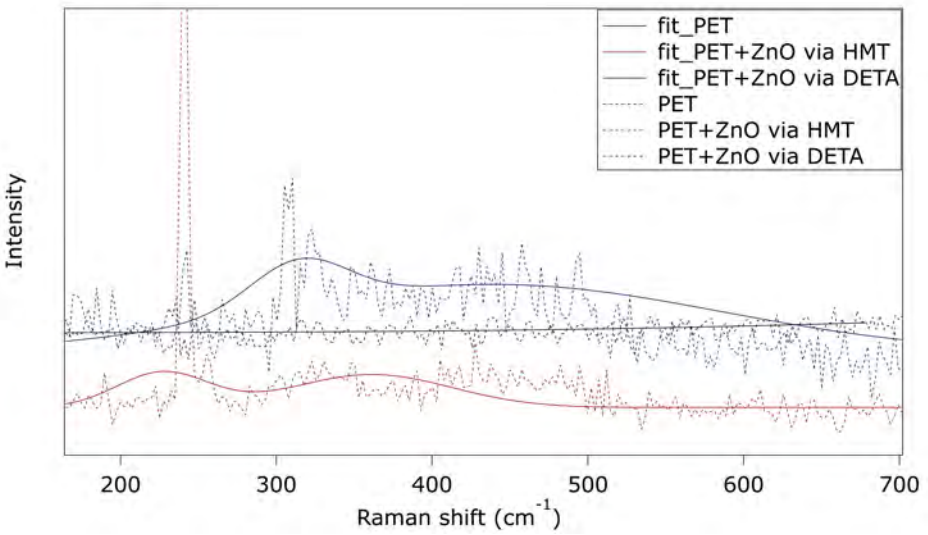

Figure 4.20: Raman spectra of PET and PET with ZnO seed layer and nanolayer.

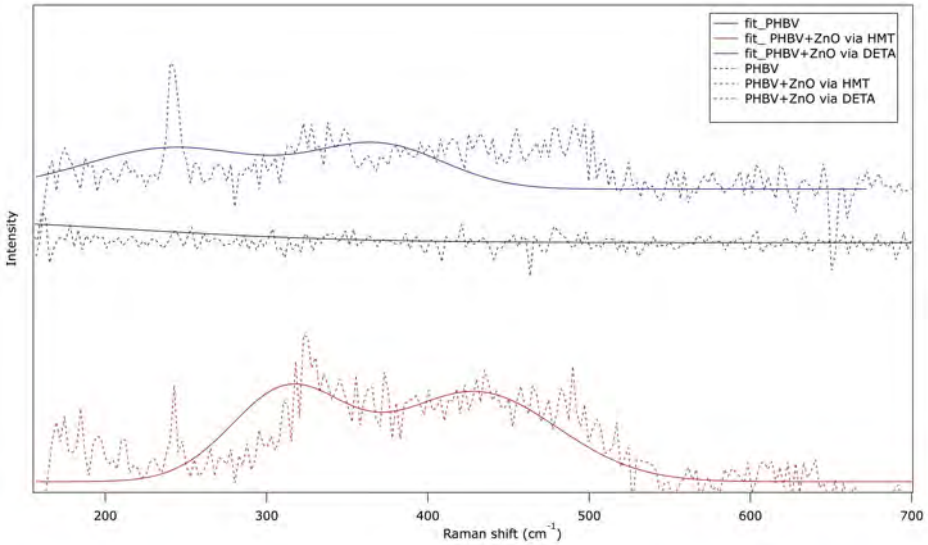

Figure 4.21: Raman spectra of PHBV2 and PHBV2 with ZnO seed layer and nanolayer.

Also to identify the ZnO nanolayer, Attenuated Total Reflectance Fourier Transform Infra Red (ATR-FTIR) spectra in the wave number range of 4000 cm^{-1} to 600 cm^{-1} were measured using a Bruker Vertex 70 Fourier transform IR spectrometer equipped with a PIKE MIRacle ATR sampling accessory with a 45° single reflection diamond/ZnSe horizontal crystal plate. The FTIR-ATR spectrum of PHBV2 with and without ZnO is shown in figure 4.22. After the addition of ZnO to PHBV2 the ratio of the symmetric (1280 cm^{-1}) and asymmetric (1260 cm^{-1}) stretching of the C-O-C bond changed. The ratio of the rocking vibration (1060 cm^{-1}) and the scissoring vibration (1040 cm^{-1}) of the CH_2 also changed. This could be an indication that the $Zn(CH_3COO)_2.2H_2O$ isn't completely transformed into ZnO [13]. Figure 4.23 shows the FTIR-ATR spectrum of PET, PET with seed layer and PET with seed layer and ZnO layer. After the addition of ZnO via the HMT and DETA method to PET with seed layer, a peak appears at 820 cm^{-1}. This peak, along with the peaks at 1623 cm^{-1} and 1597 cm^{-1}, due to the anti-symmetric COO^- stretching vibration, indicate the presence of residue from the $Zn(CH_3COO)_2.2H_2O$ precursor [14, 15]. The peaks at 1012 cm^{-1} and 999 cm^{-1} can be due to the formation of the $Zn(NH_3)_4^{2+}$-complex [16].

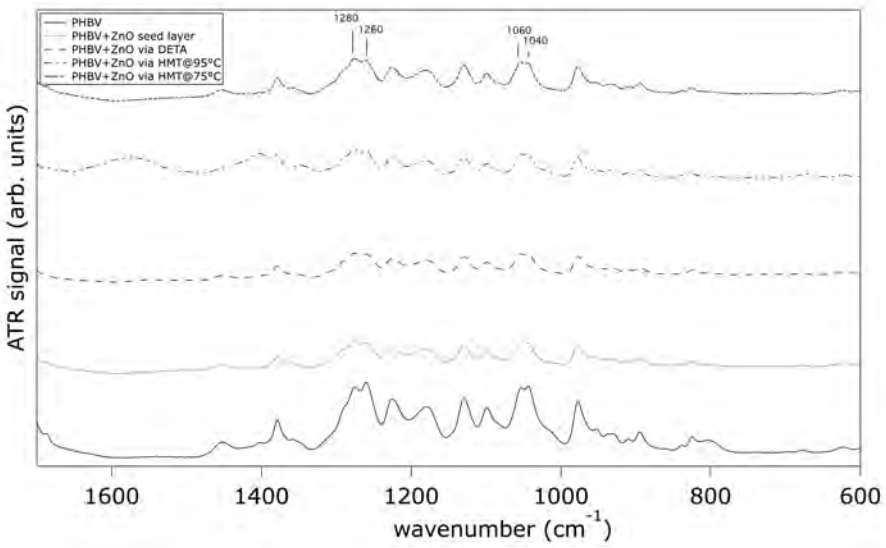

Figure 4.22: FTIR-ATR spectrum of PHBV2 with and without ZnO.

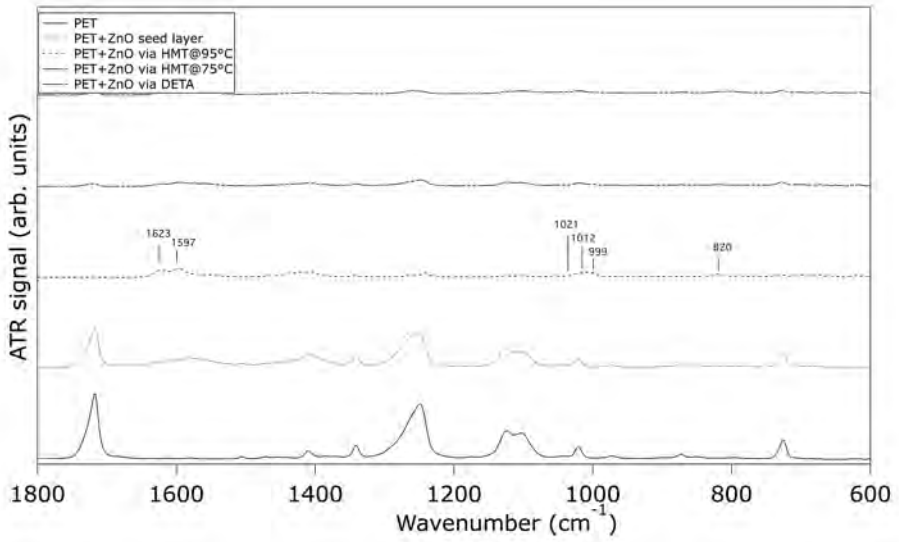

Figure 4.23: FTIR-ATR spectrum of PET with and without ZnO.

4.6 The effect of ZnO nanolayers on the physical properties of PET and PHBV

The tensile strength of the films was measured because it is an important failure criteria. The deposition of a ZnO nanolayer shouldn't decrease the tensile strength. The tensile strength (σ_{max}) was measured with a MTS/10 tensile tester using an initial speed of 5 mm/min and a 2kN load cell. Samples were prepared with a width of 6 mm and measured in a conditioned atmosphere of 23 °C and 50% RH. For each different type of sample the measurements were repeated in fivefold.

Table 4.2: The tensile strength of PET and PHBV with and without ZnO.

Substrate	σ_{max} (MPa)	Substrate	σ_{max} (MPa)
PET	149±13	**PHBV2**	13±3
PET + ZnO Seed Layer	154±23	**PHBV2 + ZnO Seed Layer**	14±6
PET + ZnO via DETA	158±10	**PHBV2 + ZnO via DETA**	17±7
PET + ZnO via HMT@95°C	146±8	**PHBV2 + ZnO via HMT@95°C**	15±2
PHBV1	19.9±0.6	**PHBV1+ ZnO**	19.8±0.5

First the tensile strength (σ_{max}) of PET and PHBV2 without and with ZnO via the chemical bath method was determined. Pure PET had a tensile strength (σ_{max}) of 149±13 MPa and PHBV2 had a tensile strength of 13±3 MPa. The tensile strength of PET and PHBV2 didn't seem to be influenced by the deposition of ZnO on the surface. PET and PHBV2 with ZnO seed layer had a tensile strength of 154±23 MPa and 14±6 MPa, respectively. PET and PHBV2 with seed layer and ZnO nanolayer via the DETA method had a tensile strength of 158±10 MPa and 17±7 MPa. PET and PHBV2 with seed layer and ZnO nanolayer via the HMT method had a tensile strength of 146±8 MPa and 15±2 MPa, respectively.

PHBV1 substrates with sputtered ZnO layers also don't lose their strength after the addition of ZnO. Pure PHBV1 had a tensile strength of 19.9±0.6 MPa and PHBV1 with ZnO nanolayer had a tensile strength of 19.8±0.5 MPa.

The GPC measurements were done using a GPC apparatus composed of a SpectroSeries P100 pump, equipped with a Shodex RI71 refractometer detector and two PL-gel 10 µ Mixed-B columns in series, thermostated at 35 °C. The eluent was chloroform (VWR, HPLC grade) at a flow rate of 1.0 ml/min. The samples were dissolved in chloroform at a concentration of 1 g/l. The injection volume was 100 µl.

That the tensile strength isn't influenced by the addition of ZnO can be linked to the gel permeation chromatography (GPC) measurements of PHBV2. The tensile strength is related to the number-average molecular weight as follows [17]:

$$\sigma_{max} = \sigma_{\infty} - \frac{a}{M_n} \quad (4.1)$$

Where σ_{∞} is the limiting tensile strength at infinite polymer chain length and a is a constant. The tensile strength starts at a low value and eventually saturates at a high value that is characteristic for infinite or very large molecular weight [17]. Thus, that the tensile strength doesn't change can be due to the high number-average molecular weights of 85 000 – 112 000 $g.mol^{-1}$, shown in figure 4.24. The weight-average molecular weight (M_w) of PHBV2 increased after the addition of ZnO, as did the number-average molecular weight. This can indicate the formation pf Zn-O-C covalent bonds. Many reports of the formation of metal-O-C covalent bonds after the deposition of metal oxide coatings on PET can be found [18, 19].

The polydispersity (D), the ratio of the weight-average molecular weight to the number-average molecular weight, decreases (fig. 4.25). This means that the molecular weight distribution curve becomes smaller and that the approximate chain lengths of the polymer chains are more uniform.

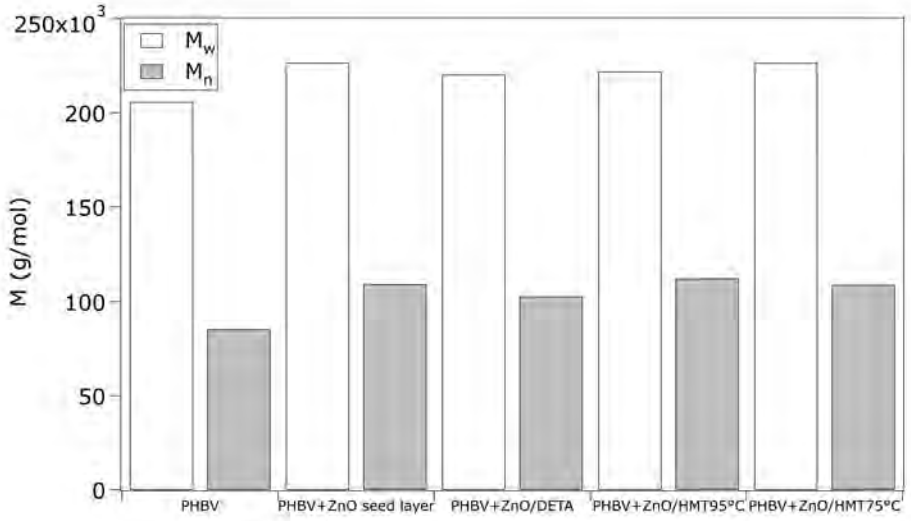

Figure 4.24: The weight-average molecular weight and number-average molecular weight of PHBV2 and PHBV2 with ZnO.

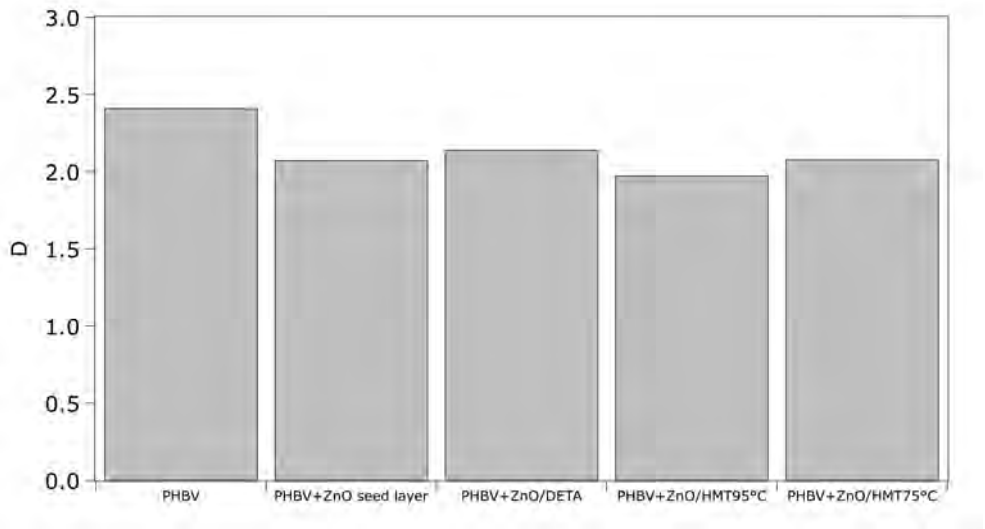

Figure 4.25: Polydispersity of PHBV2 and PHBV2 with ZnO.

Thermal analysis is important to indicate changes in the compositional and structural parameters of the polymer. TGA and DSC show that the thermal

stability of PET and PHBV isn't influenced by the addition of ZnO.

The TGA measurements were done on a horizontal TGA. The temperature was increased from room temperature to 300°C for PHBV2 and to 500°C for PET at 20°C/min. Thermogravimetric analysis (TGA) of PET and PHBV2 with and without ZnO show no decrease or increase in the decomposition temperature (T_d) (table 4.3 and 4.4). The decomposition temperature (T_d) of PHBV is 295±3°C and PHBV with ZnO has a value between 279±5°C and 292±1 °C. The T_d of PET is 421±3 °C and the T_d of PET with ZnO has a value between 423±2 °C and 430±6 °C.

DSC measurements were performed under nitrogen flow by using a DSC Q200 (TA Instruments), calibrated with Indium 99.999%. A first heating ramp of 10°C/min from room temperature to 200°C was followed by a cooling ramp of 20°C/min down to 25°C to eliminate differences in thermal history. Then two analogous cycles were performed.

The differential scanning calorimetry (DSC) measurements, shown in table 4.3 and 4.4, do not show a shift in the melting temperature (T_m) and the percentage crystallinity (%χ) of the polymers, this is in agreement with the tensile strength measurements. A DSC thermogram of PHBV2 with and without ZnO is shown in figure 4.26. The T_{m1} values of PHBV2 and PHBV2 with ZnO are between 147°C and 152 °C and the T_{m2} are between 157°C and 162°C.

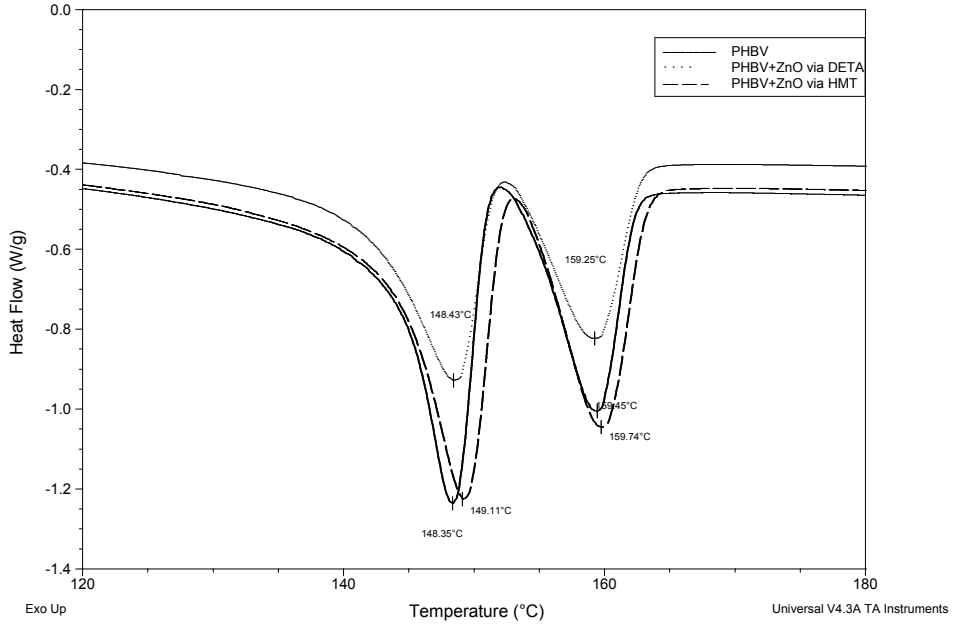

Figure 4.26: DSC thermogram of PHBV2 and PHBV2 with ZnO

The T_m value of PET can be found between 252°C and 258°C. With an $\Delta H_f°$ value of 140 J/g for PET and a value of 146 J/g for PHBV the percentage of crystallinity can be determined as follows [20]:

$$\%\text{Crystallinity} = \frac{\Delta H_f^{obs}}{\Delta H_f^{\circ}} \times 100\% \qquad (4.2)$$

Where: ΔH_f^{obs} is the observed formation enthalpy of the sample during the second cycle and ΔH_f° is the enthalpy of formation of a 100% crystalline sample of the same polymer.

The 146 J/g was chosen because PHBV2 only contains a small amount of valerate (8%), for PHBV with 12% and higher mostly 109 J/g is chosen. The percentage crystallinity (%χ) of PHBV has a value of 50±7 % and PHBV with ZnO has a value between 37±6 % and 53±6 %. PET has a crystallinity

percentage of 37±3 % and PET with ZnO has a value between 39±3 % and 43±5 %.

Table 4.3: The thermal characteristics of PET with and without ZnO.

Substrate	T_d (°C)	T_m (°C)	%χ
PET	421±3	252±3	37±3
PET + ZnO Seed Layer	424±6	252±5	43±5
PET + ZnO via DETA	423±2	258±2	39±3
PET + ZnO via HMT@95°C	430±6	253±1	41±5
PET + ZnO via HMT@75°C	423±2	255±5	43±2

Table 4.4: The thermal characteristics of PHBV2 with and without ZnO.

Substrate	T_d (°C)	T_{m1} (°C)	T_{m2} (°C)	%χ
PHBV2	295±3	148.2±0.3	159.2±0.2	50±7
PHBV2 + ZnO Seed Layer	279±5°C	147±1	158±1	50±6
PHBV2 + ZnO via DETA	279±3°C	150.2±0.9	160.7±0.7	53±6
PHBV2 + ZnO via HMT@95°C	282±3°C	149±1	160.2±0.9	43±8
PHBV2 + ZnO via HMT@75°C	292±1°C	150.3±0.6	160.8±0.6	37±6

4.7 Conclusion

The first aim was to deposit ZnO nanoparticle layers on the surface of PHBV substrates. This goal was reached.

ZnO nanoparticle layers can be deposited on top of PHBV substrates using the chemical bath and sputtering method. Though, rough surfaces make it difficult

to deposit ZnO using the chemical bath method. In this case, the more expensive sputter technique is a possible alternative.

To be able to deposit full-grown ZnO layers, it is necessary to enhance the polarity of PET and PHBV. This can be done by the deposition of a seed layer. The seed layer can be deposited using a solution of 0.03M NaOH and 0.01 M $Zn(CH_3COO)_2.2H_2O$. A minimum of 30°C is necessary to deposit ZnO seeds on PET and PHBV2 substrates.

The most dense layers for PHBV2 were formed using $Zn(CH_3COO)_2.2H_2O$ and HMT at 95 °C (table 4.5). For PET the most dense layers are formed using $Zn(NO_3)_2.6H_2O$ and DETA (table 4.5).

The mixture of DETA and $Zn(NO_3)_2.6H_2O$ has a pH of 8.4 before the deposition and a pH of 6.9 after the deposition. While the mixture of HMT and $Zn(CH_3COO)_2.2H_2O$ has a pH of 6.5 before the deposition and a pH of 5.8 after the deposition. $Zn(NO_3)_2.6H_2O$ solutions have a lower basicity. The reaction speed increases with increasing basicity and makes a part of the crystals dissolve in the solution. Probably the reaction rate is too high when depositing ZnO on PHBV substrate with $Zn(NO_3)_2.6H_2O$ solution. Decreasing the pH could improve the deposition of ZnO on PHBV2 using $Zn(NO_3)_2.6H_2O$. The pH can be decreased by decreasing the amount of DETA or HMT. For PET, the $Zn(CH_3COO)_2.2H_2O$ solutions need a higher basicity, increasing the pH could improve the deposition of ZnO on PET using $Zn(CH_3COO)_2.2H_2O$. Increasing the amount of HMT or DETA is a possible solution.

Table 4.5: Summary of the chemical bath deposition of ZnO.

Substrate	$Zn(CH_3COO)_2.2H_2O$ /DETA	$Zn(CH_3COO)_2.2H_2O$ /HMT	$Zn(NO_3)_2.6H_2O$ /DETA	$Zn(NO_3)_2.6H_2O$ /HMT
PHBV2	+	++	--	-
PET	--	-	++	+

The ZnO layers deposited using the chemical bath method have a thickness between 140 and 270 nm and the ZnO layers, deposited using the sputter technique, have a thickness of approximately 100 nm. In all the methods wurtzite ZnO with a preferential orientation along the c-axis was formed. The formation of the ZnO nanolayer left the mechanical and thermal properties of the plastics intact and extended their UV absorption to a longer wavelength. This opens opportunities for extended lifespan of the packaging material and improved protection of the packed food by the packaging material against UV radiation.

4.8 References

[1] S.H. Yi, S.K. Choi, J.M. Jang, J.A. Kim, W.G. Jung, Low-temperature growth of ZnO nanorods by chemical bath deposition, J. Colloid Interface Sci., 313 (2007) 705-710.

[2] R. Shabannia, H. Abu-Hassan, Vertically aligned ZnO nanorods synthesized using chemical bath deposition method on seed-layer ZnO/polyethylene naphthalate (PEN) substrates, Mater. Lett., 90 (2013) 156-158.

[3] M. Willander, Zinc Oxide Nanostructures: Advances and Applications, CRC Press, US, 2014.

[4] N.R. Yogamalar, A.C. Bose, Tuning the aspect ratio of hydrothermally grown ZnO by choice of precursor, J Solid State Chem, 184 (2011) 12-20.

[5] R.C. Pawar, H. Kim, C.S. Lee, Defect-controlled growth of ZnO nanostructures using its different zinc precursors and their application for effective photodegradation, Curr. Appl. Phys., 14 (2014) 621-629.

[6] D.S. Boyle, K. Govender, P. O'Brien, Novel low temperature solution deposition of perpendicularly oriented rods of ZnO: substrate effects and evidence of the importance of counter-ions in the control of crystallite growth (vol 15, pg 80, 2002), Chem Commun, (2002) 1651-1651.

[7] S. Mridha, D. Basak, Effect of concentration of hexamethylene tetramine on the structural morphology and optical properties of ZnO microrods grown by low-temperature solution approach, Phys Status Solidi A, 206 (2009) 1515-1519.

[8] J.Q. He, W. Shao, L. Zhang, C. Deng, C.Z. Li, Crystallization Behavior and UV-Protection Property of PET-ZnO Nanocomposites Prepared by In Situ Polymerization, J Appl Polym Sci, 114 (2009) 1303-1311.

[9] S. Ameen, M.S. Akhtar, H.S. Shin, Growth and characterization of nanospikes decorated ZnO sheets and their solar cell application, Chem Eng J, 195 (2012) 307-313.

[10] L. Armelao, M. Fabrizio, S. Gialanella, F. Zordan, Sol-gel synthesis and characterisation of ZnO-based nanosystems, Thin Solid Films, 394 (2001) 90-96.

[11] R. Cusco, E. Alarcon-Llado, J. Ibanez, L. Artus, J. Jimenez, B.G. Wang, M.J. Callahan, Temperature dependence of raman scattering in ZnO, Phys Rev B, 75 (2007).

[12] C.M.S. Izumi, M.L.A. Temperini, FT-Raman investigation of biodegradable polymers: Poly(3-hydroxybutyrate) and poly(3-hydroxybutyrate-co-3-hydroxyvalerate), Vib Spectrosc, 54 (2010) 127-132.

[13] R. Naphade, J. Jog, Electrospinning of PHBV/ZnO Membranes: Structure and Properties, Fiber Polym, 13 (2012) 692-697.

[14] E. Reverchon, G. Della Porta, D. Sannino, P. Ciambelli, Supercritical antisolvent precipitation of nanoparticles of a zinc oxide precursor, Powder Technol, 102 (1999) 127-134.

[15] A. Bragaru, M. Kusko, E. Vasile, M. Simion, M. Danila, T. Ignat, I. Mihalache, R. Pascu, F. Craciunoiu, Analytical characterization of engineered ZnO nanoparticles relevant for hazard assessment, J. Nanopart. Res., 15 (2013).

[16] K.M. McPeak, T.P. Le, N.G. Britton, Z.S. Nickolov, Y.A. Elabd, J.B. Baxter, Chemical Bath Deposition of ZnO Nanowires at Near-Neutral pH Conditions without Hexamethylenetetramine (HMTA): Understanding the Role of HMTA in ZnO Nanowire Growth, Langmuir, 27 (2011) 3672-3677.

[17] B.S. Mitchell, An Introduction to Materials Engineering and Science for Chemical and Materials Engineers John Wiley & Sons, Hoboken, 2004.

[18] Y. Leterrier, Durability of nanosized oxygen-barrier coatings on polymers - Internal stresses, Prog Mater Sci, 48 (2003) 1-55.

[19] P.F. S. Ben Amor; M. Jacquet, Michel Nardin, XPS characterisation of plasma treated and zinc oxide coated PET, Appl. Surf. Sci., 255 (2009) 5025-5061.

[20] X.J. Wang, Z.F. Chen, X.Y. Chen, J.Y. Pan, K.T. Xu, Miscibility, Crystallization Kinetics, and Mechanical Properties of Poly(3-hydroxybutyrate-co-3-hydroxyvalerate)(PHBV)/Poly(3-hydroxybutyrate-co-4-hydroxybutyrate)(P3/4HB) Blends, J Appl Polym Sci, 117 (2010) 838-848.

Chapter 5

The influence of a ZnO Nanoparticle Layer on the Permeability of PHBV and PET

5.1 Introduction

The second goal of my thesis was to improve the gas barrier properties of PHBV through the application of ZnO nanoparticle layers. Through the measurements of the oxygen, carbon dioxide and water vapour permeability, the influence of ZnO on the gas barrier properties of PHBV was tested.

The first hypothesis was: the deposition of ZnO nanoparticles improves the gas barrier of PHBV. Either the impermeable ZnO will prolong the tortuous path of the permeating gas molecules or ZnO will adsorb the permeating oxygen.

The second hypothesis was: more ZnO leads to a more improved gas barrier. More ZnO prolongs the route even more and will also increase the adsorption of oxygen.

5.2 Oxygen permeability (P_{O2})

The oxygen transmission rate (TR_{O2}) was measured according to the procedure described in ASTM D 3985 [1]. This method is considered to be a steady state, isostatic method using a coulometric sensor. As shown in figure 5.1, PHBV and PET substrates were placed between 2 aluminum foil masks with an open circular testing area of 5 cm^2. This surface area was determined after testing with different surface areas from 1 to 5 cm^2. Measurements at 5 cm^2 showed the smallest standard deviation. To prevent oxygen loss at the edges, the outside border of the 5cm^2 circle was glued. The test samples were put into a permeation cell. The permeation cell consists out of 2 chambers divided by the sample (Fig. 5.2). On one side of the sample O_2 gas passes and on the other

side nitrogen (N_2) gas passes. Oxygen permeates through the film entering the N_2 stream. This mixture of O_2 and N_2 gas leaves the chamber and passes through the coulometric sensor where the oxygen is measured.

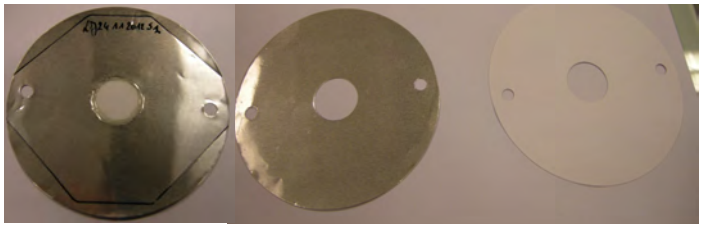

Figure 5.1: Samples prepared for permeability measurements.

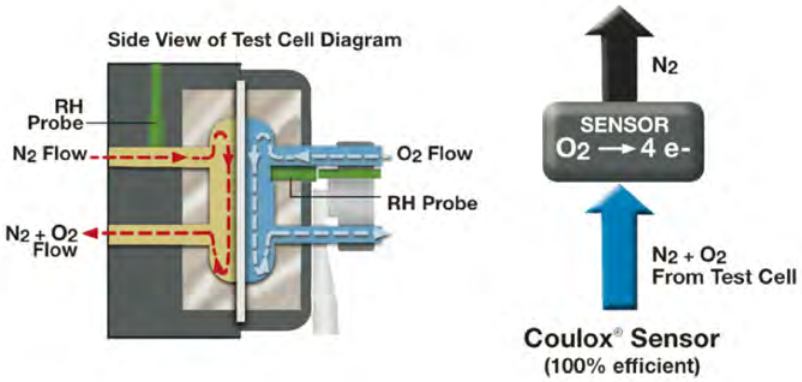

Figure 5.2: Schematic overview of an oxygen transmission test [2].

The OXTRAN module 702 and module 2/21 from MOCON were used to measure the $TR_{O2.}$ The samples were conditioned for 5 h at controlled temperature of and relative humidity (RH). The TR_{O2} was multiplied by the thickness of the samples to determine the permeability coefficient of O_2 (P_{O2}). The ZnO layers were deposited according to the methods described in chapter 4.

5.2.1 P_{O2} of PHBV and PHBV with ZnO

5.2.1.1 P_{O2} of PHBV2 and PHBV2 with ZnO

These measurements were carried out on the OXTRAN module 702. The TR_{O2} test range for this instrument is from 0.1 cc/(m^2.day) to 2000 cc/(m^2.day). Each sample was measured twice and for each type of measurement five samples were measured at 23 °C and 0% RH. An analysis of variance (ANOVA) was used to determine if there is a difference in means between the different groups. The calculated F-value of 100.55267 is higher than the F_{crit}-value of 4.05845, this indicates that there is a difference between the means. Also the p value was with 1.10^{-10} much lower than 0.05. To determine which means differ the T-test was used. The T-test assesses whether the means of two groups are statistically different from each other. The calculated P-levels are shown in table 5.1. A P-value below 0.05 indicates a significant difference. The calculated P-values show that the P_{O2} of PHBV2 differs significant from the P_{O2} of PHBV2 with ZnO.

Table 5.1: Via T-test calculated P-values for PHBV2 substrates

T-test p-level	*PHBV2+ ZnO seed layer*	*PHBV2+ ZnO seed layer +DETA*	*PHBV2+ ZnO seed layer +HMT 95°C*	*PHBV2+ ZnO seed layer +HMT 75°C*
PHBV2	0,00159	0,000001	1,21E-08	2,93E-09
PHBV2+ ZnO seed layer		0,4364	0,24664	0,43653
PHBV2+ ZnO seed layer +DETA			0,0642	0,5
PHBV2+ ZnO seed layer +HMT 95°C				0,01858
PHBV2+ ZnO seed layer +HMT 75°C				

As shown in figure 5.3, the P_{O2} of PHBV2 has a value of 13.9±0.6 cc.mm/(m^2.day.atm). This is higher than the value of 4.9 cc.mm/(m^2.day.atm) described in chapter 2 for PHBV with 8% valerate [3]. As discussed in chapter 2 this can be due to the production process. Plasticizers, such as PEG, can increase the permeability [4]. The presence of PEG has been confirmed by the GPC measurements. Figure 5.3 shows that the P_{O2} of PHBV2 decreases with

57±7 %, from 13.9±0.6 cc.mm/(m^2.day.atm) to 6±1 cc.mm/(m^2.day.atm), after the deposition of only a seed layer. The decrease in P_{O2} of PHBV2 with only a ZnO seed layer might be explained through ZnO seeds that fill up the surface pores of the PHBV2 substrate surface and lengthen the diffusion path of the oxygen particles through the polymer.

The p-values calculated via the T-test indicate no significant difference between PHBV2 with ZnO seed layer and PHBV2 with fully-grown ZnO nanoparticle layers. Figure 5.3 shows that the P_{O2} stays in the range of 5.5-6.4 cc.mm/(m^2.day.atm) for the chemical bath procedures with either HMT or DETA. This means that the hypothesis that more ZnO leads to a higher decrease in permeability doesn't stand. These observations also indicate that the adsorption of oxygen through ZnO isn't as outspoken as first thought. Above all else, the decrease in oxygen permeability can be explained by the tortuous path theory.

As indicated by the surface characterization in chapter 4, the PHBV2 substrates with ZnO nanoparticle layer are covered with nanoparticles nevertheless there are very small areas that are not covered by the ZnO nanoparticles. These areas without additional ZnO coverage might explain why the permeability doesn't decrease further after the formation of ZnO nanoparticle layers on top of the ZnO seed layers. As explained in chapter 2, defects in oxide layers, such as pinholes and cracks, often increase the permeability of layers [5, 6]. The T-test indicates that there is a difference between PHBV2 with ZnO via HMT 95°C and PHBV2 with ZnO via HMT 75°C. This supports the observations in chapter 4.3.2 that lowering the temperature of the HMT bath has a negative effect on the growth of the ZnO nanoparticle layer. However, the opposite effect is shown in figure 5.3 that shows a lower permeability coefficient for the HMT 75°C method. An explanation can be that a treatment at lower temperature has less influence on the PHBV substrate itself.

The barrier improvement factor (BIF) of the substrates is given in table 5.2. BIF is the ratio of the P_{O2} of the uncoated PHBV2 to coated PHBV2. To increase the BIF factor, the ZnO nanoparticle layers should be enhanced as discussed in chapter 4.

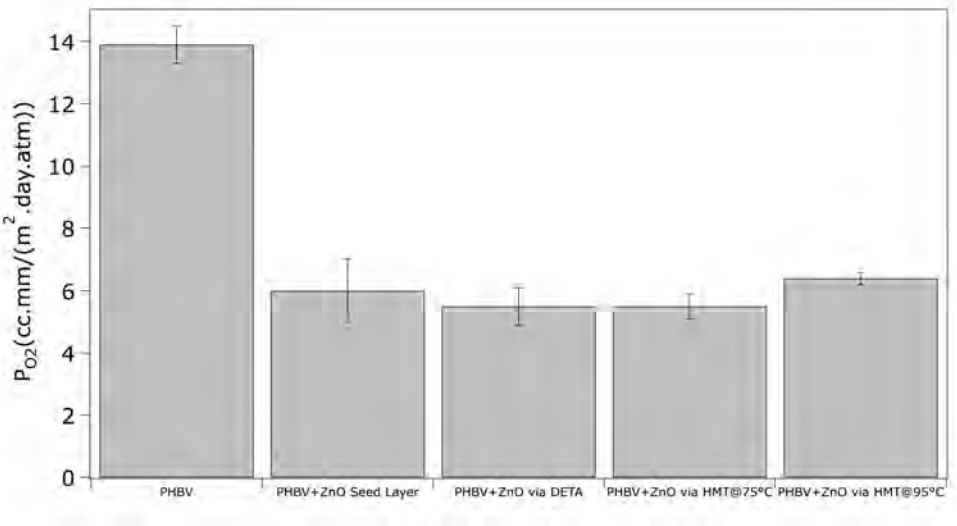

Figure 5.3: Oxygen permeability of PHBV and PHBV with ZnO.

Table 5.2: The O_2 barrier improvement factor of PHBV with ZnO.

	PHBV+ZnO Seed Layer	PHBV+ZnO via DETA	PHBV+ZnO via HMT@75°C	PHBV+ZnO via HMT@95°C
BIF	2.3	2.5	2.5	2.2

5.2.1.2 P_{O2} of PHBV1 and PHBV1 with ZnO

Sputtering the ZnO nanolayers on top of PHBV1 improves the oxygen barrier with 124.6±0.8 %. PHBV1 has a P_{O2} of 6.1±0.6 cc.mm/(m^2.day.atm) and PHBV1 with ZnO nanolayer has a P_{O2} of 4.6±0.2 cc.mm/(m^2.day.atm). A T-test analysis showed a p-level of 0.047, indicating a significant difference. The BIF factor has a value of 1.3. The reduction of P_{O2} is lower than the 38% obtained by sol gel deposition of ZnO. However, PHBV1 is ten times as thick as the PHBV2 and the permeability of a coated substrate is not completely independent of the thickness of the substrate. Very thick substrates are able to reach the same permeability as the coated substrates [7]. The ZnO nanolayer, deposited through sputtering, is approximately 100 nm thick, while using the sol gel

method the ZnO layer is between 140 and 270 nm. As is proven in literature, a thicker inorganic nanolayer decreases the permeability more. For instance, a hydrocarbon-like coating of 100 nm on PHBV has an O_2 BIF value of 1.4, while a layer of 150 nm has a BIF value of 2.7 [8]. If is assumed that the factor x_c/P_c in equation 2.17 in chapter 2 is a constant, then can be calculated, that for PHBV1 a BIF factor of 2.7 is acquired after the deposition of a 400 nm ZnO nanolayer through sputtering. This means that 0.08% of the total sample is ZnO layer. Probably the value is even lower, because increasing the thickness of the coating decreases the permeability of the coating, thus increasing the x_c/P_c value. The 0.08% is lower than the 0.3% of the total sample when depositing ZnO nanoparticle layers of 140 nm on PHBV2 using the chemical bath method. However, considering the fact that for the chemical bath method the seed layer improves the oxygen barrier and the seed layer is not thicker than 20 nm, less than 0.04% of the total sample should be ZnO to obtain a BIF factor of 2.7 using the chemical bath method. This indicates that improving the chemical bath method can increase the barrier properties of the ZnO layer even more.

5.2.1.3 Evaluation results

Comparing permeability results with literature is very difficult. There is no research found on the effect of ZnO nanoparticle layers on the permeability of PHBV. Therefore, the results couldn't be verified with other results. However the 57±7 % decrease in the P_{O2} of PHBV after the addition of ZnO nanoparticle layers through chemical bath deposition is much better than the decrease of 35 % in PHBV/ZnO nanocomposites found in literature [9]. This shows that the deposition of a ZnO nanoparticle layer has a stronger effect on the P_{O2} than the addition of ZnO nanoparticles to the polymer matrix. Comparing these results with results from other research on improving the O_2 barrier of PHBV also shows that adding a ZnO nanoparticle layer is a very effective technique. For instance, a hydrocarbon-like coating on PHBV has an O_2 BIF value of 1.4 for a 100 nm coating [8]. This is comparable with the BIF factor found using sputtering. The addition of zein interlayers improved the O_2 barrier with not more than 48 % [10]. Addition of clay particles improved the O_2 barrier with only 32 % [11]. Only composites of PHBV and bacterial cellulose whiskers show a better result of

68 % [12]. However, characterization of the ZnO nanoparticle layers formed through DETA or HMT showed that there is room for improvement in the formation of the layers. Improving the density of the ZnO layer would lead to even better results. Sputtering a ZnO layer of 12.5 nm on top of a 12.5 µm thick PEN sample resulted in an O_2 BIF of 8 [13].

Conclusion 1:

1. ***Hypothesis 1 is confirmed for the oxygen barrier of PHBV2: the addition of a ZnO nanoparticles to PHBV2 improves the oxygen barrier of PHBV2.***
2. ***Hypothesis 2 was not confirmed: more ZnO didn't lead to better oxygen barrier properties.***

5.2.2 P_{O2} of PET and PET with ZnO

These measurements were performed on the OXTRAN module 702 at 23 °C and 0% RH. Pure PET has a P_{O2} of 2.1±0.1 cc.mm/(m^2.day.atm). This is similar to the literature values of 1 to 5 cc.mm/(m^2.day.atm) [14] and lower than the P_{O2} of pure PHBV. The aromatic rings (Fig. 5.4) in the polymer chain reduce the free volume and chain mobility. Therefore, PET has less free volume than PHBV (chapter 2) and has higher barrier properties [15].

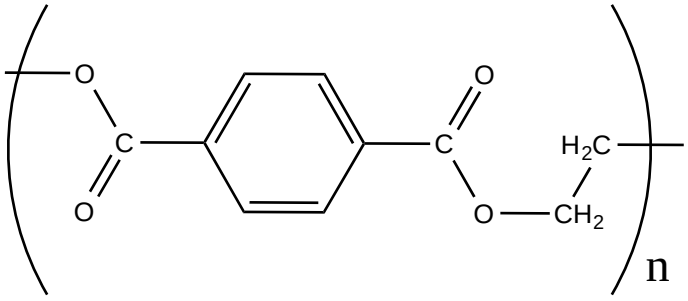

Figure 5.4: Chemical structure of PET

Again 5 samples of each different type of substrate were measured and each sample was measured twice. Through ANOVA a F-value of 7.3508, a F_{crit}-value of 3.68701 and a p-level of 0.00072 was calculated. This indicates that there is a difference between the means of the different groups. The T-test was performed to see which groups differ (Table 5.3). Table 5.3 shows that only the substrates with ZnO nanoparticle layer through the DETA method show a difference with the bare PET substrates. This is also shown in figure 5.5. As indicated by the BIF values in table 5.4, the DETA treatment seems to have increased the permeability of PET. A BIF factor of 1 means that the permeability isn't improved, below 1 indicates that the permeability increases. This observation seems to contradict with the SEM images shown in chapter 4, where more dense ZnO nanoparticle layers are shown for the DETA method than for the HMT method. A possible explanation can be that the surface of the PET substrate degrades through the pH of 8.9 of the DETA solution, leading to a better interaction with the ZnO, but increasing the permeability. Also here the T-test shows a difference between the HMT 75°C and HMT 95°C, figure 5.5 indicates that a treatment at lower temperature effects the PET substrate less.

Table 5.3: Via T-test calculated P-values for PET substrates

T-test p-level	*PET+ ZnO seed layer*	*PET+ ZnO seed layer +DETA*	*PET+ ZnO seed layer +HMT 95°C*	*PET+ ZnO seed layer +HMT 75°C*
PET	0,07229	0,00017	0,05542	0,48717
PET + ZnO seed layer		0,023	0,01928	0,12867
PET + ZnO seed layer +DETA			0,17496	0,08591
PET + ZnO seed layer +HMT 95°C				0,04241
PET + ZnO seed layer +HMT 75°C				

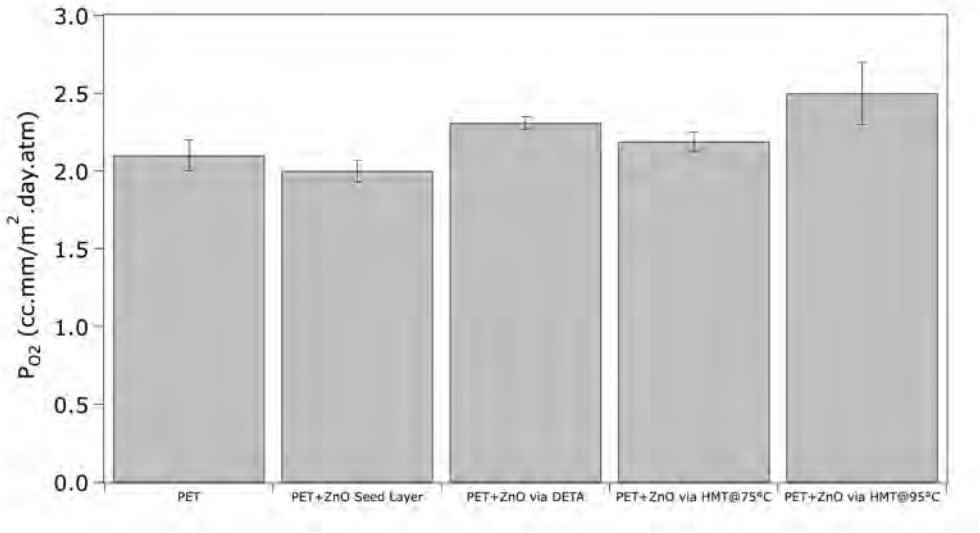

Figure 5.5: Oxygen permeability of PET and PET with ZnO.

Table 5.4: The O_2 barrier improvement factor of PET with ZnO.

	PET+ZnO Seed Layer	PET+ZnO via DETA	PET+ZnO via HMT@75°C	PET+ZnO via HMT@95°C
BIF	1	0.87	1.05	0.9

Although this study doesn't show a decrease in oxygen permeability, Bachari et all. reported a BIF of 25 after sputtering a 50 nm thick ZnO nanolayer on top of a PET substrate with a thickness of 12.5 µm [16]. Liu et all. reported that the oxygen permeability decreased six times after the addition of a AlO_x coating [17]. Plasma deposited SiO_x layers decreased the oxygen permeability with a factor 15 [18]. As indicated in chapter 2, the thickness and the permeability of the ZnO layer play a part in the improvement of the barrier. The permeability of the ZnO layer can be decreased by improvement of the density of the ZnO layer and the thickness of the ZnO layer can be increased. Using $Zn(NO_3)_2.6H_2O$ instead of $Zn(CH_3COO)_2.2H_2O$ could improve the efficiency of the ZnO layer as oxygen barrier. The permeability and thickness of the polymer also play a role. The starting P_{O2} of PET is much lower than the starting P_{O2} of PHBV, therefore, it

is more difficult to improve the O_2 barrier. The thickness of a bare PET substrate (0.25 mm) is 5 times as thick as a PHBV substrate (0.05 mm). The ZnO nanolayer however has the same thickness. Decreasing the polymer thickness increases the polymer permeability and the ZnO nanolayer can have a greater influence on the permeability.

Conclusion 2:

1. The deposition of ZnO nanoparticles on PET didn't improve the oxygen barrier of PET.

5.2.3 Influence of the temperature on PHBV2 and PHBV2 with ZnO seed layer

To determine the influence of temperature on the oxygen permeability, the TR_{O2} was measured at a controlled temperature of 10 °C, 23 °C and 38°C and 0% RH. The TR_{O2} was measured using the OXTRAN module 2/21. The test range of this module is 0.005 to 2000 cc/(m^2.day.atm). The measurements at different temperatures were only performed on PHBV2 and PHBV2 with ZnO seed layer since further growth of the layers didn't seem to influence the permeability. The study was also not performed on PHBV1, since the sputtering method was only used to show that ZnO also could be deposit on rougher surfaces. Figure 5.6 shows the increase of the P_{O2} in function of increasing temperature. As explained in chapter 2, the mobility of the molecular chains increases and the thermal expansion leads to a reduced density in the polymer. The increase in free volume will lead to an increased diffusion. In addition to this, the solubility coefficient of the O_2 will also increase with increasing temperature [19]. Increasing the temperature from 10 °C to 23 °C increased the P_{O2} with 114±12 % from 6.3±0.1 cc.mm/(m^2.day.atm) to 13.5±0.6 cc.mm/(m^2.day.atm) for PHBV2 and with 114±6 % from 1.865±0.007 cc.mm/(m^2.day.atm) to 4.0±0.1 cc.mm/(m^2.day.atm) for PHBV2 with ZnO seed layer. A temperature increase from 10 °C to 38 °C increased the P_{O2} with 437±18 % to 33.8±0.6 cc.mm/(m^2.day.atm) for PHBV2 and with 485±29 % to 10.9±0.5 cc.mm/(m^2.day.atm) for PHBV2 with ZnO seed layer. The similar percentages of increase indicate that the temperature has more influence on the polymer and less on the nanolayer. Figure 5.6 also shows that the P_{O2} of PHBV with ZnO at

38 °C is lower than the P_{O2} of PHBV2 at 23 °C, indicating that even at high temperature PHBV2 with ZnO seed layer forms a better O_2 barrier than PHBV2 at room temperature.

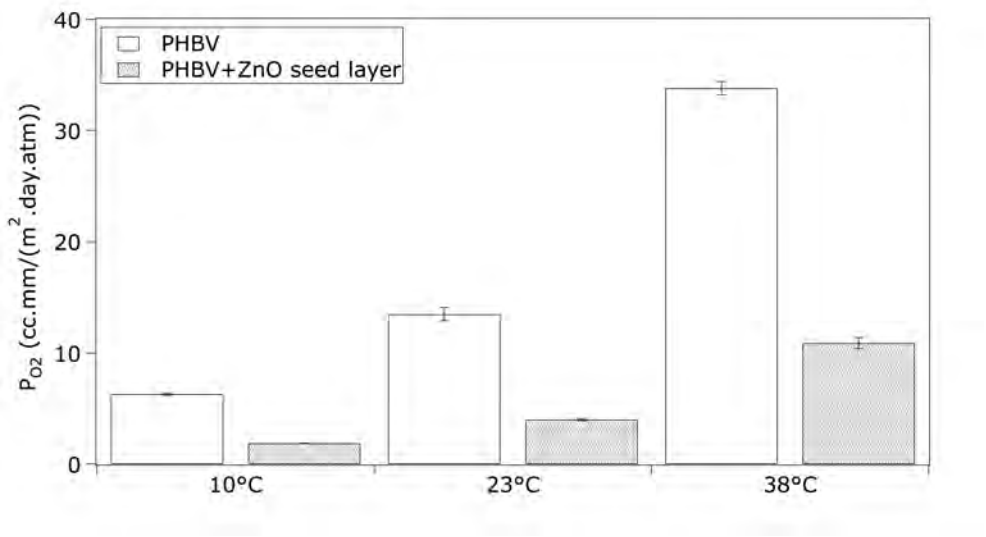

Figure 5.6: The influence of temperature on the P_{O2} of PHBV2 and PHBV2 with ZnO Seed Layer.

The E_p was determined by plotting ln P versus 1/T as described in paragraph 2.2.3.1. Figure 5.7 shows the Arrhenius plot of PHBV2 and PHBV2 with ZnO seed layer. The E_P values of PHBV2 and PHBV2 with ZnO seed layer were calculated using equation 2.16 and the slope determined in figure 5.7. The E_p of PHBV2 for O_2 at 0 % RH is 44 kJ.mol^{-1}. After adding a ZnO seed layer the E_p increases to 46 kJ.mol^{-1}. The increasing E_p suggests that O_2 interacts with the ZnO seed layer and increases the difficulty to permeate through the substrate [20]. However, the increase is only limited and confirms the defects in the ZnO layer [21]. Literature on the E_P value of PHBV for oxygen hasn't been found. The E_P value of PHBV for water vapour is reported by Shogren as 30kJ [22]. However, the PHBV mentioned in the article contained 6% and 12% valerate and not 8% and the average molecular weight of 600 000 was much higher than the average molecular weight of 220 000 from the PHBV2 samples.

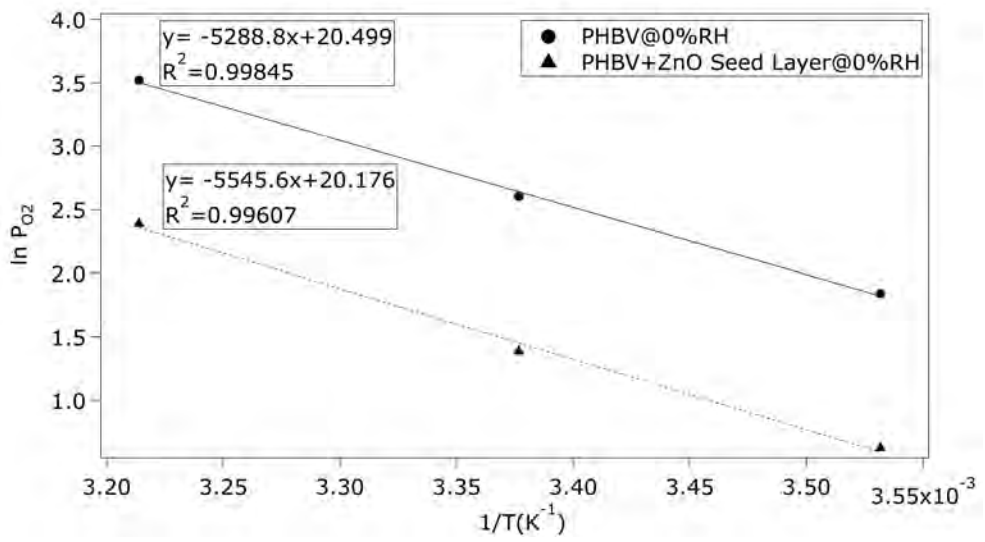

Figure 5.7: The Arrhenius plot of the P_{O2} of PHBV2 and PHBV2 with ZnO Seed Layer.

Conclusion 3:

1. The P_{O2} of PHBV2 increases with increasing temperature.

2. The PHBV2 substrate with ZnO seed layer at 38°C has a better oxygen barrier than PHBV2 without ZnO at 23°C.

3. The E_p of PHBV2 increases after the addition of ZnO.

5.2.4 Influence of temperature on the P_{O2} of PET and PET with ZnO seed layer

The measurements were performed on the OXTRAN module 2/21 under the same conditions as mentioned in paragraph 5.1.4. As shown in figure 5.8, the same observation can be made as for PHBV2. The P_{O2} increases with increasing temperature. Also here the diffusion coefficient of the polymer will increase with increasing temperature and the solubility coefficient of O_2 will also increase. Increasing the temperature from 10 °C to 23 °C increased the P_{O2} with 81±86 % from 1.4±0.5 cc.mm/(m^2.day.atm) to 2.1±0.3 cc.mm/(m^2.day.atm) for PET

and with 86±68 % from 1.4±0.3 cc.mm/(m^2.day) to 2.4±0.4 cc.mm/(m^2.day.atm) for PET with ZnO seed layer. A temperature increase from 10 °C to 38 °C increased the permeability with 157±99 % to 3.1±0.1 cc.mm/(m^2.day.atm) for PET and with 231±78 % to 4.4±0.1 cc.mm/(m^2.day.atm) for PET with ZnO seed layer. Looking at figure 5.8, an observation that can be made is that the P_{O2} for PET and PET with seed layer are practically similar at 10 °C and 23 °C with values of 1.4±0.5 and 1.4±0.3 cc.mm/(m^2.day.atm) and 2.1±0.3 and 2.4±0.4 cc.mm/(m^2.day.atm), respectively. While at 38 °C the P_{O2} for PET is 3.1±0.1 cc.mm/(m^2.day.atm) and the P_{O2} for PET with seed layer is 4.4±0.1 cc.mm/(m^2.day.atm). Thus, in the presence of ZnO the P_{O2} will increase more in the range of 23°C to 38°C. This could suggest that the solubility of oxygen in PET with ZnO seed layer is higher than the solubility of oxygen in PET at elevated temperatures.

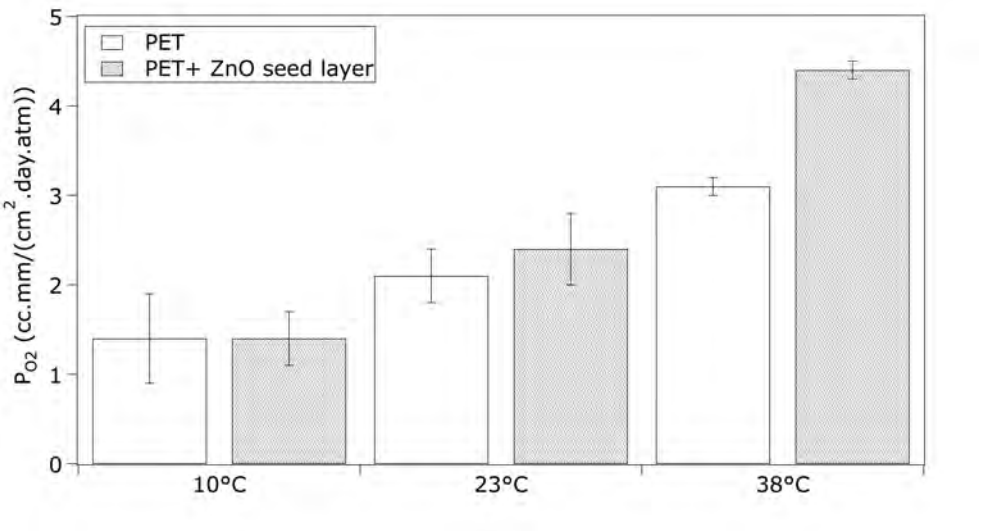

Figure 5.8: The influence of temperature on the P_{O2} of PET and PET with ZnO Seed Layer.

The E_p values were also calculated. Pure PET has an E_p value of 21 kJ.mol$^{-1,}$ while PET with ZnO has an E_p value of 29 kJ.mol^{-1}. This indicates that the PET with ZnO is more steeply temperature-dependent than PET. Thus, ZnO does have an effect on the P_{O2} of PET. It would be interesting to increase the

thickness of the ZnO nanolayer to see if the effect becomes more pronounced. The E_p value of PET is slightly lower than the values found in literature for crystalline PET of about 30-35 kJ.mol^{-1} and much lower than the 51 kJ.mol^{-1} found for rubbery PET [6, 23, 24]. The molecular weight of PET is not mentioned in the articles. However, it can be assumed that the measured PET samples have a lower molecular weight than the PET samples discussed in literature, since the diffusion of oxygen through the molecule decreases with increasing molecular weight. Also, plasticizers can increase the permeability.

Conclusion 4:

1. The P_{O2} of PET increases with increasing temperature.

2. The E_p of PET increases after the addition of ZnO.

5.2.5 Influence of the humidity on the P_{O2} of PHBV2 and PHBV2 with ZnO seed layer

To determine the influence of humidity on PHBV2, previous measurements on PHBV2 were also performed at 40 %RH and 80 %RH on the OXTRAN module 2/21. As shown in figure 5.9 the P_{O2} is hardly influenced by the humidity at 10 °C for both PHBV2 and PHBV2 with ZnO seed layer. This is due to the hydrophobic character of PHBV. There is only a weak interaction with the polar water molecules. The P_{O2} of bare PHBV2 is more or less stable between 0 % RH and 40 % RH at 23 °C and 38°C. The values at 23 °C are 13.5±0.6 cc.mm/(m^2.day.atm) and 13.15±0.07 cc.mm/(m^2.day.atm) and the values at 38 °C are 33.8±0.6 cc.mm/(m^2.day.atm) and 35.3±0.5 cc.mm/(m^2.day.atm). However, at 80 % RH the P_{O2} increases with 12.6±0.4 % at 23°C to 15.45±0.07 cc.mm/(m^2.day) and even with 19.9±0.1 % at 38°C to 42.2±0.5 cc.mm/(m^2.day). The increase in P_{O2} at 80% RH can be explained by the moderate hydrophobic character of PHBV. At higher humidity rates PHBV tends to react more with moisture from the humid air. This creates a plasticizing effect and the permeability increases [19]. For the PHBV2 with ZnO seed layer a different effect is observed (fig. 5.9). From 0% RH to 40% RH the P_{O2} increases with 26±1% at 23°C from 4.0±0.1 cc.mm/(m^2.day.atm) to 5.4±0.1

cc.mm/(m^2.day). Afterwards, in the region from 40 % RH to 80 % RH, the P_{O2} drops with 17±2 % from 5.4±0.1 cc.mm/(m^2.day.atm) to 4.5±0.1 cc.mm/(m^2.day.atm). The increase in permeability can be explained by the fact that the interaction of PHBV2 with ZnO makes the polymer more hydrophilic. The decrease in permeability at 80% RH can be explained by the fact that water molecules take in free volume at higher water activity and decrease the oxygen solubility [12]. At 38°C figure 5.9 shows that the P_{O2} of PHBV2 with ZnO seed layer from 0 %RH to 40 %RH increases with 51±8 % from 10.9±0.5 cc.mm/(m^2.day.atm) to 16.4±0.1 cc.mm/(m^2.day.atm). At 80 % RH PHBV2 with ZnO seed layer has a value that is slightly lower than the P_{O2} of PHBV2 at 23 °C and 80 % RH. The value decreased with 8.5±0.6 % to 15.0±0.1 cc.mm/(m^2.day.atm). The results show that adding a ZnO seed layer makes PHBV less susceptible to extreme humid conditions. The values of PHBV2 with ZnO seed layer at 80%RH are remarkably lower than PHBV2 without ZnO seed layer at 0% RH at the same temperature. This is due to a combination of two effects, the ZnO nanolayer decreases the diffusion rate of the polymer and water molecules occupy free volume in the polymer, decreasing the diffusion even more. The influence of temperature also decreased since the values at 80 %RH of PHBV2 at 23 °C is higher than the value of PHBV2 with ZnO seed layer at 38 °C.

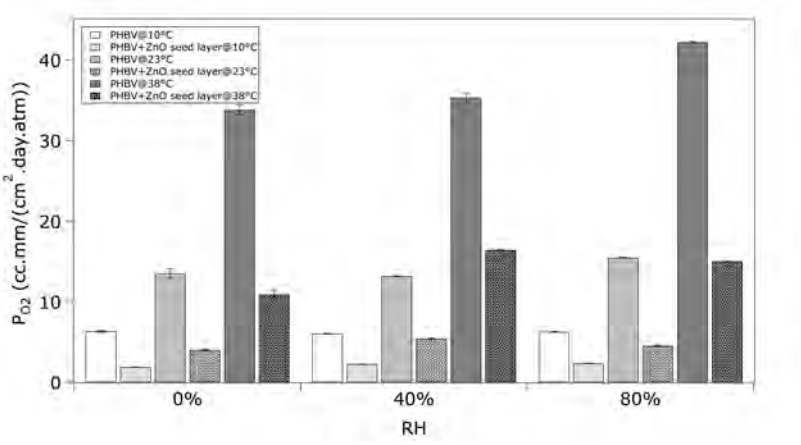

Figure 5.9: The influence of humidity on the P_{O2} of PHBV2 and PHBV2 with ZnO Seed Layer.

The E_p values for PHBV2 and PHBV2 with ZnO seed layer at 40% RH and 80 %RH were also calculated. For the PHBV2 substrates the E_p for O_2 increases from 44 kJ.mol^{-1} at 0 % RH to 50 kJ.mol^{-1} at 80 % RH. The same observation is made for the E_p for O_2 of PHBV2 with ZnO seed layer. The E_p value increases from 46 kJ.mol^{-1} at 0 % RH to 49 kJ.mol^{-1} at 80 % RH. This indicates that at higher %RH not only the polymer structure is influenced by the temperature changes, but also the interaction between the water molecules and the polymer.

Conclusion 5:

1. At 10°C humidity doesn't have an influence on the P_{O2} of PHBV2 and PHBV2 with ZnO seed layer.

2. At 23°C and 38°C PHBV2 and PHBV2 with ZnO seed layer are effected differently by humidity.

3. Adding a ZnO seed layer to PHBV2 makes PHBV2 less susceptible to extreme humid conditions.

5.2.6 Influence of the humidity on the P_{O2} of PET and PET with ZnO seed layer

For the PET substrates without and with ZnO seed layer the O_2 permeability was measured at 23 °C at a relative humidity of 40% and 80% on the OXTRAN module 2/21. As shown in figure 5.10, neither the ZnO seed layer neither the humidity seems to have an influence on the P_{O2}. The limited influence of humidity is similar to other results found in literature [25]. The water molecules don't interact with the polymer and don't cause swelling of the polymer and thus, the diffusion rate of oxygen isn't increased [25].

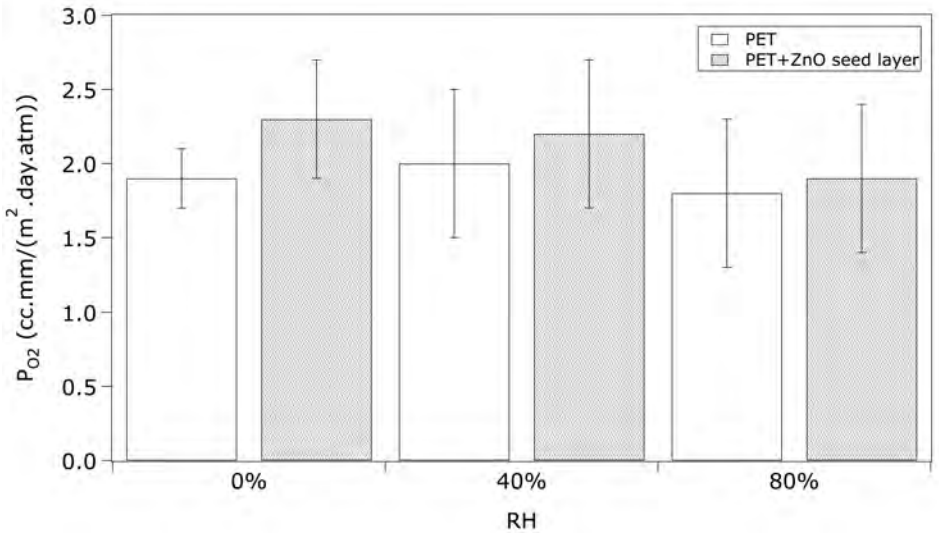

Figure 5.10: The influence of humidity on the P_{O2} of PET and PET with ZnO seed layer.

Conclusion 6:

1. Humidity has no effect on the P_{O2} of PET.

5.3 Carbon dioxide permeability (P_{CO2})

The CO_2 transmission rate (TR_{CO2}) was determined using a Permatran-C model 4/41 (Mocon) according to the ASTM F2476 norm [26]. The measuring method is similar to the measuring method of the TR_{O2}. The only two differences between the TR_{O2} and the TR_{CO2} are that O_2 gas is replaced by CO_2 gas and the sensor is an infrared detector. The substrates were prepared as indicated in chapter 4. The samples were conditioned 5h at a controlled temperature of 23°C and a relative humidity of 0% and afterwards measured under the same conditions. Each sample was measured twice and for each type of measurement five samples were measured. The permeability coefficient of CO_2 (P_{CO2}) is determined by multiplying the TR with the thickness of the samples. The test range of the Permatran module 4/41 is 10 to 500 000 cc/(m^2.day) for masked samples.

5.3.1 P_{CO2} of PHBV2 and PHBV2 with ZnO

Figure 5.11 shows the results of the P_{CO2} measurements at 23°C and 0% RH. ANOVA was used to determine if there is a significant difference between the different groups. The calculated F value (33.94224) is higher than the F_{crit} value (5.48892) and the p-level of 0.0005 is much lower than 0.05. This means there is a significant difference. The T-test (see table 5.5) shows that the measurements of the bare PHBV2 differ significantly from the PHBV2 with ZnO. As shown in figure 5.11, Pure PHBV2 has a P_{CO2} of 123±4 cc.mm/(m^2.day.atm). Formation of ZnO seed layers decreased the P_{CO2} with 69±11 %, from 123±4 cc.mm/(m^2.day.atm) to 38±14 cc.mm/(m^2.day.atm). The P_{CO2} is nine times as high as the P_{O2} value. In chapter 2 it was discussed that the kinetic diameter of CO_2 is smaller than the kinetic diameter of O_2. So the P_{CO2} value has to be higher than the P_{O2} value. There is no significant difference between the P_{CO2} measurements of the PHBV2 with ZnO seed layer and the PHBV2 with ZnO nanoparticle layer through the DETA or HMT method. Again, this is probably due to defects in the layer (Chapter 4: fig. 4.7 and 4.11). Table 5.6 shows the barrier improvement factor for CO_2. The decrease of P_{CO2} could not be compared with literature. The measurements of the P_{CO2} of PHBV are limited.

Table 5.5: Via T-test calculated P-values for PHBV substrates

T-test p-level	*PHBV2+ ZnO seed layer*	*PHBV2+ ZnO seed layer +DETA*	*PHBV2+ ZnO seed layer +HMT 95°C*	*PHBV2+ ZnO seed layer +HMT 75°C*
PHBV2	0,00583	0,04308	0,01991	0,00282
PHBV2+ ZnO seed layer		0,38587	0,23249	0,32487
PHBV2+ ZnO seed layer +DETA			0,23258	0,25281
PHBV2+ ZnO seed layer +HMT 95°C				0,35886
PHBV2+ ZnO seed layer +HMT 75°C				

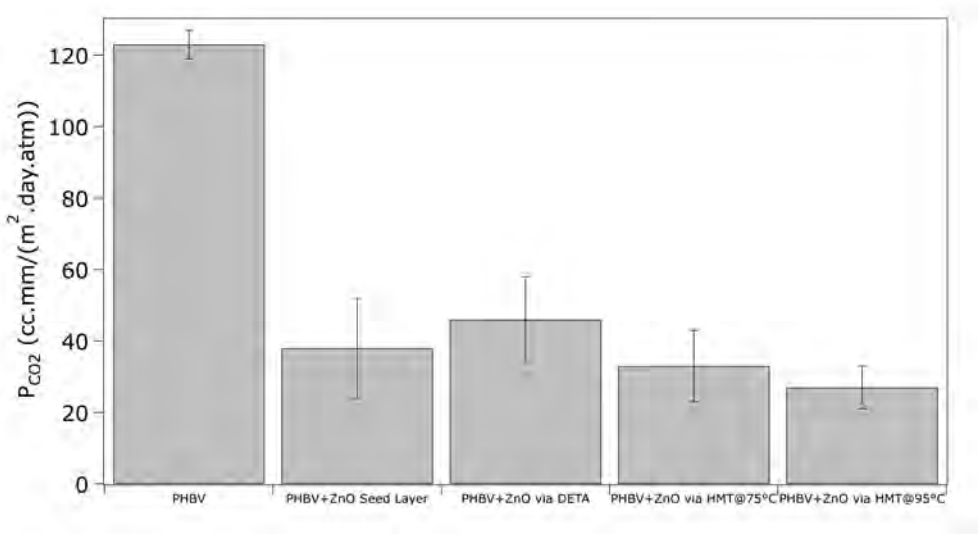

Figure 5.11: Carbon dioxide permeability of PHBV and PHBV with ZnO.

Table 5.6: The CO_2 barrier improvement factor of PHBV with ZnO.

	PHBV+ZnO Seed Layer	PHBV+ZnO via DETA	PHBV+ZnO via HMT@75°C	PHBV+ZnO via HMT@95°C
BIF	3.2	2.7	3.7	4.5

Conclusion 7:

1. ***Hypothesis 1 is confirmed for the CO_2 barrier of PHBV2: the addition of a ZnO nanoparticles to PHBV2 improves the CO_2 barrier of PHBV2.***
2. ***Hypothesis 2 was not confirmed: more ZnO didn't lead to better CO_2 barrier properties.***

5.3.2 P_{CO2} of PET and PET with ZnO

The P_{CO2} of PET was measured in the same manner as the P_{CO2} of PHBV2. As shown in figure 5.12, a value of 17.5±0.8 cc.mm/(m^2.day.atm) was obtained for sheer PET. This value is similar to the values of 15 to 20 cc.mm/(m^2.day.atm) found in literature [14]. Figure 5.12 indicates that the addition of a ZnO seed layer did not decrease the P_{CO2}. To confirm this an ANOVA analysis was performed. The F_{crit} has a value of 5.48892 and is higher than the F value of 5.03803. This indicates no significant difference. However, the p-level is 0.025 which is lower than 0.05. This means that we shouldn't conclude immediately that there is no significant difference. The T-test, shown in table 5.7, shows that there is no significant difference between PET with seed layer and pure PET. In contradiction with the PHBV2 results and the P_{O2} results of PET the formation of a ZnO nanoparticle layer through the DETA did decrease the P_{CO2}. The DETA method decreased the P_{CO2} with 37±6 % from 17.5±0.8 cc.mm/(m^2.day.atm) to 11±1 cc.mm/(m^2.day.atm). This indicates that the seed layer was not thick and dense enough to show an effect, but the layers formed with the DETA method are. Another explanation can be the CO_2 adsorption of ZnO: more ZnO adsorbs more CO_2 [27]. The BIF values are shown in table 5.8. The values of 1.2 to 1.6 are equal to or higher than the 1.2 value found for 10wt% of MXD6 in unoriented PET and lower than the 2.4 found for oriented PET and 10wt% of MXD6 [25]. The fact that it looks like the addition of ZnO always improves the P_{CO2} is because the mean values were used to determine the BIF values.

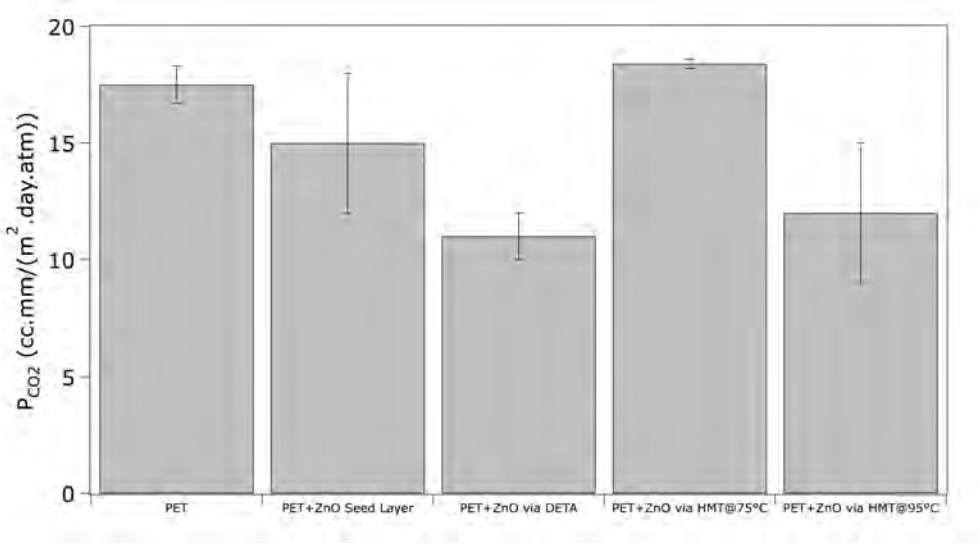

Figure 5.12: Carbon dioxide permeability of PET and PET with ZnO.

Table 5.7: Via T-test calculated P-values for PET substrates

T-test p-level	*PET+ ZnO seed layer*	*PET+ ZnO seed layer +DETA*	*PET+ ZnO seed layer +HMT 95°C*	*PET+ ZnO seed layer +HMT 75°C*
PET	0,15793	0,00989	0,13577	0,09073
PET + ZnO seed layer		0,12988	0,24449	0,10174
PET + ZnO seed layer +DETA			0,41346	0,03243
PET + ZnO seed layer +HMT 95°C				0,1143
PET + ZnO seed layer +HMT 75°C				

Table 5.8: The CO_2 barrier improvement factor of PET with ZnO.

	PET+ZnO Seed Layer	**PET+ZnO via DETA**	**PET+ZnO via HMT@75°C**	**PET+ZnO via HMT@95°C**
BIF	1.2	1.6	1	1.5

Conclusion 8:

1. ***The addition of a ZnO nanoparticle layer doesn't always improve the CO_2 barrier of PET.***
2. ***Only the ZnO nanoparticles layer deposited using the DETA method improved the CO_2 barrier of PET.***

5.3.3 Influence of the temperature on the P_{CO2} of PHBV2 and PHBV2 with ZnO seed layer

To determine the influence of temperature on the P_{CO2}, the TR_{CO2} was measured at a controlled temperature of 10 °C, 23 °C and 38°C and 0% RH. Figure 5.13 indicates that the P_{CO2} increases with 103±2 %, from 44.3±0.2 cc.mm/(m^2.day.atm) to 90.2±0.4 cc.mm/(m^2.day.atm) for PHBV2 when increasing the temperature from 10 °C to 23 °C. For PHBV2 with ZnO seed layer, the P_{CO2} increases with 124±6 % from 14.6±0.1 cc.mm/(m^2.day.atm) to 32.8±0.7 cc.mm/(m^2.day.atm). Increasing the temperature further to 38 °C shows an increase of 366±3 % to 206.5±0.6 cc.mm/(m^2.day.atm) for PHBV2 and an increase of 500±8 % to 87.6±0.6 cc.mm/(m^2.day.atm) for PHBV2 with ZnO seed layer. As explained in section 5.1.3 the increase of P_{CO2} with increasing temperature is due to the increase in both free volume of the polymer (diffusion) and solubility of CO_2 into the polymer. The higher percentages of increase for PHBV2 with ZnO seed layer shows that not only the polymer and the permeant are influenced by temperature change. The interaction of ZnO with CO_2 is also influenced by temperature change. The E_p value for CO_2 increases from 40 kJ.mol^{-1} to 47 kJ.mol^{-1} after adding a ZnO seed layer. This indicates that the ZnO seed layer reduces the permeation of CO_2.

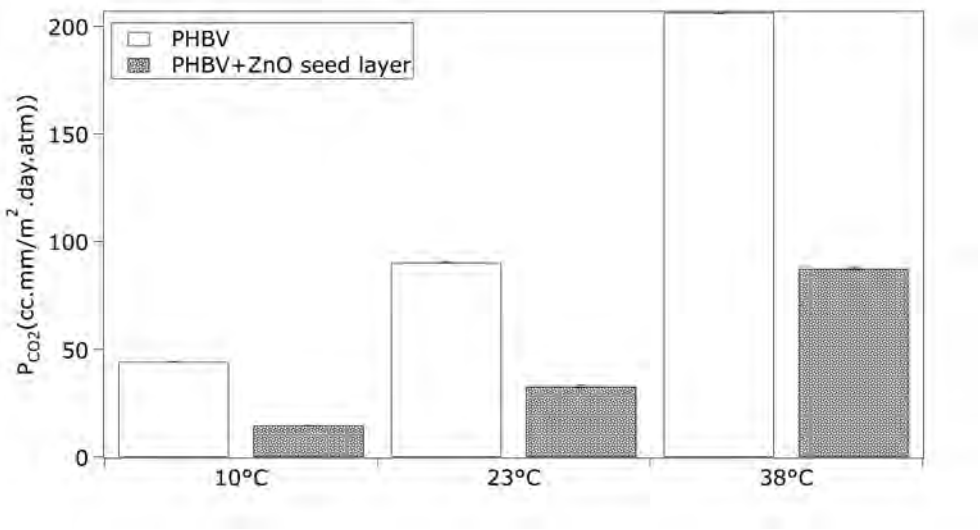

Figure 5.13: The influence of temperature on the P_{CO2} of PHBV2 and PHBV2 with ZnO Seed Layer.

Conclusion 9:

1. The P_{CO2} of PHBV2 increases with increasing temperature.

2. The PHBV2 substrate with ZnO seed layer at 38°C has a better CO_2 barrier than PHBV2 without ZnO at 23°C.

3. The E_p of PHBV2 increases after the addition of ZnO.

5.3.4 Influence of the temperature on the P_{CO2} of PET and PET with ZnO seed layer

The P_{CO2} was measured in the same manner as for PHBV2 (see 5.2.3). The P_{CO2} increases with increasing temperature (fig. 5.14). From 10 °C to 23 °C, the P_{CO2} increases with 600±500 % from 3±2 cc.mm/(m^2.day.atm) to 11±1 cc.mm/(m^2.day.atm) for PET. For PET with ZnO seed layer to P_{CO2} increases with 355±245 % from 4±2 cc.mm/(m^2.day.atm) to 13.3±0.7 cc.mm/(m^2.day.atm). Increasing the temperature from 10 °C to 38 °C increases the P_{CO2} with 804±616 % to 14.8±0.4 cc.mm/(m^2.day.atm) for PET. For PET with ZnO seed

layer the P_{CO2} increases with 466±333 % to 16±2 cc.mm/(m^2.day.atm). Figure 5.15 shows that the E_P for CO_2 cannot be determined. There is no linear relationship between the measurements. Therefore, no conclusion can be made about the temperature dependency of the P_{CO2} of PET. Probably the P_{CO2} values at 10°C are too close to the lower measuring limit of 10 cc/(m^2.day) of the Permatran module 4/41 and can't be determined correctly. However, literature supports the shown trend that an increase in temperature increases the P_{CO2} [19, 28].

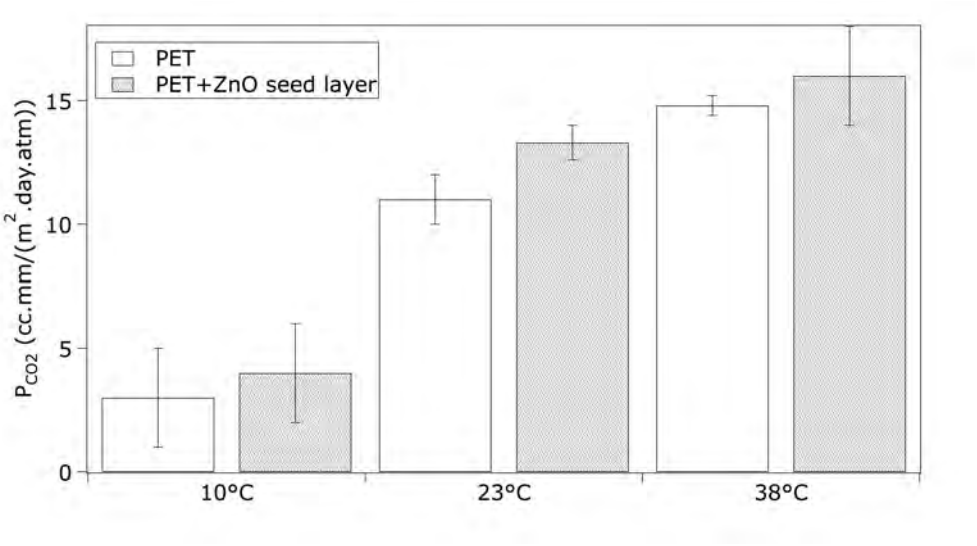

Figure 5.14: The influence of temperature on the P_{CO2} of PET and PET with ZnO Seed Layer.

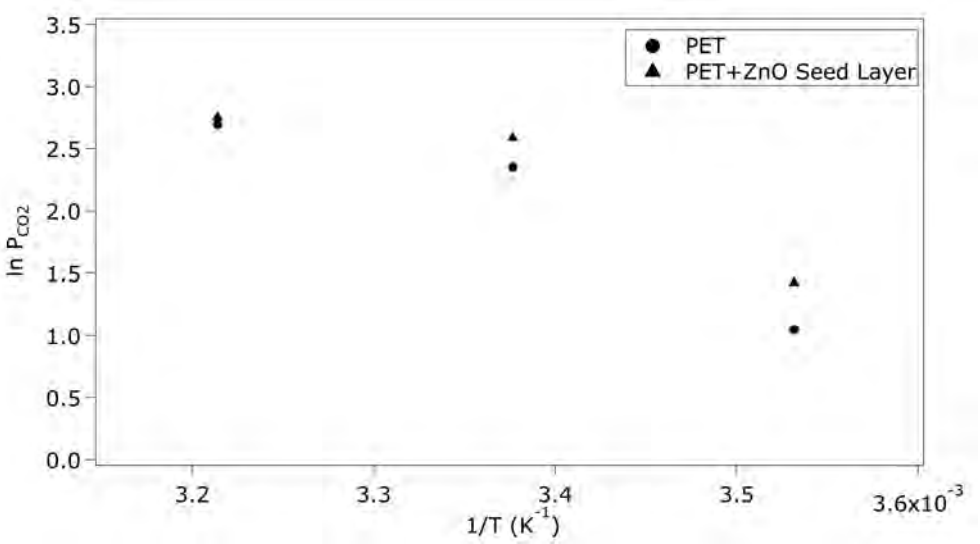

Figure 5.15: The Arrhenius plot of the P_{CO2} of PET and PET with ZnO Seed Layer.

Conclusion 10:

1. The P_{CO2} of PET increases with increasing temperature.

5.4 Water vapour permeability (P_{WV})

The P_{WV} was measured according to the procedure described in ASTM F 1249 [29]. Here, a dry chamber is separated from a chamber with a wet sponge, the wet chamber. The WV permeates through the sample and gets mixed with the N_2 gas on the other side. The amount of WV in the mixture is determined through a pressure-modulated infrared sensor. The water vapor transmission rate (TR_{WV}) was measured using a Permatran-W model 3/33 (Mocon) with a test range of 0.05 to 100 g/(cm^2.day.atm) for masked substrates. The substrates were conditioned for 5h at a controlled temperature of 23°C and a relative humidity of 100%. Afterwards, the TR_{WV} of the samples was measured under the same conditions. The permeability coefficient of WV (P_{WV}) is calculated by multiplying the TR_{WV} with the thickness of the samples. The P_{WV} is used to compare the measurements. The samples were prepared in the same manner as mentioned in section 5.1.

5.4.1 P_{WV} of PHBV and PHBV with ZnO

The P_{WV} of sheer PHBV2 is 1.6±0.1 g.mm/(m^2.day.atm) (fig. 5.16). This value is much higher than the 0.001 g.mm/(m^2.day.atm) found in literature [10, 30, 31]. However, as mentioned before, this can be due to the measuring method, the production method of PHBV or the percentage of PEG. For instance the PHBV mentioned in the articles by Fabra et al. only contain 3% and 5% valerate. As stated by Thellen et al. the water vapour permeability increases with increasing valerate content [3]. Figure 5.16 shows the P_{WV} of PHBV2 and PHBV2 with ZnO. ANOVA showed that there was a significant difference between the measurements. The F-value (13.465) was higher than the F_{crit}-value (4.81564) and the P-value (0.0049) was lower than 0.05. When adding a ZnO seed layer, the P_{WV} drops with 38±2 %, from 1.6±0,1 g.mm/(m^2.day.atm) to 1.00±0.04 g.mm/(m^2.day.atm). Again further growth of de ZnO seed layer into ZnO nanolayers didn't decrease the P_{WV} further. This was confirmed by the T-test shown in table 5.9. All p-levels are lower than 0.05 when comparing the values of pure PHBV2 substrates with PHBV2 with ZnO substrates. When comparing PHBV2 substrates with ZnO seed layer with PHBV2 substrates with seed layer and ZnO nanolayer the p-levels are higher than 0.05. The BIF values are given in table 5.10.

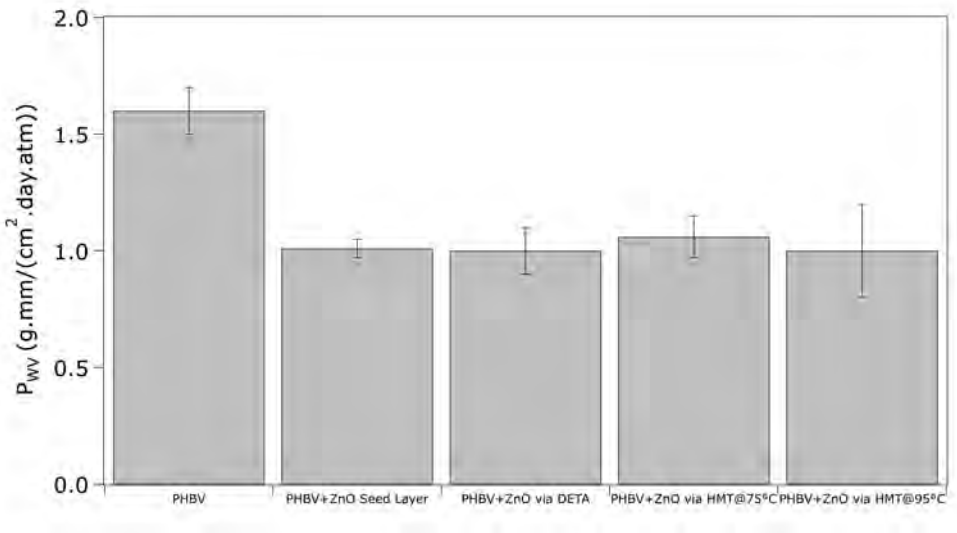

Figure 5.16: Water vapour permeability of PHBV2 and PHBV2 with ZnO.

Table 5.9: Via T-test calculated P-values for PHBV substrates

T-test p-level	*PHBV2+ ZnO seed layer*	*PHBV2+ ZnO seed layer +DETA*	*PHBV2+ ZnO seed layer +HMT 95°C*	*PHBV2+ ZnO seed layer +HMT 75°C*
PHBV2	0,00139	0,00256	0,00535	0,00302
PHBV2+ ZnO seed layer		0,37027	0,49853	0,39213
PHBV2+ ZnO seed layer +DETA			0,41628	0,31629
PHBV2+ ZnO seed layer +HMT 95°C				0,43382
PHBV2+ ZnO seed layer +HMT 75°C				

Tabel 5.10: The WV barrier improvement factor of PHBV with ZnO.

	PHBV+ZnO Seed Layer	**PHBV+ZnO via DETA**	**PHBV+ZnO via HMT@75°C**	**PHBV+ZnO via HMT@95°C**
BIF	1.5	1.6	1.5	1.6

Comparing these results with literature shows that the WV barrier improvement of 38±2 % is better than the 28 % improvement when adding bacterial cellulose whisker to PHBV with 40% HV, for PHBV with 7% HV the barrier even decreases [12]. Adding ZnO particles to the polymer matrix of PHBV with 12%HV decreases the P_{WV} with 69 % [9] and the addition of clay nanoplatelets causes a decrease in P_{WV} of 61 % [11]. Even though at the moment the decrease in P_{WV} through the addition of ZnO nanolayers is less than when using cellulose composites of PHBV, further improvement in the ZnO nanolayer structure could improve the WV barrier to a greater extent.

Conclusion 11:

1. ***Hypothesis 1 is confirmed for the WV barrier of PHBV2: the addition of a ZnO nanoparticles to PHBV2 improves the WV barrier of PHBV2.***
2. ***Hypothesis 2 was not confirmed: more ZnO didn't lead to better WV barrier properties.***

5.4.2 P_{WV} of PET and PET with ZnO

Figure 5.17 shows that the P_{WV} of pure PET is 0.25±0.04 g.mm/(m^2.day.atm). This is slightly lower than the values found in literature of 0.5-2 g.mm/(m^2.day.atm) [14]. The same remark as in paragraph 5.3.1 can be made. The method of measurement and the composition of PET can be different. As shown in figure 5.17, the addition of ZnO didn't improve the P_{WV} of PET. This was proven by the ANOVA. The F-value of 2.57204 was lower than the F_{crit}-value of 4.81564 and the p-level (0.10286) was higher than 0.05. So, no significant differences could be detected. The BIF values are given in table 5.11. The BIF values suggest that the permeability is increased through deposition of ZnO. However, the means are used to determine the BIF, standard deviation weren't taken into account. When taking the standard deviation into account, the indication that the P_{WV} increases isn't as forward as shown in the table below.

Literature shows that by sputtering a ZnO coating the P_{WV} of PET can be improved [32]. For a 100 nm thick layer the P_{WV} can be decreased with almost 90%. The PET substrate had a thickness of 75 µm. If there was a linear

connection between thickness of substrate and the necessary thickness of a ZnO nanocoating to decrease the permeability, this would mean that a ZnO nanolayer of about 330 nm should be deposited on the PET substrates of 0.25 mm. This could indicate that if thicker and denser nanolayers were produced, the P_{WV} of PET could decrease. This would correspond with literature on sputtered SiO_x coatings that report a decrease with up to factor 150 [33].

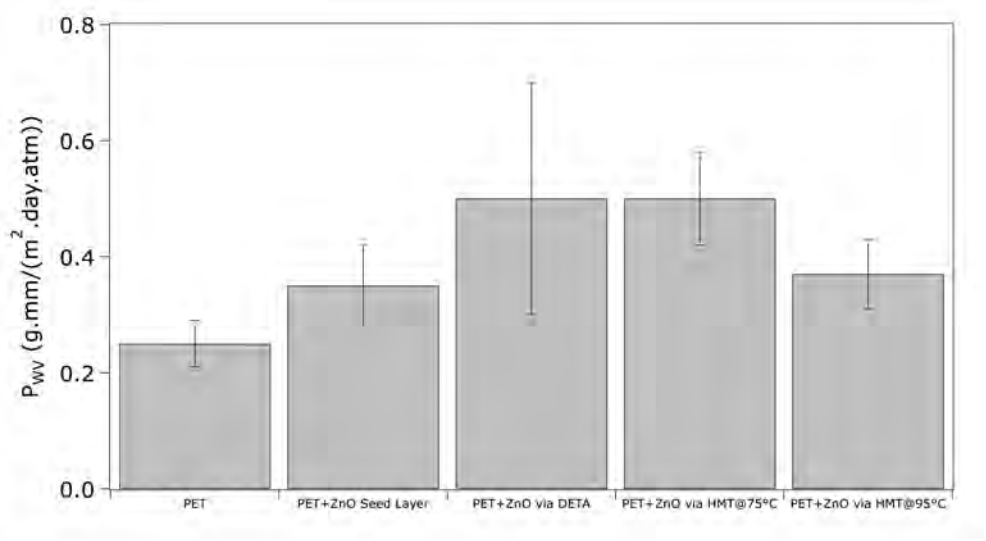

Figure 5.17: Water vapour permeability of PET and PET with ZnO.

Tabel 5.11: The WV barrier improvement factor of PET with ZnO.

	PET+ZnO Seed Layer	PET+ZnO via DETA	PET+ZnO via HMT@75°C	PET+ZnO via HMT@95°C
BIF	0.7	0.5	0.7	0.5

Conclusion 12:

1. ***The addition of a ZnO nanoparticle layer doesn't improve the WV barrier of PET.***

5.4.3 Influence of the temperature on the P_{WV} of PHBV and PHBV with ZnO seed layer

To determine the influence of temperature on the P_{WV}, the TR_{WV} was measured at a controlled temperature of 10 °C, 23 °C and 38°C and 100% RH. The same observation can be made as for P_{O2} and P_{CO2}. The P_{WV} increases with increasing temperature for both PHBV2 and PHBV2 with ZnO seed layer. This is again due to the same reasons as mentioned in the previous paragraphs, the free volume of the polymer increases and the solubility of the permeant increases. Figure 5.18 indicates that the P_{WV} increases in the region of 10 °C to 23 °C. For PHBV2 the P_{WV} increases with 206±51 % from 0.55±0.07 g.mm/(cm^2.day.atm) to 1.65±0.07 g.mm/(cm^2.day.atm). For PHBV2 with ZnO seed layer the P_{WV} increases with 238±62 % from 0.27±0.02 g.mm/(cm^2.day.atm) to 0.9±0.1 g.mm/(cm^2.day.atm). In the region from 10 °C to 38 °C the P_{WV} increases with 955±152 % to 5.7±0.1 g.mm/(cm^2.day) for PHBV2 and with 1200±100 % to 3.49±0.01 g.mm/(cm^2.day) for PHBV2 with ZnO seed layer.

The E_p value for WV also increases when adding a ZnO seed layer to the PHBV substrate, from 61 kJ.mol^{-1} to 67 kJ.mol^{-1}. The permeation of the water vapour molecules decreases due to the addition of ZnO.

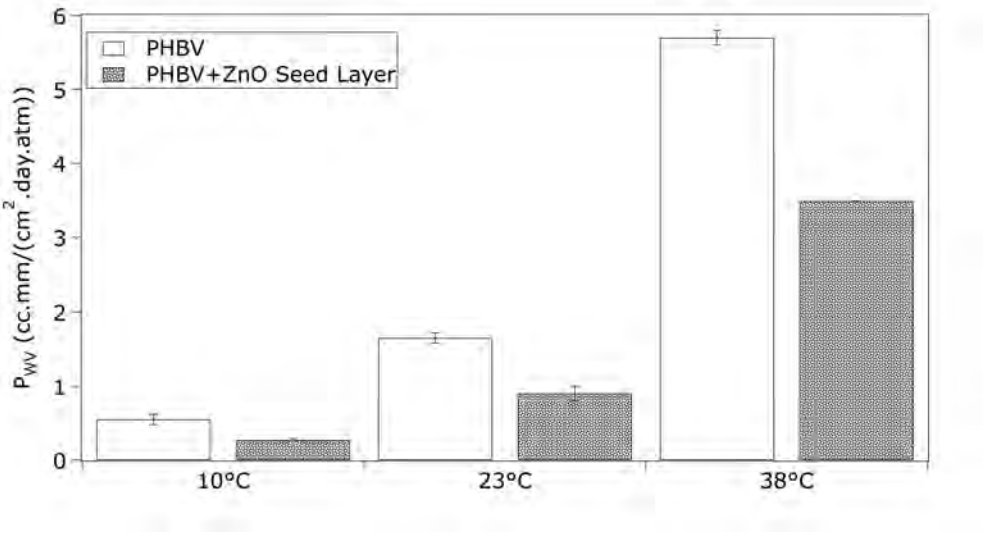

Figure 5.18: The influence of temperature on the P_{WV} of PHBV2 and PHBV2 with ZnO Seed Layer.

Conclusion 13:

1. The P_{WV} of PHBV2 increases with increasing temperature.

2. The E_p of PHBV2 increases after the addition of ZnO.

5.4.4 Influence of the temperature on P_{WV} of PET and PET with ZnO seed layer

The TR_{WV} was measured in the same manner as in paragraph 5.3.4. The P_{WV} increases with increasing temperature (Fig. 5.19). From 10 °C to 23 °C the P_{WV} of PET increases with 87±27 % from 0.14±0.01 g.mm/(cm^2.day.atm) to 0.26±0.02 g.mm/(cm^2.day.atm). For PET with ZnO seed layer the P_{WV} increases with 143±82 % from 0.15±0.03 g.mm/(cm^2.day.atm) to 0.34±0.05 g.mm/(cm^2.day.atm). In the region from 10 °C to 38 °C the P_{WV} increases with 575±55 % to 0.94±0.01 g.mm/(cm^2.day.atm) for PET and with 678±222 % to 1.1±0.1 g.mm/(cm^2.day.atm) for PET with ZnO seed layer. PET and PET with ZnO seed layer have the same E_P value of 51 kJ.mol^{-1}. This confirms what has

been stated in paragraph 5.3.2, ZnO doesn't decrease the permeability. A denser layer of ZnO is necessary to decrease the permeability.

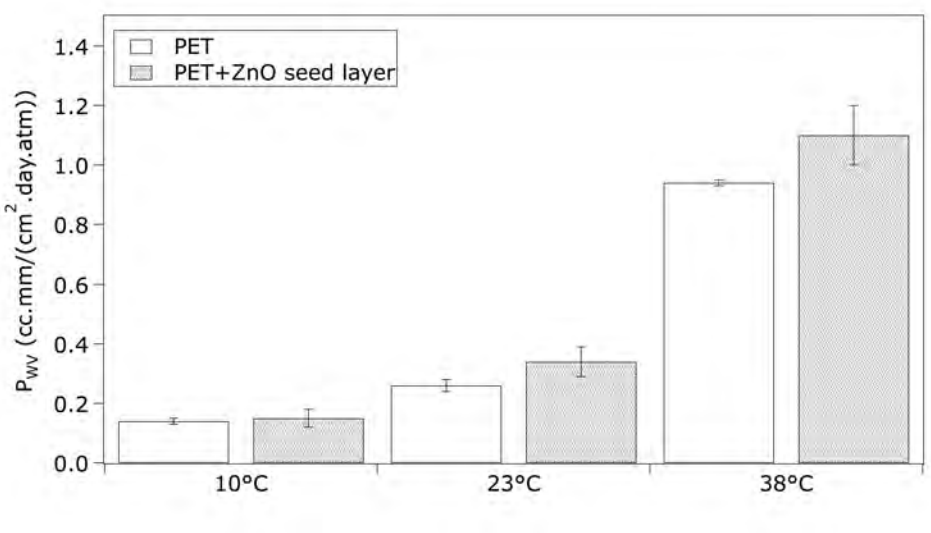

Figure 5.19: The influence of temperature on the P_{WV} of PET and PET with ZnO Seed Layer.

Conclusion 14:

1. The P_{WV} of PET increases with increasing temperature.

5.4.5 Influence of the humidity on P_{WV} of PHBV2 and PHBV2 with ZnO seed layer

To determine the influence of humidity on $P_{WV,}$ the TR_{WV} was measured at a temperature of 23 °C at 40 %RH, 80 %RH and 100 %RH. As shown in figure 5.20, the P_{WV} increases with increasing %RH. This result is consistent with the result for P_{O2} discussed in paragraph 5.1. The water vapour differential partial pressure increases due to the moisture affinity of PHBV2, increasing the solubility and diffusion coefficients. The water absorption causes a plasticizing effect increasing the P_{WV}. The P_{WV} increases with 145±1 % from 0.43±0.001 g.mm/(cm^2.day.atm) to 1.053±0.001 g.mm/(cm^2.day.atm) for PHBV in the region from 40 %RH to 80 %RH. For PHBV with ZnO seed layer the P_{WV}

increases with 156±6 % from 0.207±0.001 g.mm/(cm^2.day.atm) to 0.53±0.01 g.mm/(cm^2.day.atm). From 40 %RH to 100 %RH the P_{WV} increases with 284±17 % to 1.65±0.07 g.mm/(cm^2.day.atm) for PHBV and with 335±50 % to 0.9±0.1 g.mm/(cm^2.day.atm) for PHBV with ZnO seed layer. The P_{WV} of PHBV2 at 80%RH is higher than the P_{WV} of PHBV2 with ZnO seed layer at 100%RH indicating that the ZnO seed layer protects the polymer against water absorption.

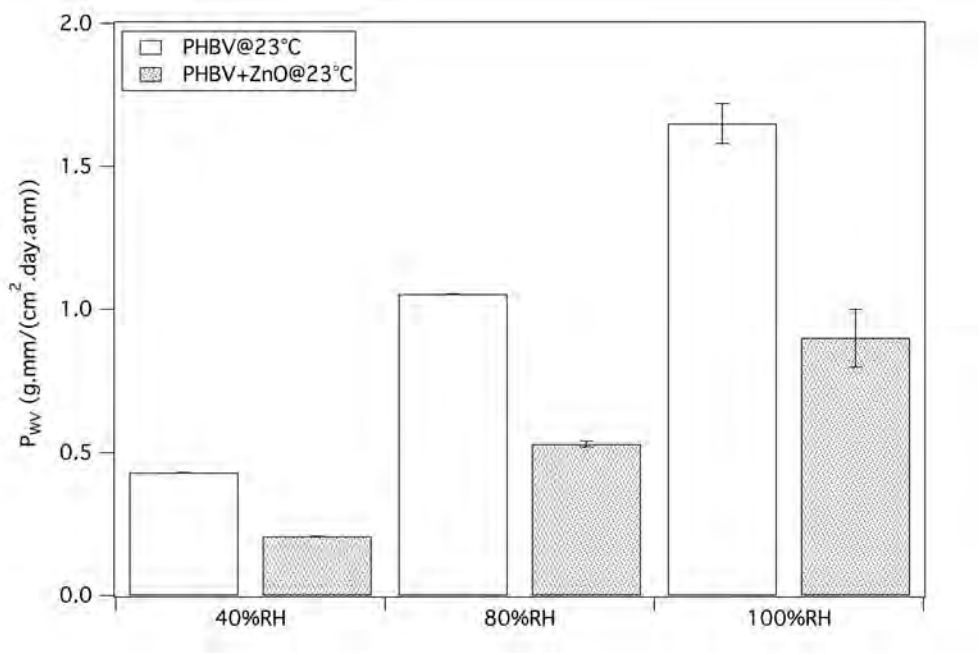

Figure 5.20: The influence of humidity on the P_{WV} of PHBV2 and PHBV2 with ZnO Seed Layer.

Conclusion 15:

1. The P_{WV} of PHBV2 and PHBV2 with ZnO seed layer increases with increasing humidity.

2. The P_{WV} of PHBV2 with ZnO seed layer at 100%RH is lower than the P_{WV} of PHBV2 at 80%RH.

5.5 Conclusion

A first conclusion that can be made is that ZnO nanoparticles can be used to improve the O_2, CO_2 and WV barrier properties of PHBV. ZnO seed layers even provide better O_2 barriers than other known techniques.

The ZnO nanoparticle layer did not improve the O_2 and WV barrier properties of PET, although literature shows that ZnO should improve the barrier properties. A small increase in the CO_2 barrier properties was detected after the addition of ZnO nanolayers through the DETA and the HMT method. This indicates that the ZnO isn't dense enough and that more ZnO is necessary to improve the gas barrier. Further optimization of the ZnO nanolayers and thicker ZnO nanolayers are necessary to improve the barrier properties of PET.

For PET and PHBV2, the P_{CO2} always has a higher value than the P_{O2} due to the smaller kinetic diameter of CO_2. The hydrophilic character of the polymer influences the P_{WV}.

The polymer determines the influence of the temperature and the magnitude of E_P is determined through the polymer and the ZnO. Through the addition of ZnO the P_{O2}, P_{CO2} and P_{WV} values at 23 °C are reduced compared to those of sheer PHBV2 at 23 °C. The P_{O2} and P_{CO2} values of PHBV2 with ZnO at 38 °C are also similar to the P_{O2} and P_{CO2} of pure PHBV2 at 23°C. This indicates that PHBV2 with ZnO seed layer can be used at higher temperatures than pure PHBV2 for the same applications. For PET the P_{O2}, P_{CO2} and P_{WV} values increase with increasing temperature. Through the addition of ZnO the P_{O2}, P_{CO2} and P_{WV} values of PET at 23 °C aren't reduced compared to those of sheer PET at 23 °C.

PHBV2 has an E_P value for O_2 (44 $kJ.mol^{-1}$) that is larger than the E_P value for CO_2 (40$kJ.mol^{-1}$). This is logical, since the activation energy increases with increasing kinetic diameter of the permeant, as is stated in chapter 2. The E_p value of WV (61 $kJ.mol^{-1}$) is higher than the E_p values for CO_2 and O_2. Here the hydrophilic groups in PHBV2 play a role. They make it more difficult for WV to permeate through the polymer, therefore the permeation rate is lower and the E_p value is higher. The same observations can be made for PET. The addition of ZnO increases the E_p value of PET because it is more difficult for the permeant

to permeate through the polymer. The E_p value of PHBV2 is higher than the E_p value of PET. This seems confusing since more free volume leads to lower E_P values and higher permeability due to lower E_P. However these presumptions can only be made for the same type of polymers. As indicated in equation 2.15, E_p is a combination of E_D and H_S. This results in lower E_p values for more polar polymers. PET is more polar than PHBV and therefore has a lower E_p value.

Table 5.12 shows that the percentage of decrease in P_{O2} is similar for the PHBV2 without and the PHBV2 with ZnO seed layer in the same temperature interval. The same observation can be made for P_{WV}. However the P_{CO2} of PHBV2 at 38°C increases less than the P_{CO2} of PHBV2 with ZnO seed layer. The increase of the P_{WV} is also higher than the increase of the P_{O2} and P_{CO2}. These results indicate that it is the polymer that determines the temperature dependency and not ZnO.

Table 5.12: The influence of temperature on PHBV and PET with and without ZnO.

$T_{interval}$	Substrate	P_{O2} increase (%)	P_{CO2} increase (%)	P_{WV} increase (%)
10°C ➔ 23°C	PHBV	114±12	103±2	206±51
	PHBV+ZnO seed layer	114±6	124±6	238±62
	PET	81±86	600±500	87±27
	PET+ZnO seed layer	86±68	355±245	143±82
10°C ➔ 38°C	PHBV	437±18	366±3	955±152
	PHBV+ZnO seed layer	485±29	500±8	1200±100
	PET	157±99	804±616	575±55
	PET+ZnO seed layer	231±78	466±333	678±222

For PET the P_{O2}, P_{CO2} and P_{WV} values are also similar in the same temperature interval.

The humidity study on PHBV2 and PHBV2 with ZnO shows that for the P_{WV} the PHBV tends to react with moisture from the humid air at higher humidity. This creates a plasticizing effect and the permeability increases. The P_{WV} changes in a similar way for PHBV2 and PHBV2 with ZnO seed layer when changing the humidity. However the P_{O2} is influenced differently for PHBV2 and PHBV2 with ZnO seed layer. This indicates that the oxygen interacts with the ZnO protecting the polymer against humidity changes. ZnO nanolayers protect the PHBV2 against humidity. The P_{O2} value of PHBV2 with ZnO seed layer at 80 %RH is lower than the P_{O2} value of pure PHBV2 at 0% RH and this for 10 °C, 23 °C and 38 °C. The P_{WV} of PHBV2 with ZnO seed layer at 100 %RH is also lower than the P_{WV} of pure PHBV at 80 %RH. This indicates that PHBV with ZnO seed layer can be used in more humid conditions.

Even though the deposition of ZnO nanoparticle layers on PHBV2 substrates show a noticeable improvement in the barrier properties, the ZnO layer needs to be optimized. The defects in the ZnO nanoparticle layer deposited through the chemical bath method need to be removed. This can be done by changing the pH of the deposition solution, increasing deposition temperature or increasing the deposition time. A dense, defect-free layer could lead to even further improvement in barrier properties, making it a better solution than the nanocomposites.

For the PET substrates the ZnO nanoparticle layers need to be denser or more ZnO is necessary to adsorb the gas molecules. An optimization of the chemical bath method could provide this. $Zn(NO_3)_2.6H_2O$ can be used instead of $Zn(CH_3COO)_2.2H_2O$ to improve the density of the layer. Another factor that needs to be taken in consideration is the smaller transmission rate of PET. Therefore it is recommended to measure on samples with a larger surface. A larger sample provides a smaller measuring error.

5.6 References

[1] ASTM, Standard Test Method for Oxygen Gas Transmission Rate Through Plastic Film and Sheeting Using a Coulometric Sensor, in, ASTM Book of Standards, 2010.

[2] Permeation and its impact on Packaging, in, Lippke, 2013.

[3] C. Thellen, M. Coyne, D. Froio, M. Auerbach, C. Wirsen, J.A. Ratto, A Processing, Characterization and Marine Biodegradation Study of Melt-Extruded Polyhydroxyalkanoate (PHA) Films, J Polym Environ, 16 (2008) 1-11.

[4] K.L. Yam, The Wiley Encyclopedia of Packaging Technology, 3rd ed., John Wiley & Sons, USA, 2009.

[5] A. Gruniger, P.R. von Rohr, Influence of defects in SiOx thin films on their barrier properties, Thin Solid Films, 459 (2004) 308-312.

[6] A.P. Roberts, B.M. Henry, A.P. Sutton, C.R.M. Grovenor, G.A.D. Briggs, T. Miyamoto, A. Kano, Y. Tsukahara, M. Yanaka, Gas permeation in silicon-oxide/polymer (SiOx/PET) barrier films: role of the oxide lattice, nano-defects and macro-defects, J Membrane Sci, 208 (2002) 75-88.

[7] A.L.B. Otto G. Piringer, Plastic Packaging Materials for Food: Barrier Function, Mass Transport, Quality Assurance, and Legislation, John Wiley & Sons, 2008.

[8] L. Belard, F. Poncin-Epaillard, P. Dole, L. Averous, Plasma-polymer coatings onto different biodegradable polyesters surfaces, European Polymer Journal, 49 (2013) 882-892.

[9] A.M. Diez-Pascual, A.L. Diez-Vicente, ZnO-Reinforced Poly(3-hydroxybutyrate-co-3-hydroxyvalerate) Bionanocomposites with Antimicrobial Function for Food Packaging, Acs Appl Mater Inter, 6 (2014) 9822-9834.

[10] M.J. Fabra, A. Lopez-Rubio, J.M. Lagaron, On the use of different hydrocolloids as electrospun adhesive interlayers to enhance the barrier properties of polyhydroxyalkanoates of interest in fully renewable food packaging concepts, Food Hydrocolloid, 39 (2014) 77-84.

[11] M.D. Sanchez-Garcia, J.M. Lagaron, Novel Clay-Based Nanobiocomposites of Biopolyesters with Synergistic Barrier to UV Light, Gas, and Vapour, J Appl Polym Sci, 118 (2010) 188-199.

[12] M. Martinez-Sanz, M. Villano, C. Oliveira, M.G.E. Albuquerque, M. Majone, M. Reis, A. Lopez-Rubio, J.M. Lagaron, Characterization of polyhydroxyalkanoates synthesized from microbial mixed cultures and of their nanobiocomposites with bacterial, New Biotechnol, 31 (2014) 364-376.

[13] B. Guedri, S. Ben Amor, J.L. Gardette, M. Jacquet, A. Rivaton, Lifetime improvement of poly(ethylene naphthalate) by ZnO adhesive coatings, Polym. Degrad. Stabil., 88 (2005) 199-205.

[14] L. Avérous, Pollet, E., Environmental Silicate Nano-Biocomposites, Springer-Verlag, London, 2012.

[15] H.J. Lehermeier, J.R. Dorgan, J.D. Way, Gas permeation properties of poly(lactic acid), J Membrane Sci, 190 (2001) 243-251.

[16] E.M. Bachari, S. Ben Amor, G. Baud, M. Jacquet, Photoprotective zinc oxide coatings on polyethylene terephthalate films, Mat Sci Eng B-Solid, 79 (2001) 165-174.

[17] Z. Liu, X.X. Ma, Z.H. Sun, F.J. Xu, Properties of Aluminum Oxide (AlOx) Barrier Coatings Deposited on Poly (Ethylene Terephthalate) (PET) Substrates by Reactive Magnetron Sputtering, Rare Metal Materials and Engineering, 41 (2012) 268-271.

[18] J. Schneider, D. Kiesler, M. Leins, A. Schulz, M. Walker, U. Schumacher, U. Stroth, Development of Plasma Polymerised SiOx Barriers on Polymer Films for Food Packaging Applications, Plasma Processes and Polymers, 4 (2007) S155-S159.

[19] L.K. Massey, Permeability Properties of Plastics and Elastomers, USA, 2003.

[20] R. Pantani, G. Gorrasi, G. Vigliotta, M. Murariu, P. Dubois, PLA-ZnO nanocomposite films: Water vapor barrier properties and specific end-use characteristics, European Polymer Journal, 49 (2013) 3471-3482.

[21] L. Korner, A. Sonnenfeld, P.R. von Rohr, Silicon oxide diffusion barrier coatings on polypropylene, Thin Solid Films, 518 (2010) 4840-4846.

[22] R. Shogren, Water vapor permeability of biodegradable polymers, J Environ Polym Degr, 5 (1997) 91-95.

[23] R. Auras, B. Harte, S. Selke, Effect of water on the oxygen barrier properties of poly(ethylene terephthalate) and polylactide films, J Appl Polym Sci, 92 (2004) 1790-1803.

[24] A. Polyakova, R.Y.F. Liu, D.A. Schiraldi, A. Hiltner, E. Baer, Oxygen-barrier properties of copolymers based on ethylene terephthalate, J Polym Sci Pol Phys, 39 (2001) 1889-1899.

[25] Y.S. Hu, V. Prattipati, S. Mehta, D.A. Schiraldi, A. Hiltner, E. Baer, Improving gas barrier of PET by blending with aromatic polyamides, Polymer, 46 (2005) 2685-2698.

[26] ASTM, Standard Test Method for the Determination of Carbon Dioxide Gas Transmission Rate (CO2TR) Through Barrier Materials Using An Infrared Detector, in, ASTM Book of Standards, 2013.

[27] D. Gouvea, S.V. Ushakov, A. Navrotsky, Energetics of CO2 and H2O Adsorption on Zinc Oxide, Langmuir, 30 (2014) 9091-9097.

[28] Permeability Properties of Plastics and Elastomers.

[29] ASTM, Standard Test Method for Water Vapor Transmission Rate Through Plastic Film and Sheeting Using a Modulated Infrared Sensor, in, ASTM book of standards, 2013.

[30] M.D. Sanchez-Garcia, J.M. Lagaron, S.V. Hoa, Effect of addition of carbon nanofibers and carbon nanotubes on properties of thermoplastic biopolymers, Compos Sci Technol, 70 (2010) 1095-1105.

[31] M.J. Fabra, A. Lopez-Rubio, J.M. Lagaron, Nanostructured interlayers of zein to improve the barrier properties of high barrier polyhydroxyalkanoates and other polyesters, J Food Eng, 127 (2014) 1-9.

[32] J. Fahlteich, M. Fahland, W. Schonberger, N. Schiller, Permeation barrier properties of thin oxide films on flexible polymer substrates, Thin Solid Films, 517 (2009) 3075-3080.

[33] A. Bieder, A. Gruniger, P.R. von Rohr, Deposition of SiOx diffusion barriers on flexible packaging materials by PECVD, Surf Coat Tech, 200 (2005) 928-931.

Chapter 6

The influence of a ZnO nanoparticle layer on the UV -degradation of PHBV

6.1 Introduction

Exposure of polymers to sunlight may lead to changes in the chemical composition of polymers, such as reduction in molecular weight, formation of crosslinks or oxidation of functional groups. These changes in chemical composition cause changes in mechanical properties, appearance and permeability. However, the photochemical reaction in polymers can only take place when the absorbed light is energetic enough [1].

Solar radiation consists of approximately 46% infrared radiation, 46% visible light and only 8% UV light [2]. It is the UV radiation that causes the most important damage. To be able to break the bonds in a polymer, the radiation has to be sufficiently energetic. Most single covalent bonds need energies from 165 to 420 kJ/mol to be broken [3]. The radiation of wavelengths from 720 to 280 nm is sufficient to cause damage:

$$E_{720nm} = h.\frac{c}{\lambda} = 6.626.10^{-34}Js.\frac{3.10^{8}m.s^{-1}}{720.10^{-9}m} = 0.0276.10^{\cdot-17}J \quad (6.1)$$

$$E_{720nm} \text{ for 1 mole of photons} = 0.0276.10^{-17}J.6{,}022.10^{23}\ mol^{-1}$$

$$= 0.166.10^{6}\ J.mol^{-1} = 166\ kJ.mol^{-1} \quad (6.2)$$

$$E_{280\,nm} = h.\frac{c}{\lambda} = 6.626.10^{-34}Js.\frac{3.10^{8}m.s^{-1}}{280.10^{-9}m} = 0.0710.10^{\cdot-17}J \quad (6.3)$$

$$E_{280\,nm} \text{ for 1 mole of photons} = 0.0710.10^{\cdot -17} J.\, 6{,}022.\, 10^{23}\ mol^{-1}$$

$$= 0.428.\, 10^{6}\ J.\, mol^{-1} = 428\ kJ.\, mol^{-1} \qquad (6.4)$$

Even though radiation from the near ultraviolet region (300-400nm) causes the most covalent bonds to break, radiation from wavelengths below 190 nm are required to break stronger bonds, such as C-H and O-H [1, 4].

The components of the polymers that make it possible to absorb radiation are the chromophores. There are different types of chromophores in polymers. The first type, type A, are the isolated "internal in-chain" and "end-chain" impurity chromophores. These result from the polymerization process; products of thermal- and/or photo-oxidation; or probes added deliberately. Type B chromophores are part of the molecular structure of the polymer and the third type are the "external" low molecular impurity chromophores, often present in the rest of polymerization catalyzers, commercial additives such as antioxidants, thermal- and photo- stabilizers, pigments, dyes, lubricants, plasticizers, etc. [1].

Even though there are polymers that do not absorb at wavelengths above 300 nm, such as polyethylene, polypropylene and polystyrene, they do degrade due to the presence of chromophores acting as photochemical impurities or structural defects, which do absorb UV light [4].

Photo-degradation in polymers proceeds according to a general scheme involving initiation, propagation and termination [1]. This will result in crosslinking and chain scission.

The photo-degradation reaction of PHBV has not been studied to a great extent [5, 6]. However, it can be concluded from the few literature sources found that due to UV-radiation, cracks develop in the surface of PHBV, discoloration occurs and the tensile strength decreases [5-7]. It can also be presumed that PHBV undergoes the same type of reactions as PHB. Possible reactions involved in PHB photo-degradation are shown in Fig. 6.1 [8]. PHB can undergo a series of

reactions initiated by a free radical (Fig 6.1.1). First dehydration of the asymmetric carbon occurs (I). The formed radical reacts with oxygen to form species II. Species II can react with another molecule and eventually form end carbonyl groups (III) and end polymer radicals. The crosslinking reactions (Fig. 6.1.2) consist of the recombination of free radicals formed by chain scission in previous steps, such as species I and II. The Norrish I (Fig. 6.1.3) and Norrish II (Fig. 6.1.4) type reactions are common reactions when the polymer contains ketone groups [1]. During the Norrish I reaction the cleavage of the carbonyl carbon and the α-carbon results in the formation of free radicals. These radicals participate in further degradation. The Norrish II scission is a reaction of the carbonyl carbon with the γ-carbon. An unsaturated polymer chain end and a polymer chain with an end carbonyl are formed [5].

In this chapter the photo-degradation process of PHBV2 will be studied to determine if PHBV2 undergoes a similar reaction as PHB.

To slow down the photo-degradation in polymers, stabilisers are added. Possible stabilisers are UV absorbers (e.g. benzophenones), anti-oxidants (e.g. phenols) and quenchers (e.g. nickel chelates) [4]. As discussed in chapter 1, ZnO is a known inorganic UV absorber and adsorbs the harmful UV-light [9-12], but also shows photo-catalytic activity and can accelerate the degradation of organic molecules [10, 13]. ZnO deposited on top of plastics, such as PP, PC, PEN and PET, acts as a photo-protector [14-19], while ZnO in ZnO/PLA composites show a photo-catalytic effect [13]. The effect of ZnO nanolayers on the photo-protection or photo-degradation of PHBV hasn't been reported before. Therefore, the effect of UV radiation on PHBV2 with ZnO will be studied.

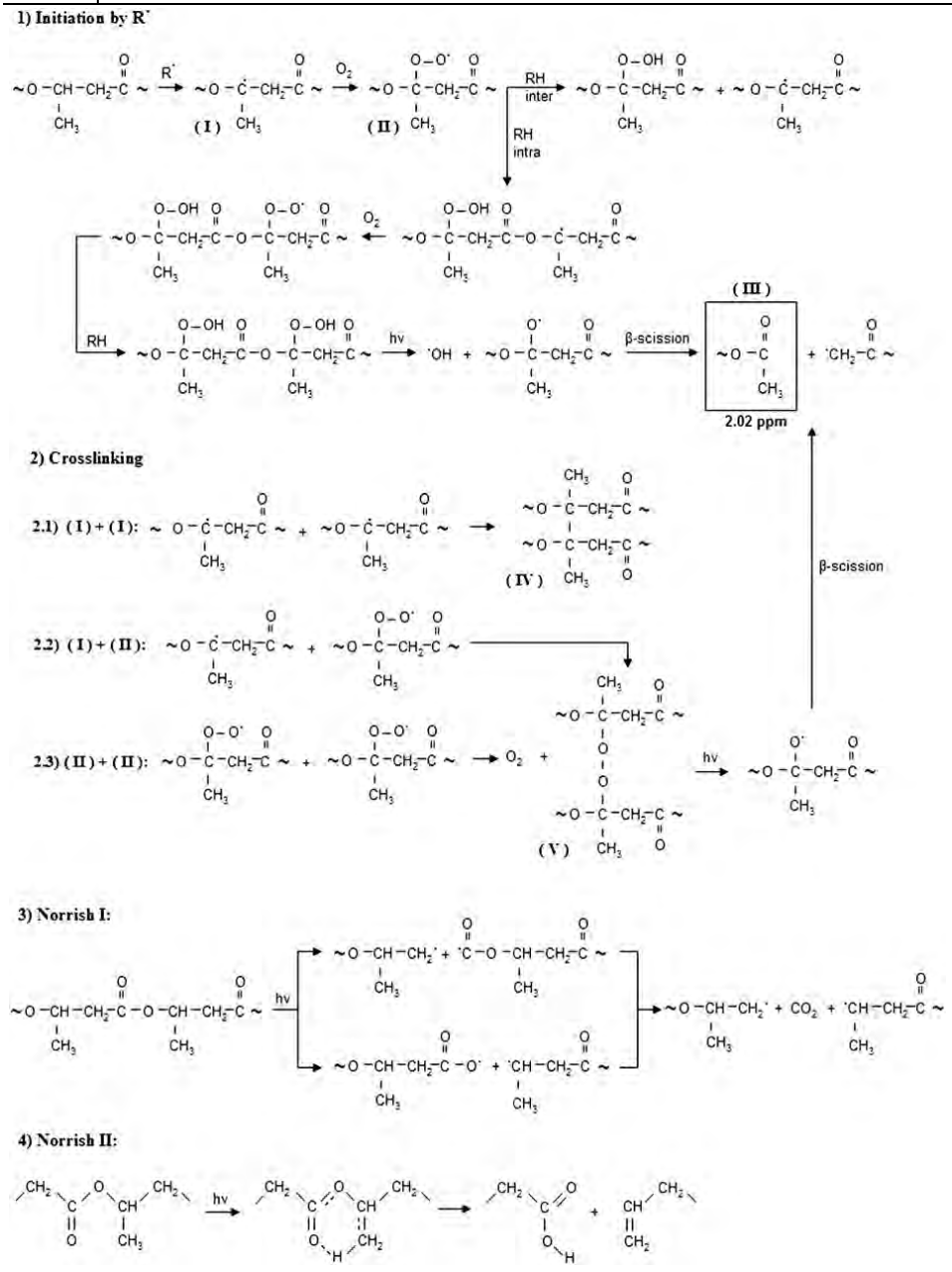

Figure 6.3: Reactions involved in PHB photodegradation process [8].

6.2 Interaction of PHBV2 with UV radiation

To understand the reaction of PHBV2 treated with UV radiation, it is important to know the interaction of PHBV2 with UV radiation. Therefore, the optical transmittance of PHBV2 and PHBV2 with ZnO was measured in the wavelength ranging from 200 nm to 800 nm on a UV–VIS–NIR Varian Cary 500 spectrophotometer.

Fig 6.2 shows that the area of 0% transmittance is extended from 250 nm to 368 nm after the deposition of the ZnO nanolayer. This indicates that after the deposition of ZnO, the UV light is blocked in the near UV region from 300 to 368 nm. As is discussed in chapter 1 and chapter 4, the absorption of ZnO at 368 nm is near the absorption of bulk ZnO and can be linked to the band gap of ZnO (3.37 eV) [20]. The energetic value of the absorbed radiation decreases from 480 $kJ.mol^{-1}$ to 325 $kJ.mol^{-1}$ (eq. 6.1 and 6.2) after the addition of ZnO. While in uncoated PHBV the C-O (358 $kJ.mol^{-1}$) and C-C (347 $kJ.mol^{-1}$) bonds could be broken under the influence of UV-light, ZnO prevents the absorption of sufficient energetic radiation to break these bonds [3].

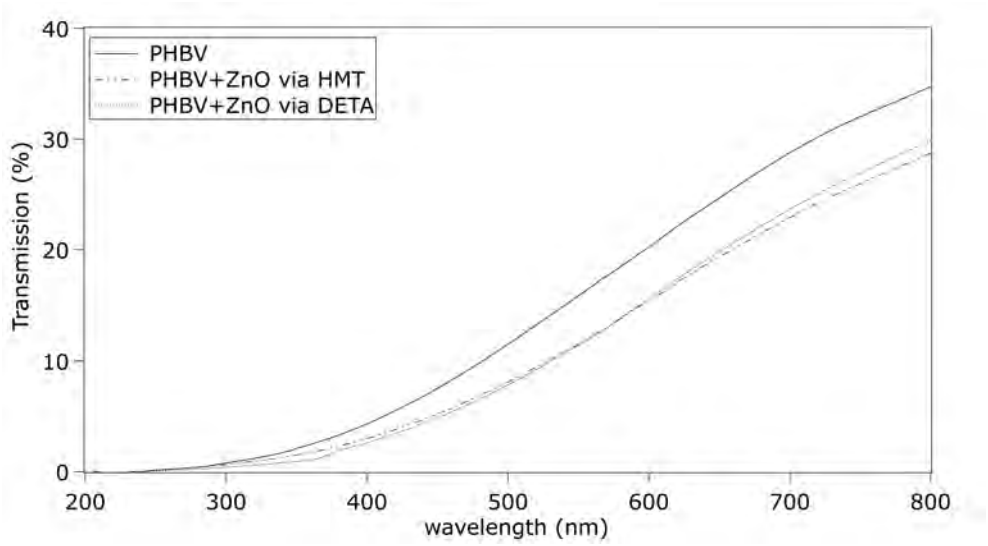

Figure 6.2: UV-VIS transmittance spectra of PHBV2 and PHBV2 with ZnO nanolayer.

6.3 Influence of UV-radiation on PHBV2 and PHBV2 with ZnO layer

6.3.1 Sample treatment

The effects of sunlight on PHBV2 and PHBV2 with ZnO were determined using the QUV apparatus of Q-Lab. The tests were performed according to the ISO 4582 norm [21]. The samples were irradiated for 2, 4, 8, 12, 24 and 36h with UV-B light with a wavelength of 313 nm at a constant temperature of 70±3 °C and intensity of 0.48W.m^{-2}.nm^{-1}. For each period of radiation, the measurements were repeated 5 times. The UVB-313 lamp was chosen because short-wave UV is the primary cause of polymer degradation. As shown in figure 6.3, the UVB-313 nm lamp emits the shortest wavelengths of sunlight found on the earth surface, but also emit shorter wavelengths, below the solar cutoff of 295 nm. Consequently, the UVB-313 lamp accelerates the polymer damage and shows fast and cost-effective results [22].

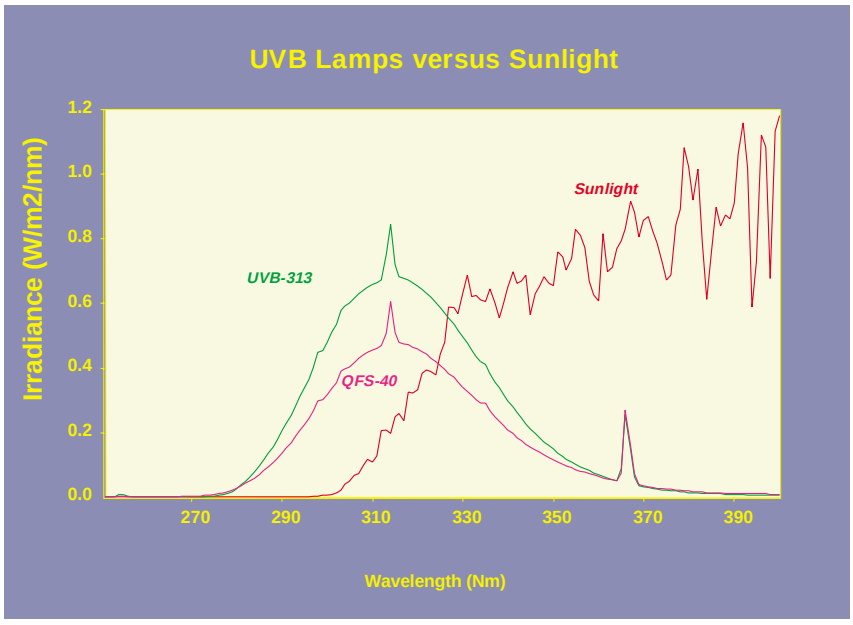

Figure 6.3: The UV spectrum of a UVB-313 nm lamp [22].

6.3.2 Influence of UV radiation on the chemical composition of PHBV2 and PHBV2 with ZnO

Weight loss can indicate deterioration of a polymer. Therefore, the percentage weight difference between the radiated and not radiated samples was calculated as followed:

$$\%\Delta w = \frac{w_b - w_a}{w_b} \times 100 \quad (6.5)$$

Where: w_b is the weight of the sample before UV exposure and w_a is the weight of the sample after UV exposure.

The weight of the samples was measured using an analytical balance with a precision of 0.1 mg.

Figure 6.4 shows an increase in the percentage weight difference of PHBV2 and PHBV2 with ZnO indicating that the UV light causes the polymer to degrade. Only the PHBV2 and PHBV2 + ZnO via the DETA method did not tear after 36h of UV treatment, hence after 36h of radiation only the weight difference of the samples of PHBV2 and PHBV2 + ZnO via DETA method could be determined. The weight difference increases more rapidly for PHBV2 than for PHBV2 with ZnO. There is also a difference between PHBV2 with ZnO seed layer and PHBV2 with ZnO seed layer and ZnO nanolayer. The weight difference of PHBV2 with ZnO seed layer starts to increase more rapidly between 4h and 8h of radiation, while the weight difference of PHBV2 with ZnO seed layer and ZnO nanolayer via the DETA or HMT method starts to increase more rapidly between 8h and 24h. This indicates that the thickness of the layer and consequently the amount of ZnO have an effect on the UV-protection properties of ZnO.

Attenuated total reflectance spectroscopy (ATR) was used to determine the modifications in the chemical structure of PHBV2. The ATR spectra in the wave number range of 600 to 4000 cm^{-1} were measured using a Bruker Vertex 70 Fourier transform IR spectrometer equipped with a PIKE MIRacle ATR sampling accessory with a 45° single reflection diamond/ZnSe horizontal crystal plate.

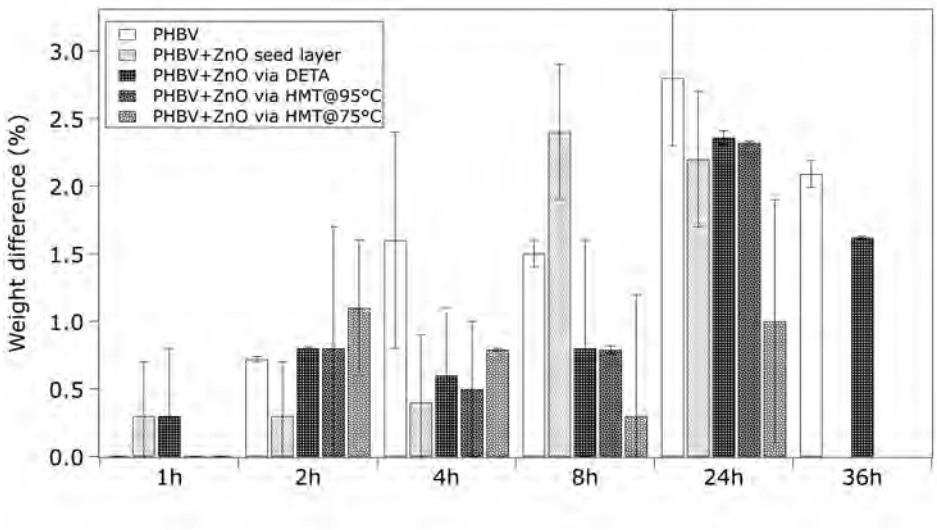

Figure 6.4: Weight difference in UV-radiated PHBV2 without and with ZnO layers deposited as indicated.

To calculate the keto carbonyl (1718 cm^{-1}) and ester carbonyl (1740 cm^{-1}) indices and the crystallinity index (CI), the following equations were used [8, 23]:

$$\text{Keto carbonyl bond index} = \frac{I_{1718}}{I_{1465}} \tag{6.6}$$

$$\text{Ester carbonyl bond index} = \frac{I_{1740}}{I_{1465}} \tag{6.7}$$

$$\text{Crystallinity index} = \frac{I_{1228}}{I_{1718}} \tag{6.8}$$

Where *I* is the intensity of the peak and the number is the frequency at which the peak appears.

Table 6.1 shows the keto carbonyl index of PHBV2 and PHBV2 with ZnO. After a minimum of between 8h and 12h of UV radiation the PHBV samples show an increase in keto carbonyl index. This is due to the formation of carbonyl groups through deterioration of the carbon backbone and indicates that reactions I and II initiated by free radicals (Figure 6.1) take place during the photo-degradation

of PHBV2. PHBV2 with ZnO showed only a small increase in keto carbonyl index, indicating the protection against photo-degradation by ZnO and confirming the mass loss measurements. The ester carbonyl index is shown in table 6.2. For the PHBV2 samples a small increase in ester carbonyl index can be detected after radiation of minimum 8h, this would indicate that the Norrish II reactions take place, although to a limited extent, since there was no extra absorption around 1640 cm^{-1}, characteristic for C=C bonds [8]. The ester carbonyl index does not change for the PHBV2 substrates with ZnO. This indicates that the ZnO protects PHBV2 against photo-degradation. Table 6.3 shows a small decrease in crystallinity index (CI) for PHBV2 after 8h to 12h of radiation. This can be linked to the loss in tensile strength, discussed in following paragraph. The decrease in crystallinity is in contradiction with literature reports on the photo-degradation of PHB. For PHB the crystallinity increases with increasing exposure time [8]. This could indicate that the intensities of 1228 and 1718 cm^{-1} are inadequate to determine the crystallinity and a more reliable method needs to be developed [24]. There are no noticeable changes in the crystallinity index of PHBV2 with ZnO, indicating that ZnO protects PHBV2 against photo-degradation.

Table 6.1: The keto carbonyl index of PHBV2 and PHBV2 with ZnO deposited as indicated.

PHBV	Before radiation	After radiation	PHBV+ZnO Seed Layer	Before radiation	After radiation
1h	13±0	6.9±0.7	**1h**	7.3±0.1	3±3
2h	6±6	0.6±0.3	**2h**	6.4±0.7	4.2±0.6
4h	5±2	9±6	**4h**	1.0±0.7	5±2
8h	6±2	8±3	**8h**	7±3	7±2
12h	6.2±0.2	33±2	**12h**	3.2±1.0	6±3
24h	6±0.3	37±3	**24h**	3±0.5	4.1±0.8
36h	6±0.1	32±1	**36h**	13±3	7±5
PHBV+ZnO via DETA	**Before radiation**	**After radiation**	**PHBV+ZnO via HMT@95°C**	**Before radiation**	**After radiation**
1h	6±4	8±5	**1h**	3±1	5.3±0.9
2h	1.9±0	1.2±0.8	**2h**	3±1	4.0±0.4
4h	6±3	1±1	**4h**	0.41±0.07	3±1
8h	3±2	0.2±0.1	**8h**	2±1	3±2
12h	3.2±0.5	10±1	**12h**	6.9±0.4	12.0±0.7
24h	3±2	14±8	**24h**	6.6±0.6	13±2
36h	14±3	2±1	**36h**	6±3	9±7
PHBV+ZnO via HMT@75°C	**Before radiation**	**After radiation**			
1h	17±4	16±9			
2h	3±2	4±1			
4h	3±1	6±9			
8h	4±6	4±3			
12h	6.5±0.4	12.2±0.4			
24h	6.7±0.3	12.3±0.3			
36h	6±3	41±18			

Table 6.2: The ester carbonyl index of PHBV2 and PHBV2 with ZnO deposited as indicated.

PHBV	Before radiation	After radiation	PHBV+ZnO Seed Layer	Before radiation	After radiation
1h	5±0	2.9±0.3	**1h**	5.4±0.3	0.6±0.3
2h	1±1	0.7±0.2	**2h**	2.6±0.2	2.03±0.05
4h	0.6±0.6	3±2	**4h**	0.8±0.2	1.7±0.7
8h	2±2	3.5±0.9	**8h**	5±3	3.2±0.8
12h	2.58±0.09	10±1	**12h**	1.7±0.3	0.4±0.5
24h	2.5±0.1	12±4	**24h**	1.8±0.1	0.57±0.8
36h	2.50±0.06	8.2±0.5	**36h**	4.6±0.9	0.7±0.4
PHBV+ZnO via DETA	**Before radiation**	**After radiation**	**PHBV+ZnO via HMT@95°C**	**Before radiation**	**After radiation**
1h	0.6±0.8	2±1	**1h**	0.24±0.02	2.5±0.2
2h	3±3	0.8±0.4	**2h**	1±1	2±2
4h	1.0±0.5	0.7±0.4	**4h**	0.5±0.5	2±2
8h	0.3±0.2	0.95±0.0.06	**8h**	1.3±0.2	1.6±0.9
12h	1.7±0.1	6±4	**12h**	2.80±0.02	3.5±0.2
24h	1.6±0.6	1.3±0.5	**24h**	2.6±0.2	3.65±0.06
36h	4.4±0.7	1.5±0.5	**36h**	2±1	1±1
PHBV+ZnO via HMT@75°C	**Before radiation**	**After radiation**			
1h	4.3±0.2	5±4			
2h	1.3±0.1	2.0±0.5			
4h	2±3	2±1			
8h	3±1	2.0±0.8			
12h	2.7±0.1	3.66±0.10			
24h	2.7±0.1	3.56±0.04			
36h	2±1	2±3			

Table 6.3: The crystallinity index of PHBV2 and PHBV2 with ZnO deposited as indicated.

PHBV	Before radiation	After radiation	PHBV+ZnO Seed Layer	Before radiation	After radiation
1h	0.6±0.03	0.580±0.003	**1h**	0.66±0.03	0.59±0.01
2h	0.63±0.06	0.7±0.2	**2h**	0.7±0.1	0.66±0.01
4h	0.56±0.01	0.7±0.2	**4h**	0.62±0.05	0.61±0.05
8h	0.64±0.01	0.57±0.02	**8h**	0.62±0.01	0.54±0.05
12h	0.562±0.001	0.382±0.004	**12h**	0.56±0.03	0.52±0.04
24h	0.571±0.005	0.379±0.004	**24h**	0.56±0.03	0.48±0.02
36h	0.560±0.005	0.39±0.01	**36h**	0.50±0.02	0.4±0.3
PHBV+ZnO via DETA	**Before radiation**	**After radiation**	**PHBV+ZnO via HMT@95°C**	**Before radiation**	**After radiation**
1h	0.61±0.01	0.59±0.06	**1h**	0.563±0.005	0.571±0.007
2h	0.68±0.08	0.7±0.2	**2h**	0.7±0.3	0.7±0.1
4h	0.73±0.09	1±1	**4h**	0.6±0.1	0.5±0.1
8h	0.64±0.05	1.1±0.5	**8h**	0.8±0.2	0.8±0.2
12h	0.60±0.02	0.60±0.03	**12h**	0.54±0.06	0.400±0.005
24h	0.64±0.09	0.7±0.1	**24h**	0.593±0.007	0.403±0.006
36h	0.53±0.02	0.7±0.2	**36h**	0.54±0.03	0.53±0.03
PHBV+ZnO via HMT@75°C	**Before radiation**	**After radiation**			
1h	0.64±0.01	0.57±0.03			
2h	0.9±0.3	0.7±0.1			
4h	0.60±0.02	0.8±0.1			
8h	0.8±0.2	0.62±0.09			
12h	0.51±0.01	0.400±0.001			
24h	0.50±0.02	0.404±0.003			
36h	0.478±0.003	0.4±0.3			

Another way to determine the change in crystallinity is the use of differential scanning calorimetry (DSC) measurements. DSC measurements were performed under nitrogen flow by using a DSC Q200 (TA Instruments), calibrated with Indium 99.999%. A first heating ramp of 10°C/min from room temperature to 200°C was followed by a cooling ramp of 20°C/min down to 25°C to eliminate differences in thermal history. Then two analog cycles were performed to compare the melting temperature (T_m) of PHBV2 and PHBV2 with ZnO nanolayer and the enthalpy of fusion of the polymer was obtained for the melting peaks to calculate the percentage of crystallinity of each sample with following equation:

$$\%\text{Crystallinity} = \frac{\Delta H_f^{obs}}{\Delta H_f^{\circ}} \times 100\% \quad (6.9)$$

Where: ΔH_f^{obs} is the observed fusion enthalpy of the sample after the second cycle and ΔH_f° is the enthalpy of fusion of a 100% crystalline sample of the same polymer. For PHBV ΔH_f° is 146.6 J.g^{-1} [25].

The determination of the %crystallinity with DSC also didn't provide a clear answer about what happens to the crystallinity after UV-radiation (Table 6.4). The crystallinity increases with increasing duration of the UV treatment for PHBV2. This is in agreement with literature [8]. The increase in crystallinity is due to chain scission. For PHBV2 with ZnO the %crystallinity sometimes increases and sometimes decreases. The difficulty in determining the crystallinity for PHBV with ZnO is that the exact amount of ZnO is unknown and therefore cannot been taken into account in the calculations [26]. As shown in table 6.5, the melting temperatures of all the samples remain the same. A possible explanation for this can be that only the surface of PHBV2 undergoes degradation and the level of degradation is too low to have an effect on the melting temperature.

Table 6.4: The % crystallinity of PHBV2 and PHBV2 with ZnO deposited as indicated.

%Crystallinity	PHBV	PHBV+ZnO seed layer	PHBV+ZnO via Deta	PHBV+ZnO via HMT@95	PHBV+ZnO via HMT@75
0h	41	42	42	49	49
1h	56	50	59	37	36
2h	53	41	45	38	37
4h	41	51	65	48	40
8h	41	59	55	53	38
12h	67	43	41	44	36
24h	51	41	31	29	39
36h	66	30	34	46	44

Table 6.5: The melting points of PHBV2 and PHBV2 with ZnO deposited as indicated.

T_{m1}	PHBV	PHBV+ZnO seed layer	PHBV+ZnO via Deta	PHBV+ZnO via HMT@95	PHBV+ZnO via HMT@75
0h	148	147	147	149	149
1h	148	148	149	149	149
2h	148	146	150	149	150
4h	149	146	151	149	151
8h	148	149	151	152	151
12h	148	149	152	150	151
24h	147	150	151	148	150
36h	147	148	152	150	148
T_{m2}	PHBV	PHBV+ZnO seed layer	PHBV+ZnO via Deta	PHBV+ZnO via HMT@95	PHBV+ZnO via HMT@75
0h	159	159	159	160	160
1h	159	159	160	160	160
2h	159	157	160	160	161
4h	160	157	161	160	161
8h	159	159	161	162	161
12h	159	160	162	161	162
24h	158	161	161	159	161
36h	157	159	162	160	158

6.3.3 Influence of UV radiation on the mechanical properties of PHBV2 and PHBV2 with ZnO

An increase in crystallinity can indicate tensile strength loss. Therefore, the tensile strength of PHBV2 and PHBV2 with ZnO was determined. The measurements were performed on a MTS/10 tensile tester using an initial speed of 5 mm/min and a 2kN load cell. The prepared samples had a width of 6 mm and were measured in a conditioned atmosphere of 23°C and 50% relative humidity.

The tensile properties of a polymer are also correlated to the weight-average molecular weight [27]. Therefore, the molecular mass distribution of PHBV2 was analysed using a GPC apparatus composed of a SpectroSeries P100 pump, equipped with a Shodex RI71 refractometer detector and two PL-gel 10 µ Mixed-B columns in serie, thermostated at 35 °C. The eluent was chloroform (VWR, HPLC grade) at a flow rate of 1.0 ml/min. The samples were dissolved in chloroform at a concentration of 1 g/l. The injection volume was 100 µl. Only one of the five samples of each radiation period was measured.

The loss in tensile strength (σ) of PHBV2 and PHBV2 with ZnO, shown in figure 6.5, confirms the degradation of the polymer. However, the loss in tensile strength is only observed after an UV treatment between 24 hours and 36h of radiation. Literature shows that a UV treatment of 10h doesn't show a decrease in tensile strength of PHBV(5%), while a treatment of 100h does show a decrease in the tensile strength of PHBV(12%) [5, 6]. Photo-degradation of several other polymers, such as PP and PET, show that the degradation is dependent on the extent and degree of radiation. Thus, it can be concluded that a treatment with an UVB-313nm lamp between the 24h and 36h is necessary to detect a decrease in tensile strength. As discussed in chapter 4 (eq. 4.1), the tensile properties of a polymer are correlated to the number-average molecular weight (M_n) [27]. A decrease in tensile strength implies a decrease in number-average molecular weight. As shown in Fig. 6.6 the number-average molecular weight (M_n) of PHBV2 and PHBV2 with ZnO seed layer does decrease, indicating chain scission [28]. The number-average molecular weight starts to decrease between the 24h and 36h UV-treatment for PHBV2 and between the 12h and

24h of treatment for PHBV2 with ZnO seed layer. This can be supported by the loss of weight-average molecular weight (M_w) shown in figure 6.7. The increase in the ratio M_z/M_w (Fig. 6.8) indicates that both the crosslinking and chain scission process, shown in fig 6.1, take place after irradiation. Chain scission causes a decrease in molecular weight and the higher molecular weight fraction can be explained by the formation of crosslinks [29]. The faster decrease in molecular weight of PHBV2 with ZnO seed layer could contradict the weight loss measurements. However, the fraction of keto and carbonyl groups (see paragraph 6.3.2) supports the weight loss measurements.

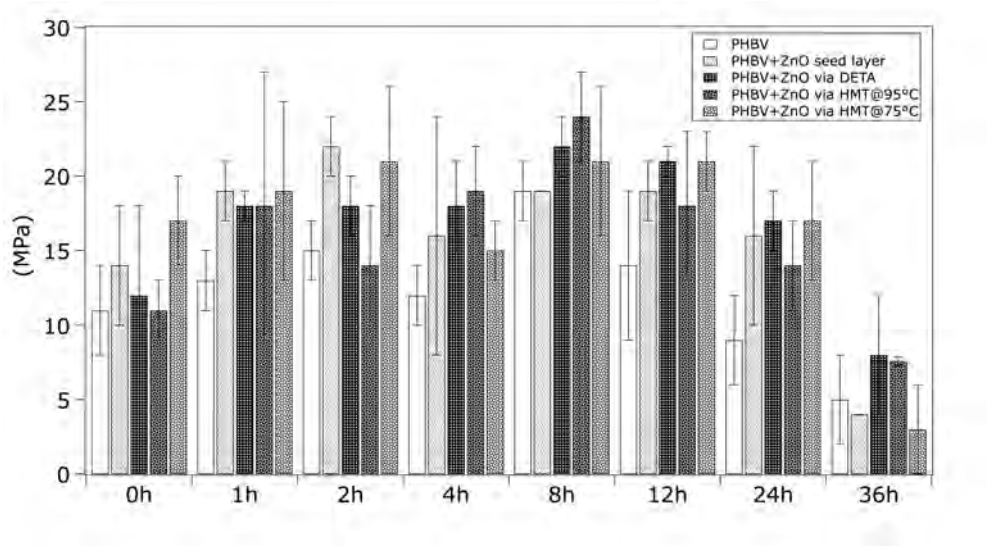

Figure 6.5: Tensile strength of UV-radiated PHBV without and with ZnO layers deposited as indicated.

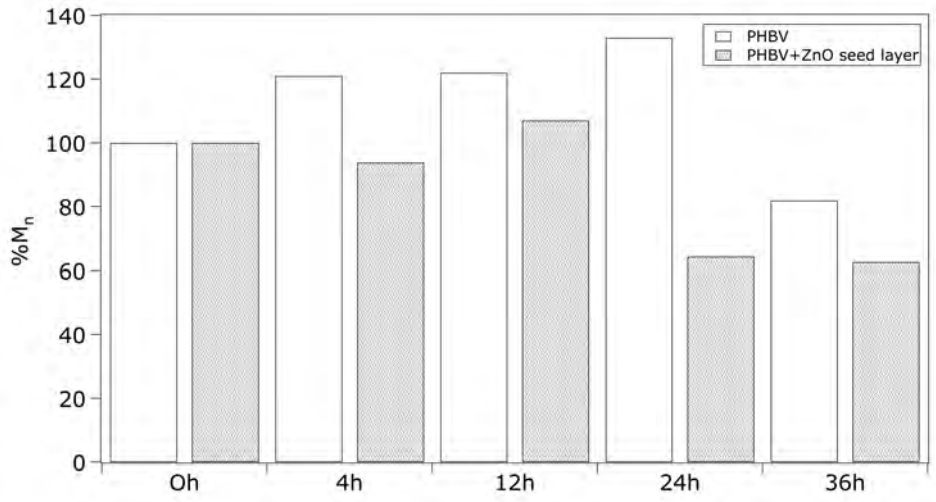

Figure 6.6: Number average moleculare weight of UV-radiated PHBV2 and UV-radiated PHBV2 with ZnO seed layer.

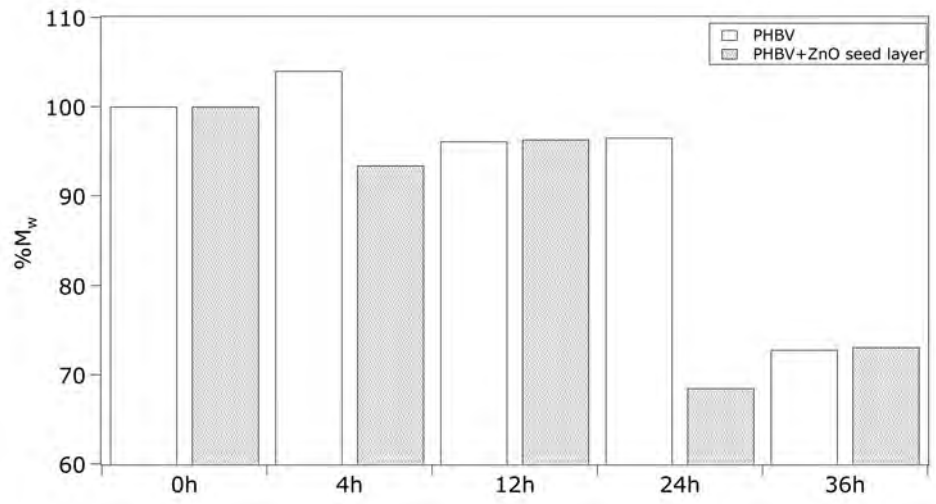

Figure 6.7: Weight average molecular weight of UV-radiated PHBV2 and UV-radiated PHBV2 with ZnO seed layer.

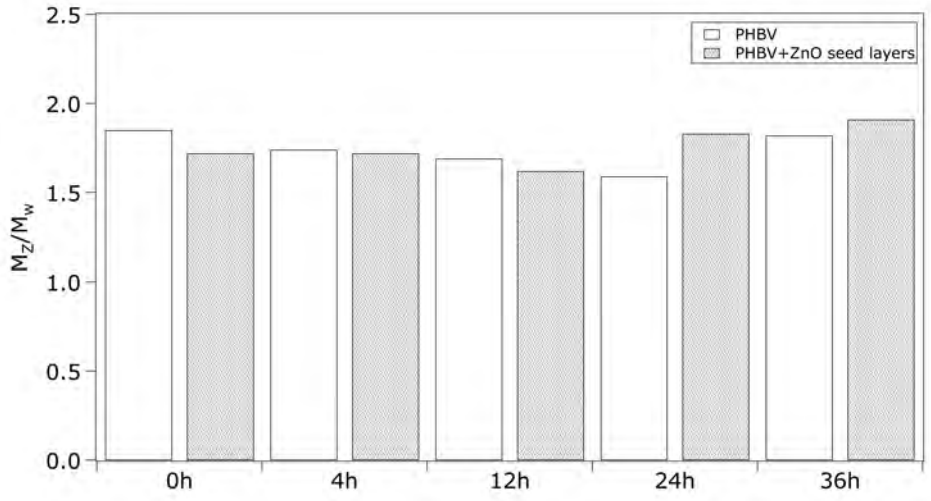

Figure 6.8: Ratio M_z/M_w of UV-radiated PHBV2 and UV-radiated PHBV2 with ZnO seed layer.

6.3.4 Influence of UV radiation on the appearance of PHBV2 and PHBV2 with ZnO

As indicated in the introduction the appearance of the polymer can change due to UV degradation. Colour difference and yellowing can indicate that the polymer is degrading. Due to chain scission and crosslinking, the polymer degrades in smaller pieces, causing the colour to change. The formation of carboxyl end groups and acetaldehyde causes yellowing of the polymer [30]. Therefore, CIELAB Colour differences and yellowing were measured with the Datacolour Microflash MF200D. ΔE represents the colour difference between the non-irradiated and the UV-irradiated samples and can be calculated using following equation:

$$\Delta E = \Delta L^2 + \Delta a^2 + \Delta b^2 \qquad (6.10)$$

Where: ΔL^* indicates the lightness and Δa^* and Δb^* describe the colour position as vectors of red, green, yellow and blue. Yellowing is represented by the yellow

index Δb^*.

Figure 6.9 shows that for PHBV2 and PHBV2 with ZnO seed layer the colour difference increases with increasing UV-radiation time. This indicates that the polymer is influenced by exposure to UV light. Another observation that can be made is that PHBV2 with ZnO seed layer and ZnO nanolayer via the DETA and HMT method at 95°C shows less increase in colour difference. This indicates that the ZnO protects the PHBV2 substrate against UV light as suggested by the UV transmission spectra in figure 6.2. As discussed, yellowing is also an indication of polymer degradation. In figure 6.10 the yellow index Δb is shown. The more positive Δb, the yellower the substrate is after exposure to UV light and the more negative, the more blue. After a minimum of 8h of radiation the substrates became more yellow. The same observation as with the colour differences can be made, the PHBV and PHBV with ZnO seed layer show a higher increase in Δb.

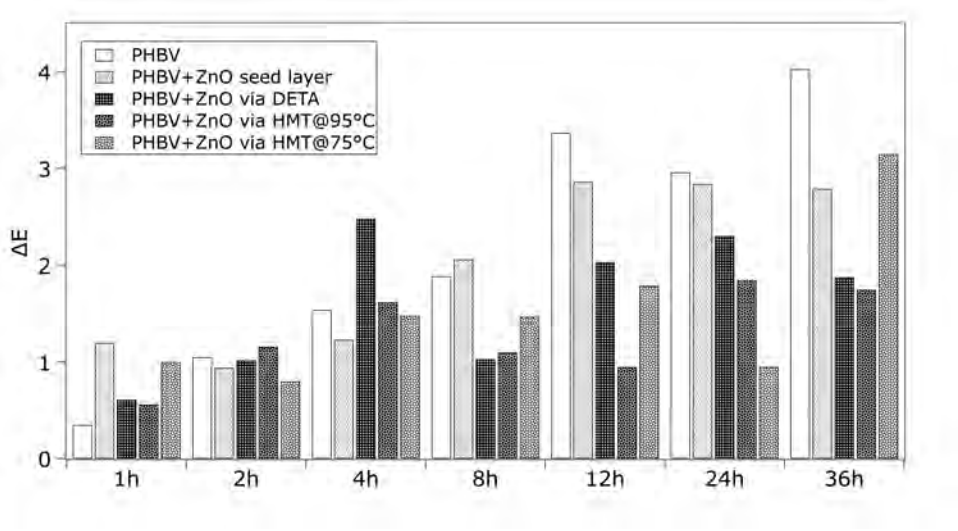

Figure 6.9: Colour difference in UV-radiated PHBV2 without and with ZnO layers deposited as indicated.

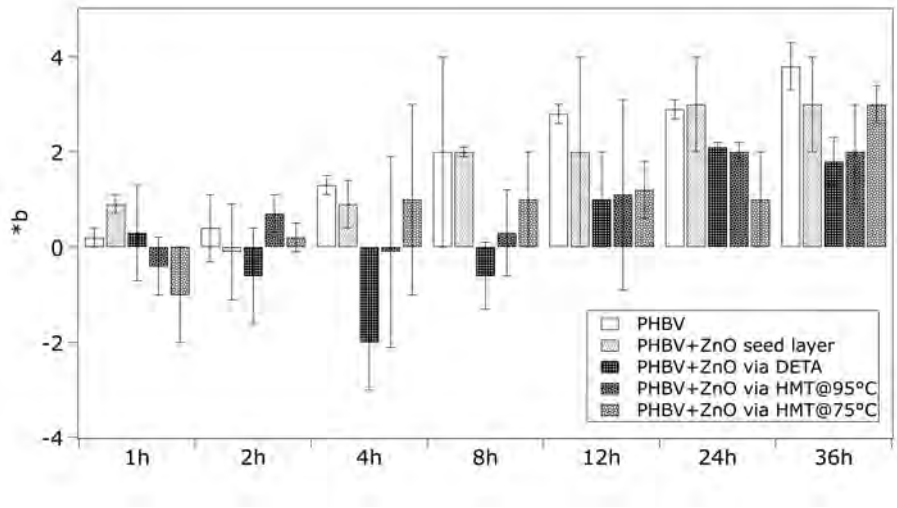

Figure 6.10: Yellowing of UV-radiated PHBV2 without and with ZnO layers deposited as indicated.

6.3.5 Influence of UV radiation on the permeability properties of PHBV2 and PHBV2 with ZnO

The oxygen permeability was measured using an OX-TRAN module 702 (Mocon) and the CO_2 permeability was determined using a Permatran-C model 4/41 (Mocon). The substrates were conditioned 5h at a controlled temperature of 23°C and a relative humidity of 0%. The water vapor transmission rate was measured using a Permatran-W model 3/33 (Mocon) and the substrates were conditioned for 5h at a controlled temperature of 23°C and a relative humidity of 100%.

Figure 6.11 to 6.13 show the results of the permeability study. Exposing PHBV2 to UV light decreases WV, CO_2 and O_2 permeability. When the UV-radiation time increases, the permeability decreases. The decrease in permeability can be explained by the decrease in the diffusion coefficients by the formation of chemical crosslinks, as confirmed by the GPC measurements, and the decrease of free volume. Another explanation is the observation that UV degradation happens in the amorphous part of PHBV2, as confirmed by the DSC measurements. The %crystallinity of PHBV2 increases and the permeability

decreases [31]. The WV permeability of PHBV2 with ZnO seed layer shows the same results. The O_2 and CO_2 permeability of PHBV2 with ZnO seed layer stays stable after 2h of radiation, this indicates again that the ZnO acts as a UV protection layer. The decrease in WV permeability of PHBV2 with ZnO seed layer is probably due to the fact that high humidity makes PHBV2 swell and opens op the surface area and makes it easier for UV light to reach the PHBV2 polymer [1].

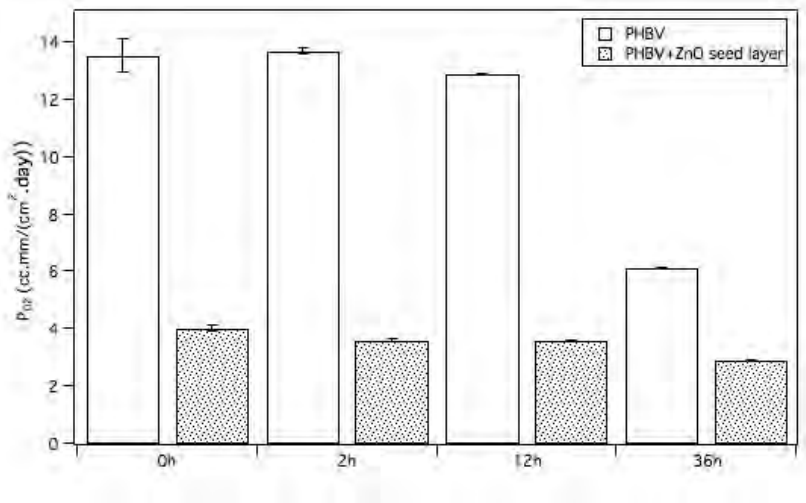

Figure 6.11: Oxygen permeability of UV-radiated PHBV and PHBV with ZnO seed layer.

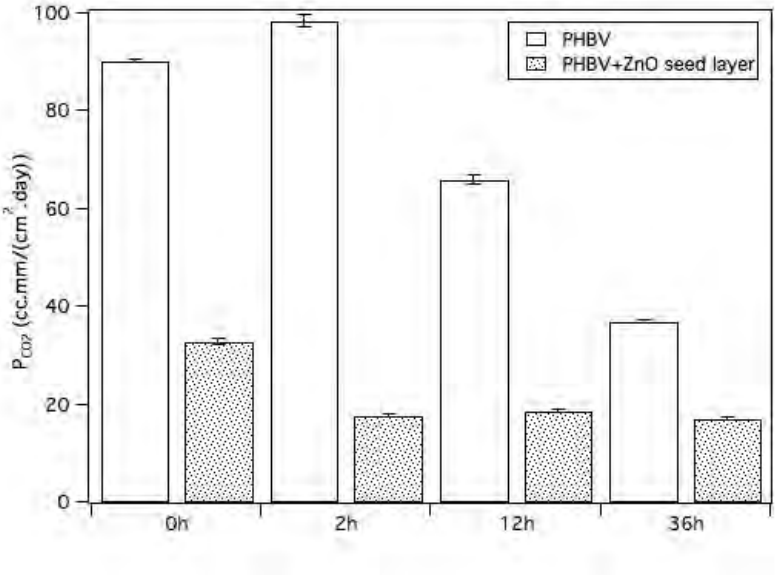

Figure 6.12: CO_2 permeability of UV-radiated PHBV and PHBV with ZnO seed layer.

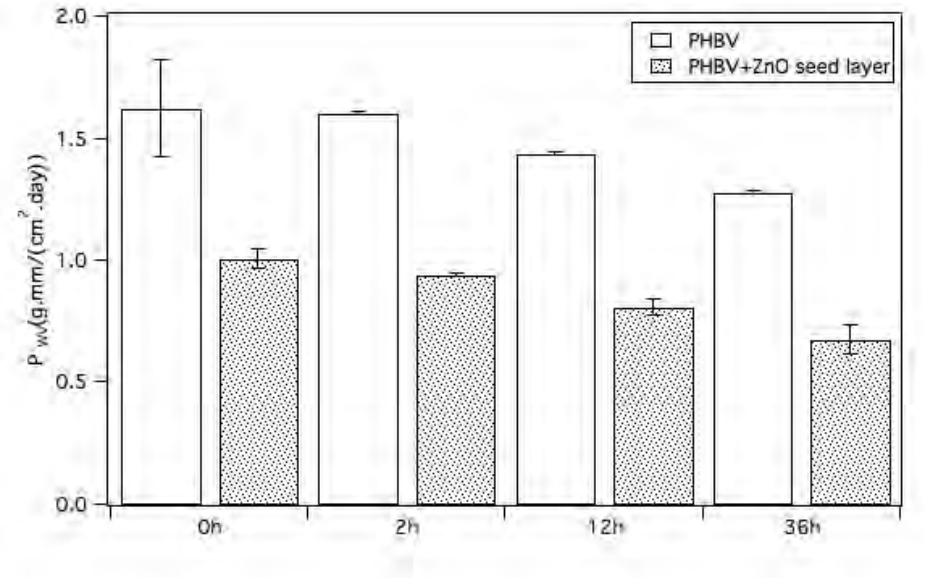

Figure 6.13: Water vapour permeability of UV-radiated PHBV and PHBV with ZnO seed layer.

6.4 Conclusion

It can be concluded that PHBV2 undergoes photo-degradation and that the UV degradation of PHBV2 follows a process, similar to PHB, of crosslinking and chain scission as indicated by GPC and permeability measurements. The ATR measurements showed that the degradation takes place following the β-oxidation reaction and in limited extent the Norrish I and Norrish II reaction. However, radiation of at least 8h is necessary to influence the properties of PHBV2. A radiation of 8h was necessary to show an increased mass loss in PHBV2. The tensile strength, M_n and M_w only decreased after 24h of irradiation. While an increase in keto and ester carbonyl bond index was already visible after 12h of radiation. Yellowing of the polymer is visible after 8h. A decrease in O_2, CO_2 and WV permeability is noticeable after 12h.

The optical transmittance spectra of PHBV2 and PHBV2 with ZnO showed that ZnO can be used to prevent the breakdown of C-O and C-C bonds. The mass loss in PHBV2 after UV radiation is suppressed by the addition of ZnO. The mass loss is increased after 24h instead of 8h. The keto-carbonyl index of PHBV2 increases only slightly and the ester-carbonyl index doesn't change after the addition of a ZnO layer to the PHBV2 substrates. The discoloration and yellowing only increase with a small amount. The thicker ZnO layers, deposited using DETA and HMT, showed a larger decrease in discoloration. The O_2 and CO_2 permeability of PHBV2 with ZnO seed layer stays stable, this indicates again that the ZnO acts as a UV protection layer. The water vapor permeability of PHBV2 with ZnO decreased. The swelling of PHBV2 prevents the ZnO of protecting the polymer against UV degradation.

In general, it can be concluded that deposition of ZnO layers can protect PHBV2 against UV degradation and prevent the deterioration of the polymer after a period of time. This is in concurrence with other literature reports about the deposition of ZnO on top of plastics, such as PP, PC, PEN and PET [14-19].

6.5 References

[1] J.F. Rabek, Photodegradation of Polymers, Springer, Berlin, 1996.

[2] A. Qahtan, S.P Rao, N. Keumala, The effectiveness of the sustainable flowing water film in improving the solar-optical properties of glazing in the tropics, Energy and buildings, 77 (2014) 247-255.

[3] H.F. Mark, Encyclopedia of Polymer Science and Technology, Concise, third ed., John Wiley & Sons, Hoboken, New Jersey, 2013.

[4] D.W. Van Krevelen, Te Nijenhuis, K., Properties of Polymers, Elsevier, Amsterdam, 2009.

[5] J. Park, J.G. Park, W.M. Choi, C.S. Ha, W.J. Cho, Synthesis and photo- and biodegradabilities of poly[(hydroxybutyrate-co-hydroxyvalerate)-g-phenyl vinyl ketone], J Appl Polym Sci, 74 (1999) 1432-1439.

[6] A. Lopez-Rubio, J.M. Lagaron, Improvement of UV stability and mechanical properties of biopolyesters through the addition of beta-carotene, Polym. Degrad. Stabil., 95 (2010) 2162-2168.

[7] E. Ikada, Relationship between photodegradability and biodegradability of some aliphatic polyesters, Journal of Photopolymer Science and Technology, 12 (1999) 251-256.

[8] R.K. Sadi, G.J.M. Fechine, N.R. Demarquette, Photodegradation of poly(3-hydroxybutyrate), Polym. Degrad. Stabil., 95 (2010) 2318-2327.

[9] M. Rashvand, Z. Ranjbar, S. Rastegar, Nano zinc oxide as a UV-stabilizer for aromatic polyurethane coatings, Progress in Organic Coatings, 71 (2011) 362-368.

[10] J.F. Wang, T. Tsuzuki, L. Sun, X.G. Wang, Reducing the Photocatalytic Activity of Zinc Oxide Quantum Dots by Surface Modification, J Am Ceram Soc, 92 (2009) 2083-2088.

[11] Z.A. Lewicka, W.W. Yu, B.L. Oliva, E.Q. Contreras, V.L. Colvin, Photochemical behavior of nanoscale TiO2 and ZnO sunscreen ingredients, J Photoch Photobio A, 263 (2013) 24-33.

[12] K. Ellmer, A. Klein, B. Rech, Transparent Conductive Zinc Oxide: Basics and Applications in Thin Film Solar Cells, Springer, Berlin, 2007.

[13] P.O. Bussiere, J. Peyroux, G. Chadeyron, S. Therias, Influence of functional nanoparticles on the photostability of polymer materials: Recent progress and further applications, Polym. Degrad. Stabil., 98 (2013) 2411-2418.

[14] E.M. Bachari, S. Ben Amor, G. Baud, M. Jacquet, Photoprotective zinc oxide coatings on polyethylene terephthalate films, Mat Sci Eng B-Solid, 79 (2001) 165-174.

[15] A. Moustaghfir, E. Tomasella, A. Rivaton, B. Mailhot, M. Jacquet, J.L. Gardette, J. Cellier, Sputtered zinc oxide coatings: structural study and application to the photoprotection of the polycarbonate, Surf Coat Tech, 180 (2004) 642-645.

[16] L. Guedri-Knani, J.L. Gardette, M. Jacquet, A. Rivaton, Photoprotection of poly(ethylene-naphthalate) by zinc oxide coating, Surf Coat Tech, 180 (2004) 71-75.

[17] B. Guedri, S. Ben Amor, J.L. Gardette, M. Jacquet, A. Rivaton, Lifetime improvement of poly(ethylene naphthalate) by ZnO adhesive coatings, Polym. Degrad. Stabil., 88 (2005) 199-205.

[18] A. Moustaghfir, E. Tomasella, M. Jacquet, A. Rivaton, B. Mailhot, J.L. Gardette, E. Beche, ZnO/Al2O3 coatings for the photoprotection of polycarbonate, Thin Solid Films, 515 (2006) 662-665.

[19] K. Lahtinen, T. Kaariainen, P. Johansson, S. Kotkamo, P. Maydannik, T. Seppanen, J. Kuusipalo, D.C. Cameron, UV protective zinc oxide coating for biaxially oriented polypropylene packaging film by atomic layer deposition, Thin Solid Films, 570 (2014) 33-37.

[20] J.Q. Xu, Y.P. Chen, D.Y. Chen, J.N. Shen, Hydrothermal synthesis and gas sensing characters of ZnO nanorods, Sensor Actuat B-Chem, 113 (2006) 526-531.

[21] ISO, Plastics -- Determination of changes in colour and variations in properties after exposure to daylight under glass, natural weathering or laboratory light source, in, 2007.

[22] UV Weathering and Related Test Methods, in, Cabot, USA.

[23] F. Masood, T. Yasin, A. Hameed, Comparative oxo-biodegradation study of poly-3-hydroxybutyrate-co-3-hydroxyvalerate/polypropylene blend in controlled environments, Int Biodeter Biodegr, 87 (2014) 1-8.

[24] Y. Kann, M. Shurgalin, R.K. Krishnaswamy, FTIR spectroscopy for analysis of crystallinity of poly(3-hydroxybutyrate-co-4-hydroxybutyrate) polymers and its utilization in evaluation of aging, orientation and composition, Polym Test, 40 (2014) 218-224.

[25] X.J. Wang, Z.F. Chen, X.Y. Chen, J.Y. Pan, K.T. Xu, Miscibility, Crystallization Kinetics, and Mechanical Properties of Poly(3-hydroxybutyrate-co-3-hydroxyvalerate)(PHBV)/Poly(3-hydroxybutyrate-co-4-hydroxybutyrate)(P3/4HB) Blends, J Appl Polym Sci, 117 (2010) 838-848.

[26] H.Y. Yu, Z.Y. Qin, Z. Zhou, Cellulose nanocrystals as green fillers to improve crystallization and hydrophilic property of poly(3-hydroxybutyrate-co-3-hydroxyvalerate), Progress in Natural Science-Materials International, 21 (2011) 478-484.

[27] B.S. Mitchell, An Introduction to Materials Engineering and Science for Chemical and Materials Engineers John Wiley & Sons, Hoboken, 2004.

[28] S.K. Sharma, et al., A Handbook of Applied Biopolymer Technology: Synthesis, Degradation and Applications, RSC Publishing, 2011.

[29] A. Tanaka, et al., Influence of Morphology on Photo-Degradation of Low Density Polyethylene Films, Polym. Eng. Sci., 40 (2000) 2007-2013.

[30] T.E.L. John Scheirs, Modern Polyesters: Chemistry and Technology of Polyesters and Copolyesters, John Wiley & Sons, Chichester, 2005.

[31] S. Singh, A.K. Mohanty, T. Sugie, Y. Takai, H. Hamada, Renewable resource based biocomposites from natural fiber and polyhydroxybutyrate-co-valerate (PHBV) bioplastic, Compos Part a-Appl S, 39 (2008) 875-886.

Chapter 7

Summary and Outlook

7.1 Summary

Nowadays packaging has become indispensable in the food industry. While decades ago most food was sold separately, nowadays almost everything is packed in pots, cans, bottles, boxes, etc.. Packaged goods are easier to transport and to identify and products are better protected during transport and storage. Food is not only protected against shocks and vibrations, but also against environmental factors. For example, temperature, humidity, light, and oxygen can have a major impact on the shelf life of food products. Nowadays some products are shipped from one continent to another. Thus the shelf life of the products is more important than ever. To prolong the shelf life of food, barrier materials are used. Barrier materials can protect the product against O_2, CO_2, WV and UV light.

Plastic is one of the most commonly used packaging materials. More than 50% of the products are packed in plastic. Plastics have the advantage that they are light weight and can be produced in various forms. In spite of some great characteristics, there are also several disadvantages associated with the use of plastics. For the production not only crude oil is needed, but also energy that causes the release of greenhouse gases, such as methane and CO_2. In addition, plastics are not biodegradable and they contribute to the waste problem. Bioplastics on the other hand are produced from biomass and / or are biodegradable. They are considered to be an interesting material to replace conventional plastics. Bio-PET, Bio-PP and Bio-PE are gradually taking the place of their conventional counterparts. However, these materials are based only on biomass and are non-biodegradable. A more interesting bioplastic is PLA. PLA is both based on biomass and is biodegradable. However, PLA has the disadvantage to be thermally unstable and brittle. Therefore PHA’s are seen as a better alternative. PHBV belongs to the group of the PHA's and has similar mechanical properties to PP. It is a semi-crystalline polymer having a melting

point around 180 ° C, depending on the concentration of valerate. However, the gas barrier of this material does not meet the requirements of a high barrier, 1 cc.mm/(m^2.dag.atm) and therefore should be optimized.

There are several methods to optimize the gas barrier properties of PHBV. One can blend the polymer with another polymer with higher barrier properties. Layers of high-barrier material can be coated on the polymer surface or high barrier particles can be mixed in the polymer matrix. In the packaging industry, mixing inorganic particles, such as AlO_x, SiO_x and MMT, in the polymer matrix, is considered to be a good method to improve the gas barrier properties. However, mixing inorganic particles into a polymer matrix also has disadvantages. Often, the chemical incompatibility between the inorganic particle and the polymer matrix causes the formation of agglomerates and decreases the barrier properties. A possible solution to this is the application of barrier layers on the polymer surface. For this study, ZnO nanolayers were deposited on the surface of the bioplastic PHBV. ZnO was chosen because ZnO adsorbs O_2, protects against UV light and has antibacterial properties.

There are several techniques available to deposit ZnO nanolayers onto the surface of polymers. However, most of these techniques, such as CVD, have deposition temperatures above 200 ° C. These temperatures are too high, as PHBV will decompose at temperatures above 200 ° C. It is therefore important that a technique with a deposition temperature below 100 ° C was used. Techniques such as ALD and sputtering meet these conditions, but are expensive. A cheaper solution was the use of the sol gel technique, in combination with the chemical bath method. Another advantage of this technique is that by adjustment of the parameters, such as pH, temperature and concentration, the shape of the deposited particles can be adjusted. Nanoparticles with a high aspect ratio provide better barrier properties than particles with a low aspect ratio. The deposition differs from substrate to substrate. Therefore it is important to adjust the deposition parameters, such as pH, deposition temperature and duration of the deposition, to get the best deposition conditions. The deposition of ZnO nanolayers on PHBV hasn't been studied before and the existing sol gel methods often have annealing

temperatures above 100 ° C. Therefore the ZnO layer was optimized using a PET substrate.

In chapter 4, the synthesis of ZnO nanolayers was discussed. ZnO nanolayers can be deposited on top of PHBV substrates using the chemical bath and sputtering method. For rough surfaces the sputter technique is recommended. The polarity of both PHBV and PET substrates need to be enhanced by a seed layer to deposit a fully-grown ZnO layer. The seed layer can be deposited using a solution of 0.03M NaOH and 0.01 M $Zn(CH_3COO)_2.2H_2O$. A minimum temperature of 30°C is necessary to deposit ZnO seeds layers on PET and PHBV substrates. The most dense layers for PHBV were formed using the HMT method with $Zn(CH_3COO)_2.2H_2O$ at 95 °C (table 4.4). For PET the most dense layers were formed using the DETA method with $Zn(NO_3)_2.6H_2O$ (table 4.4). $Zn(NO_3)_2.6H_2O$ solutions have a lower basicity. The reaction speed increases with increasing basicity and makes a part of the crystal dissolve in the solution. Probably the reaction rate is too high when depositing ZnO on PHBV substrate with $Zn(NO_3)_2.6H_2O$ solution. Decreasing the pH could improve the deposition of ZnO on PHBV using $Zn(NO_3)_2.6H_2O$. For PET, the $Zn(CH_3COO)_2.2H_2O$ solutions need a higher basicity, increasing the pH could improve the deposition of ZnO on PET using $Zn(CH_3COO)_2.2H_2O$.

The deposition of ZnO seed and nanolayers on PHBV resulted in an improvement of the O_2, CO_2 and WV barrier properties of PHBV (Chapter 5). However, a ZnO nanolayer did not improve the O_2 and WV barrier properties of PET, although literature shows that ZnO should improve the barrier properties. A small increase in the CO_2 barrier properties was detected after the addition of ZnO nanolayers through the DETA and the HMT method. This indicates that the ZnO isn't dense enough and that more ZnO is necessary to improve the gas barrier. Further optimization of the ZnO nanolayers and thicker ZnO nanolayers are necessary to improve the barrier properties of PET. $Zn(NO_3)_2.6H_2O$ can be used instead of $Zn(CH_3COO)_2.2H_2O$ to improve the density of the layer. Another factor that needs to be taken in consideration is the smaller transmission rate of PET. Therefore it is recommended to measure on samples with a larger surface. A larger sample provides a smaller measuring error.

A temperature increase increases the permeability of the polymer. Through the addition of ZnO, PHBV can be used at higher temperatures than pure PHBV for the same applications. PHBV has an E_P value for O_2 (44 $kJ.mol^{-1}$) that is larger than the E_P value for CO_2 (40$kJ.mol^{-1}$). The E_p value of WV (61 $kJ.mol^{-1}$) is higher than the E_p values for CO_2 and O_2. The same observations can be made for PET. The addition of ZnO increases the E_p value of PET because it is more difficult for the permeant to permeate through the polymer. The E_p value of PHBV is higher than the E_p value of PET. PET is more polar than PHBV and therefore has a lower E_p value.

PHBV tends to react with moisture from the humid air at higher humidity. This creates a plasticizing effect and the permeability increases. The P_{WV} changes in a similar way for PHBV and PHBV with ZnO seed layer when changing the humidity. However the P_{O2} is influenced differently for PHBV and PHBV with ZnO seed layer. This indicates that the oxygen interacts with the ZnO protecting the polymer against humidity changes. ZnO nanolayers protect the PHBV against humidity. This indicates that PHBV with ZnO seed layer can be used in humid conditions.

Even though the deposition of ZnO nanolayers on PHBV substrates show a noticeable improvement in the barrier properties, the ZnO layer needs to be optimized. The defects in the ZnO nanolayer deposited through chemical bath method need to be removed. This can be done by changing the pH of the deposition solution, increasing deposition temperature or increasing the deposition time. A dense, defect-free layer could lead to even further improvement in barrier properties, making it a better solution than the nanocomposites.

In Chapter 6 it was shown that ZnO protects PHBV against UV light. However, radiation of at least 8h is necessary to influence the properties of PHBV. The UV degradation of PHBV follows a process, similar to PHB, of crosslinking and chain scission as indicated by GPC and permeability measurements. The ATR measurements showed that the degradation takes place following the β-oxidation reaction and in limited extent the Norrish I and Norrish II reaction.

The optical transmittance spectra of PHBV and PHBV with ZnO showed that ZnO can be used to prevent the breakdown of C-O and C-C bonds. The mass loss in PHBV after UV radiation is suppressed by the addition of ZnO. The keto-carbonyl index of PHBV increases only slightly and the ester-carbonyl index doesn't change after the addition of a ZnO layer to the PHBV substrates. The discoloration and yellowing only increase with a small amount. The thicker ZnO layers deposited using DETA and HMT showed a larger decrease in discoloration. The O_2 and CO_2 permeability of PHBV with ZnO seed layer stays stable, this indicates again that the ZnO acts as a UV protection layer. The water vapor permeability of PHBV with ZnO decreased. The swelling of PHBV prevents the ZnO of protecting the polymer against UV degradation.

Therefore it can be concluded that ZnO nanolayers form good barrier layers. They increase the O_2, CO_2 and WV barrier of PHBV and protect PHBV against UV light.

7.2 Outlook

This study shows that ZnO nanolayers can be deposited on plastic and bioplastic surfaces at temperatures as low as 95 °C. Low temperature deposition can provide for applications and benefits in a wide variety of sectors. The commercialization of biobased and/or biodegradable plastics as packaging material by improving their gas barrier or the reduction of production costs of solar cells by replacing heavy rigid substrates through flexible materials are only two examples of what can be achieved [1, 2].

Therefore it is important to further optimize the deposited ZnO nanolayers. The influence of the pH can be further researched by adding more alkaline substances to the mixture. By variation of pH and molar concentration the density of the layers can be improved or the deposition time can be decreased [3]. Another way to decrease deposition time and layer defects solution is to use the sputtering technique. The advantages and disadvantages of CBD and sputtering should be compared.

The deposition of ZnO nanolayers improves the gas barrier and UV barrier of PHBV and PET. The results of the UV degradation show that more ZnO leads to a more pronounced UV barrier. Therefore it is important to research if a ZnO nanolayer with less defects also leads to more improved gas barrier properties of PHBV and PET. It is also shown by the permeability study that the ratio of the thickness of the ZnO nanolayer and the thickness of the polymer substrate plays a role in improving the barrier properties of PET and PHBV [4]. It is important to create the best barrier with the least amount of ZnO. Therefore the optimal ratio of the thickness of the substrate and the ZnO nanolayer should be determined.

The determination of P_{CO2} of PHBV can lead to increased work on the improvement of the CO_2 barrier. MAP packaging is gaining popularity and therefore materials with a good CO_2 barrier are becoming more important [5]. The determination of the E_p values of PHBV and PHBV with ZnO will facilitate the prediction of the gas permeability of the substrates at different temperatures [6].

The improved UV barrier of PHBV with ZnO opens opportunities for extended lifespan of the packaging material and improved protection of the packed food by the packaging material against UV radiation. However this does not mean that the biodegradation properties of PHBV will decrease. Research shows that addition of nanoclays to bioplastics accelerates the biodegradability [7]. It would be interesting to determine if the biodegradation of PHBV accelerates in the presence of ZnO.

ZnO is commonly used as antimicrobial agent. Antimicrobial packaging can extend the shelf life and maintain the product quality of food [8]. Therefore, it is interesting to research the antibacterial properties of PHBV and PET with ZnO nanolayers.

Another hot topic in the food packaging industry is the migration of nanoparticles from food contact polymers into the food product. The European regulation EC 1935/2004 states that nanomaterials in food packaging should not pose a danger to human health [9]. Recent research indicates that the nanoparticles of food contact polymers do not reach the food product [10].

However it would be interesting to confirm these results with migration test on the PHBV substrates with ZnO. To limit the chance that the ZnO reaches the food product the ZnO nanolayers should be sandwiched in between two PHBV substrates.

7.3 References

1. J A Kilner, S.J.S., S J C Irvine, P P Edwards, *Functional Materials for Sustainable Energy Applications*. 2012, Cambridge: Woodhead Publishing Limited.
2. Siracusa, V., et al., *Biodegradable polymers for food packaging: a review.* Trends In Food Science & Technology, 2008. **19**(12): p. 634-643.
3. Kumar, P.S., et al., *Biodegradability study and pH influence on growth and orientation of ZnO nanorods via aqueous solution process.* Applied Surface Science, 2012. **258**(18): p. 6765-6771.
4. Leterrier, Y., *Durability of nanosized oxygen-barrier coatings on polymers - Internal stresses.* Progress in Materials Science, 2003. **48**(1): p. 1-55.
5. Sandhya, *Modified atmosphere packaging of fresh produce: Current status and future needs.* Lwt-Food Science and Technology, 2010. **43**(3): p. 381-392.
6. Massey, L.K., *Permeability Properties of Plastics and Elastomers*. Vol. William Andrew Publishing. 2003, USA.
7. Lagaron, J.M. and A. Lopez-Rubio, *Nanotechnology for bioplastics: opportunities, challenges and strategies.* Trends in Food Science & Technology, 2011. **22**(11): p. 611-617.
8. Rhim, J.W., H.M. Park, and C.S. Ha, *Bio-nanocomposites for food packaging applications.* Progress in Polymer Science, 2013. **38**(10-11): p. 1629-1652.
9. *regulation (EC) No 1935/2004 on materials and articles intended to come into contact with food and repealing Directives 80/590/EEC and 89/109/EEC*. 2004 07.08.2009 [cited 2014 25 November]; Available from: http://eur-lex.europa.eu/LexUriServ/LexUriServ.do?uri=CONSLEG:2004R1935:20090807:EN:PDF.

10. Franz, R.S., Angela; Bott, Johannes, *Migration measurement and modelling of nanoparticles from food contact polymers*, in *245th National Meeting of the American-Chemical-Society*2013: New Orleans, LA.